Diese Dissertation haben begutachtet:

………………………   …………………………

TECHNISCHE UNIVERSITÄT WIEN
Vienna University of Technology

DISSERTATION

TISSUE ENGINEERING APPROACHES TO IMPROVE
PERIPHERAL NERVE REGENERATION

ausgeführt zum Zwecke der Erlangung des akademischen Grades eines
Doktors der technischen Wissenschaften unter der Leitung von

a.o.Univ.Prof. Dipl.-Ing. Dr.techn. Heinz Redl

Institut für Verfahrenstechnik, Umwelttechnik und Technische Biowissenschaften

Eingereicht an der Technischen Universität Wien
Fakultät für Technische Chemie

Christina M.A.P. Schuh, MSc
0300501
Landgutgasse 32
1100 Wien

Wien, am 16. Februar 2016

Eidesstattliche Erklärung

Hiermit erkläre ich an Eides statt, dass ich die vorliegende Dissertation *„Tissue Engineering Approaches to Improve Peripheral Nerve Regeneration"* selbstständig verfasst und keine anderen als die angegebenen Quellen und Hilfsmittel verwendet habe.

Wien, am 16.2.2016   Christina M.A.P. Schuh

Table of contents

KURZFASSUNG

Läsionen peripherer Nerven betreffen 5% aller traumatischen Verletzungen (etwa 300.000 Fälle pro Jahr in Europa) und sind eine häufige Ursache für langwierige Krankenhausaufenthalte, die wiederum das Gesundheitssystem belasten. Der goldene Standard zur Behandlung peripherer Nervenläsionen ist das autologe Nerventransplantat, dessen Einsatz allerdings durch begrenzte Verfügbarkeit transplantierbarer Nerven limitiert ist. Weiters führt das autologe Nerventransplantat nicht immer zu funktionell zufriedenstellenden Ergebnissen. In dieser Dissertation wurden mehrere vielversprechende alternativen Ansätze zur Verbesserung der peripheren Nervenregeneration getestet.

Schwann'sche Zellen und deren Phenotypwechsel-assoziierte Formung von Büngner Bändern sind sowohl eine Vorraussetzung, als auch ein kritischer Faktor in der Nervenregeneration. Isolierung, Kultivierung und Reimplantation an die Defektstelle haben sich als große Herausforderung herausgestellt. Alternativen zu nativen Schwann'schen Zellen wurden in der Differenzierung von mesenchymalen Stammzellen in Richtung "Schwannzell-artige Zellen" gefunden. Kapitel I beschreibt die "Extrakorporale Stoßwellentherapie" als Methode zur Verbesserung von Schwannzell Isolierung und Kultivierung, aber auch zur Steigerung der Differenzierungseffizienz von mesenchymalen Stammzellen Richtung Schwannzell-artige Zellen.

Luminale Füllungen in Nervenkonduits stehen seit mehreren Jahren im Fokus wissenschaftlicher Diskussionen. Meinungen und Ideen reichen von Gelen, über Einzelfasern in unterschiedlicher Anzahl und Durchmesser, Kombination von Gelen und Fasern, Multikanal-Tuben, bis hin zu verschiedenen Wachstumsfaktoren und /oder Zellen. In Kapitel II wurde mit Hilfe von Elektrospinning eine parallel ausgerichtete Faserstruktur aus Fibrin und PGLA hergestellt, mit Schwannzellartigen Zellen besiedelt und für den potentiellen Einsatz *in vivo* getestet.

Kapitel III konzentriert sich auf Seidenfibroin als neuartiges Nervenkonduitmaterial, seiner Herstellung und Funktionalisierung. Durch die exzellente Biokompatibilität ist Seidenfibroin ein interessanter Kandidat für die Überbrückung von Nervendefekten. Wir beschreiben eine neuartige Methode um Seidenfibrointuben mechanisch und topographisch so zu verändern, dass diese als Nerventubus verwendet werden können. Der gewebte Tubus aus roher Seide wird aufeinanderfolgend degummiert mit einem Boratpuffersystem und mit einem ternären Lösungsmittel ($CaCl_2$/H_2O/Ethanol), Ameisensäure und Methanol behandelt. Um die Adhäsion, Viabilität und Proliferation von Schwannschen Zellen zu verbessern, wurde ein Protokoll entwickelt um Laminin kovalent an Seide zu binden.

ABSTRACT

Peripheral nerve injuries show a prevalence of about 5% of traumatic injuries (approximately 300.000 cases per year in Europe) and are a frequent cause of hospitalization, displaying a major burden to patients, and the social health-care systems and the economy. Injuries to peripheral nerves often result in large defects in the continuity of the severed nerve. Bridging of a large defect with an autologous interfascicular nerve graft is considered to be the gold standard. Albeit it is best available treatment, transplantation of an autologous nerve graft does not always provide a satisfactory outcome. In this thesis several alternative approaches have been developed to improve peripheral nerve regeneration.

Schwann cells are a crucial factor in peripheral nerve regeneration. Isolation, culture and re-implantation to the defect site have been proven to be challenging. Alternatives to native cultures are mesenchymal stem cells differentiated into Schwann cell-like cells. Chapter I illustrates the method "Extracorporeal Shockwave Treatment" to facilitate native Schwann cell isolation and culture, and to improve differentiation of mesenchymal stem cells into Schwann cell-like cells.

Nerve conduit luminal fillers have been topic of discussion for many years. Ideas of an ideal luminal filler range from gels, to single fibres of different diameters and number, to composite gel/fibre fillers, multiple channels containing different growth factors and/or cells. In chapter II we investigated electrospinning as a method to align fibrin/PGLA fibres to create a biomimicking tissue-like material seeded with Schwann cell-like cells *in vitro* for potential use as an *in vivo* scaffold.

Chapter III focuses on a novel nerve conduit material, its fabrication and functionalization. Due to its excellent biocompatibility silk fibroin has attracted considerable interest as a biomaterial for use as a conduit in peripheral nerve regeneration. We describe a novel procedure to produce silk fibroin nerve conduits: a braided tubular structure of raw Bombyx mori silk is subsequently degummed with a borate buffer system and processed with the ternary solvent $CaCl_2/H_2O$/ethanol, formic acid and methanol to improve its mechanical and topographical characteristics. Furthermore a protocol has been established to covalently bind laminin to silk fibroin utilizing carbodiimide chemistry, resulting in improved adhesion, viability and proliferation of Schwann cells.

General Introduction

Background

Peripheral nerve injuries show a prevalence of about 5% of traumatic injuries (approximately 300.000 cases per year in Europe (1)) and are a frequent cause of hospitalization, displaying a major burden to patients, and the social health-care systems and the economy (2). The treatment of complete transections of a nerve trunk - are either direct end-to-end coaptation of opposing nerve stumps for small gap lengths (< 5mm) or the use of autograft tissue (the sural nerve is the most used donor nerve) for longer gap lengths. However, such treatments are not ideal solutions, as direct suturing is only possible for a small sub-set of injuries, whereas the use of a nerve autograft, when available with appropriate length and thickness, may induce a neurological deficit at the donor site. Moreover, in long nerve defect injuries or in major nerve injuries like the sciatic nerve the grafts needed for interfascicular reconstruction are not available due to a limited source.

The main advantage of nerve autografts is their morphologically native structure, which provides not only guiding structures and the ideal tissue density, but also Schwann cells producing extracellular matrix molecules favourable for outgrowing axons into the distal nerve stump. However, transplantation of an autologous nerve graft does not always provide a satisfactory outcome (3). A growing body of literature states the inferiority of sensory compared to motor nerve grafts in regard to re-innervation and functional outcome. It is evident that peripheral sensory nerves are still used as autografts because loss of motor function is not acceptable. Finding alternatives for autologous nerve grafting has become one of the major topics of investigation in the field of regenerative medicine in the last decades.

The human nervous system

The human nervous system is comprised of billions of connected nerve cells, responsible for motor functions, cognitive functions, processing incoming information and regulating vital functions such as breathing and the hormonal balance. It is divided into the central nervous system (CNS) and the peripheral nervous system (PNS). The two parts of the CNS are the brain and the spinal cord; ganglia and nerves exterior the brain and spinal cord build the PNS. The most apparent difference between the CNS and the PNS is the processing of information: while the CNS is responsible to handle all involuntary information, the (PNS) handles voluntary information.

Transmitting information from the CNS, nerves are called "motor neurons" and the process of transmission "efferent", while transmission into the CNS is called "afferent" and the nerves "sensory neurons". (4)
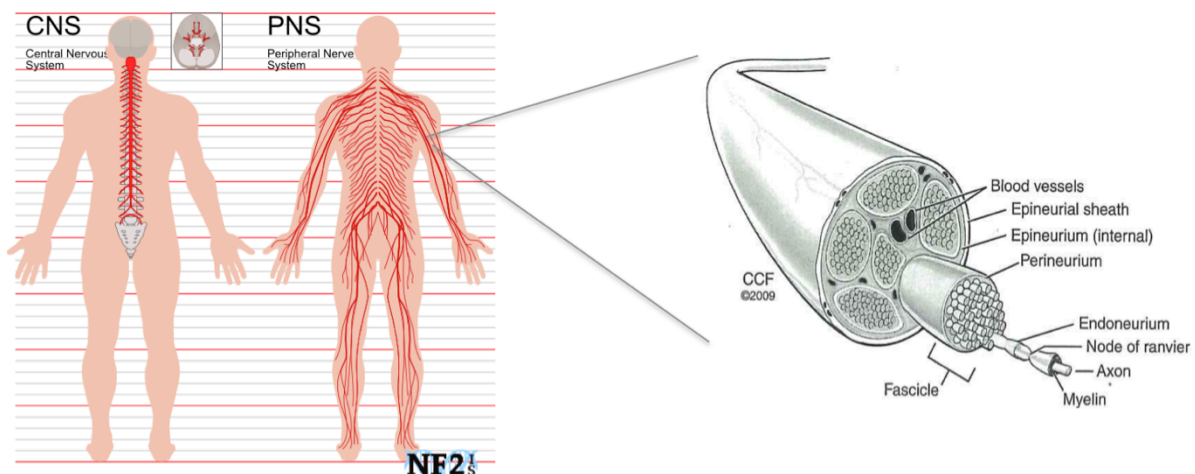
Figure 1: Schematic depiction of the CNS and PNS (http://www.nf2is.org/nerves.php), and peripheral nerve anatomy (3)

Nerve anatomy. A neuron is segmented in the perykaryon - the cell body - and the axon and dendrites - the cell extensions. In the peripheral nervous system, Schwann cells are wrapped around an axon producing myelin, which acts as an insulator and enables the saltatoric conduction. Their cell organelles are exterior to the myelin sheath. Between the individual Schwann cells, there are the Nodes of Ranvier, which are gaps of approximately 1 μm in length, responsible for the saltatoric conduction. The Schwann cells, including the Nodes of Ranvier, are again surrounded by mostly longitudinal fibrous connective tissue, the basal lamina (4). Together, the Schwann cells and the basal lamina build the endoneurium. The perineurium embraces a variable number of nerve fibres to a fascicle and consists of the fibroblastic interior pars epithelialis and the exterior connective tissue, the pars fibrosa. Tissue

between the fascicles is called epineurium, the epineural sheath builds the surrounding layer on the outside. With collagen and elastic fibres it is responsible for the flexibility and tear strength of the nerve fibres and integrates blood vessels.

Peripheral Nerve Injury and Regeneration

Historically Sir Herbert Seddon was the first to categorize nerve injuries according to their severity: neuropraxia, axonotmesis and neurotmesis. *Neuropraxia* describes a defect where the axon, myelin sheath and epineurium are damaged but not disrupted. In *axonotmesis* the axon and myelin sheath are disrupted, but the epineurium remained intact. *Neurotmesis* is the disruption of the axon and all protective structures, including the epineurium. (4)

In the 1950 severity of a nerve injury was further divided into five categories, according to a scale established by Sidney Sunderland. Starting with the first degree injury, where continuity of the nerve preserved and spontaneous recovery occurs after minutes to weeks, the categories increase in severity until degree five, where the axon and all encapsulating structures are disrupted and nerve recover is not possible unless surgically intervened (Table 1). (5)

Sunderland Terminology	Description
First degree	• Nerve in continuity • Compression of ischemic etiology • Local conduction block • Spontaneous recovery in minutes to weeks
Second degree	• Injury to axon • Encapsulation structures intact • Wallerian degeneration occurs • Recovery 1-3 mm per day • Spontaneous recovery is length dependent
Third degree	• Injury to axon • Endoneurium disrupted, epineurium and perineurium intact • Wallerian degeneration occurs • Spontaneous recovery is length dependent
Fourth degree	• Injury to axon • Disruption in all encapsulating elements, but epineurium is intact • Wallerian degeneration occurs • Requires surgical intervention for recovery
Fifth degree	• Injury to axon • Disruption in all encapsulating elements • Wallerian degeneration occurs • Requires surgical intervention for recovery

Table 1: Sunderland Classification of Peripheral Nerve Injuries; Adapted from Carp 2015 (6)

After peripheral nerve injury, a rapid process of degenerative events called "Wallerian degeneration" occurs. The degenerative processes are again followed by regenerative events (depicted in Figure 2), provided that the injured nerve stumps are in close vicinity and the regenerating axons from the proximal stump are able to enter the vacated endoneural sheaths in the distal stump.
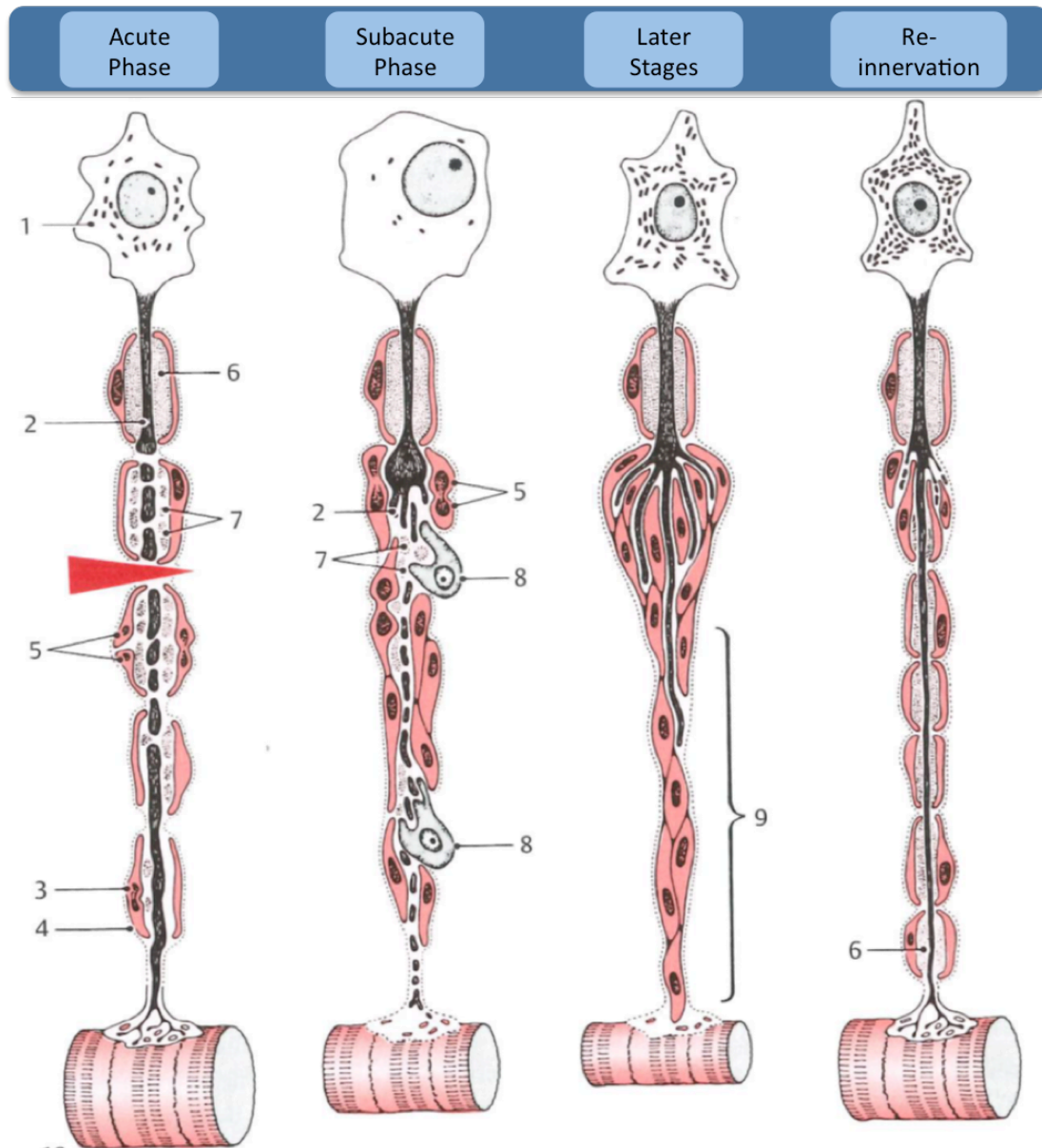
Figure 2: Scheme of the degeneration and regeneration of a dissected motor axon, illustrating the acute phase, subacute phase, later stages and re-innveration. 1: perikaryon; 2: proximal segment of the axon; 3: Schwann cell; 4: basal lamina; 5: proliferating Schwann cell; 6: myelin sheath; 7: myelin debris; 8: macrophage; 9: Bands of Büngner; adapted from (4)

In the **acute phase** (1-4 days after neurotmesis) the distal part of the axon undergoes Wallerian degeneration and resident Schwann cells start to proliferate. Proximal to the injury

Wallerian degeneration only takes place up to the first internode. This process is accompanied by local inflammation mainly due to the activation of resident macrophages (7) and infiltration of macrophages through the epineurium (8).

After 10 to 21 days (**subacute phase**) atrophy of the target muscle can be seen and the bands of Büngner are formed by proliferating Schwann cells. Removal of myelin and axonal debris is achieved by Schwann cells and recruited macrophages. The proximal stump of the axon already shows sprouting and the motor end plate is degenerating.

In **later stages** of axonal regeneration proliferating Schwann cells align to form the bands of Büngner and restructure the extracellular matrix that contains growth-promoting molecules such as laminin and fibronectin. The growth cone of the regenerating axons actively synthesizes transmembrane integrin molecules, for example, integrin-type alpha5-beta1, which interacts with fibronectin, thereby ensuring the axonal growth. Atrophy of the muscle advances, the chromatolysis of the rough endoplasmatic reticulum is regressing. (4)

The gold standard and other approaches

In peripheral nerve injuries accompanied by segmental loss, spontaneous regeneration does not occur. Therefore autologous nerve grafting is necessary in order to bridge the gap and restore continuity of the nerve. Interfascicular grafting is recommended (9). Nerve fascicles are resected from a solely sensitive donor nerve and transplanted between the proximal and the distal stump. The graft provides the ideal nerve conduit concerning adhesion molecules and neurotrophic factors, once it underwent Wallerian degeneration. Due to the common need for long grafts, the sural nerve is by far the nerve used most for autografting.

The use of artificial tubular conduits to restore continuity of the proximal and distal stump of a transected nerve has been the subject of a large number of investigations (over 600 publications on Pubmed). Nerve stumps are placed inside a biological or synthetic tube and sutured to it. The tube protects the nerve gap from ingrowth of connective tissue and axoplasmic fluid is retained at the defect site. However, regeneration inside a hollow tube differs from autografting, as the regenerative matrix is not remodelled from existing tissue, but has to be newly established. Regeneration occurs in five phases, shown in Figure 3. Starting with the fluid phase: axoplasmic fluids flush the tube and neurotrophic factors accumulate. Subsequently, in the matrix phase, acellular fibrin from the nerve stumps form within the tube. In the third phase, the cellular phase, Schwann cells migrate along the fibrin

cables to form bands of Büngner. The axonal phase is characterized by axon sprouting and elongation from proximal stump to the distal stump along the before formed tissue cable. In the last phase Schwann cells from the tissue cable wrap around the newly formed axons and myelinate them.

(1) fluid phase

accumulation of neurotrophic factors and ECM molecules

(2) matrix phase

fibrin cable formation

(3) cellular phase

Schwann cell migration, proliferation and alignment and tissue cable formation

(4) axonal phase

growth of daughter axons (proximal to distal) across de novo tissue cable

(5) myelination phase

myelination of regenerated immature axons forming mature axonal fibres

Figure 3: Scheme of peripheral nerve regeneration within a hollow tube; Daly *et al.* 2012, adapted from Belkas *et al.* 2004 (1,10)

The question of conduit design has been subject of discussion for decades. An ideal conduit should protect the site of injury from the infiltration of surrounding tissues, while at the same time retaining a certain degree of porosity to allow diffusion of soluble factors through the tube wall, as well as limiting the migration and organization of myofibroblasts, which are responsible for the undesired synthesis of scar tissue (11). The conduit should also provide adequate mechanical strength and flexibility to support the regenerating nerve fibres, as well as to be able to be coapted to the proximal and distal nerve stump, and should be biocompatible and biodegradable. Positive effects have been observed with surface functionalization (12,13) and regenerative cells seeded on extracellular-matrix-improved surfaces (14). While the presence of a conduit between the transected stumps is sufficient to induce regeneration, the microstructural, mechanical and compositional features of the tubular construct itself have been observed to significantly affect the quality of regeneration (11,15). Luminal fillers have been topic of discussion for many years. Ideas of an ideal luminal filler range from gels, to single fibres of different diameters and number, to composite gel/fibre fillers, multiple channels (16–20) containing different growth factors (Nerve growth factor, vascular endothelial growth factor, fibroblast growth factor,… (21–23)) and/or cells (mesenchymal stem cells or Schwann cells) (24,25).

Schwann cells

In early embryonic development a single-cellular-layer sheet is formed, called the neural plate. Folding of the neural plate (neurulation) results in the precursor of the central nervous system - the neural tube. The cells of the neural folds transform into neural crest cells, which again differentiate into different cell types like sensory neurons, glial cells, myoblasts or Schwann cells precursor cells. (26) These precursors undergo further differentiation steps towards mature Schwann cells, seen in Figure 4.

In their mature state, myelinating Schwann cells are wrapped around an axon, producing myelin. Myelin is composed of lipids and proteins, acting as an insulator. In contrast to most biological membranes, it has a higher proportion of lipids (70-85%) (27). The short gaps between the myelin producing Schwann cells, are known as "Nodes of Ranvier". Along these discontinuous sites, membrane depolarization occurs, resulting in rapis, saltatoric conduction (28). Main components of myelin are Myelin Associated Glycoprotein (MAG) and protein zero (P0). Structurally MAG has a single transmembrane domain, separating the glycosylated extracellular part from an intracellular carboxy-terminal domain. MAG is located in the periaxonal glial membranes of myelin sheaths, next to the axon- functioning in adhesion and

12

signaling between myelin-forming cells and the axolemma. (27) P0 is the most abundant myelin protein in the PNS (>50%). Structurally it is a type I membrane glycoprotein, having a positively charged domain on the extracellular side of the membrane, contributing to stabilization of the major dense line in the PNS. (27)
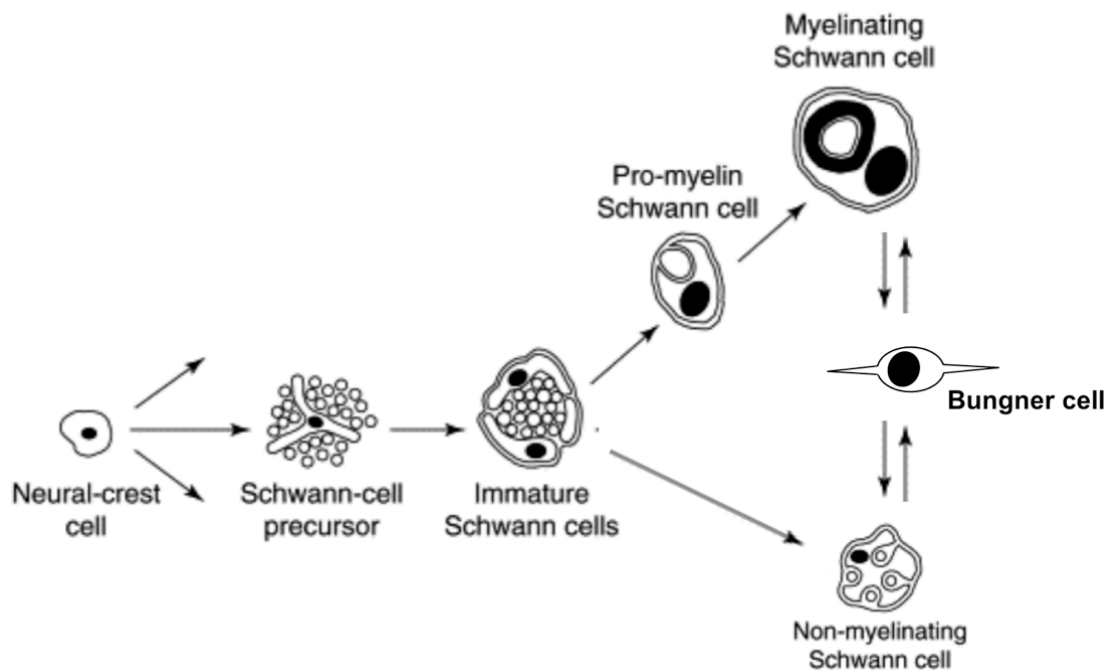
Figure 4: Schwann cell transition in a schematic overview; Neural crest cells transform into Schwann cell precursor and immature Schwann cells. The third transition offers two options: myelinating and non-myelinating Schwann cells; After injury, mature Schwann cells, independent of myelination status, switch into the activated „Bungner cell" status; adapted from Jessen and Mirsky 1999 (29) and Arthur-Farraj et al. 2012 (30);

Schwann cells are a crucial factor in peripheral nerve regeneration. While in the uninjured nerve, they are non-proliferating and ensheating the axon, in the injured nerve they switch towards the activated state, also known as "repair cell" or "Bungner cell" (30). In the activated state Schwann cells start proliferating, building the so-called bands of Bungner from the site of injury to the target muscle. Schwann cells within the bands of Bungner build a guidance substrate, secreting several growth factors like the brain derived neurotrophic factor (BDNF) (31), the glial derived neurotrophic factor (GDNF) (32) and other neurotrophic factors (33), and expressing adhesion molecules like the neural cell adhesion molecule (NCAM), cadherin and integrins (34). Neurotrophin receptor P75, also known as P75NTR or CD271 is expressed during proliferation, strongly correlating with it (35). Since neurotrophins are key mediators for myelination, the absence of P75 inhibits future myelination (36). The combination of secreted factor and adhesion molecules stimulates and guides axonal outgrowth.

13

Aim

Injuries to a peripheral nerve often result in large defects in the continuity of the severed nerve. Bridging of a large defect with an autologous interfascicular nerve graft is considered to be the gold standard. Albeit it is best available treatment, transplantation of an autologous nerve graft does not always provide a satisfactory outcome. This PhD thesis aims to improve regeneration of peripheral nerves after traumatic injury in a three-staged approach:

I. Improving Schwann cell isolation and culture, as well as Schwann cell-like cell differentiation using extracorporeal shockwave treatment.

II. Development of a fibrin based luminal filler containing activated Schwann cell-like cells.

III. Functionalizing silk fibroin to serve as an improved biomaterial for nerve regeneration

I) Improving Schwann cell isolation, culture and Schwann cell-like cell differentiation

Recently Hausner *et al.* (37) showed a novel approach of accelerating regeneration after peripheral nerve injury. In a rat sciatic nerve autograft model extracorporeal shockwave treatment resulted in a significantly accelerated functional recovery without causing any adverse effects. As shockwaves were applied on the site of defect (as opposed to the neural cell bodies) we hypothesize that extracorporeal shockwave treatment could have beneficial effects on *in vitro* Schwann cell cultures and investigated the effect of shockwave treatment on the isolation efficacy and purity and quality of culture.

Furthermore it was shown in an *in vitro* setup that a variety of cells react to shockwave treatment with increased ATP release and proliferation (38), and we hypothesize that also adipose derived stem cells could react to shockwave treatment with increased reactivity to stimuli, eg differentiation into Schwann cell-like cells.

II) Fibrin and activated Schwann cells as a potential luminal filler for nerve guidance conduits

The formation and controlled degradation of fibrin is one of the major components in natural wound healing. Fibrin is an especially important factor in nerve regeneration: after injury, nerve stumps leak fibrin plasma exudate into the affected area, forming fibrin cables that enable Schwann cells to migrate towards the distal stump and form Bands of Büngner (1,39).

In this chapter, we investigate electrospinning as a method to align fibrin/PGLA fibres to create a biomimicking tissue-like material seeded with Schwann cell-like cells (SCLs) *in vitro* for potential use as an *in vivo* scaffold.

III) Functionalizing silk fibroin to serve as an improved biomaterial for nerve regeneration

In the last few years, silk fibroin (SF) has attracted considerable interest as a biomaterial suitable for applications towards peripheral nerve regeneration. SF has been shown to possess characteristics that favour its use as a nerve guidance, such as mechanical stability, slow degradation rate, biocompatibility and its ability to support nerve regeneration (40,41). We first hypothesized that a hollow silk tube would be suitable to bridge an 8 mm nerve gap in a rat sciatic model, however found options *in vitro* to possibly further improve the outcome *in vivo*.

One possibility to improve the outcome *in vivo* is to apply silk fibroin guiding structures inside the tube. These silk fibroin fibres could be functionalized with laminin to provide an ideal growth substrate, containing pro-migratory and pro-regenerative ECM molecules such as laminin and collagens isolated from the human placenta. Laminin is known to promote neurite outgrowth *in vitro* (42) and *in vivo* (43) and collagens are upregulated after injury by pro-regenerative Schwann cells inducing cell proliferation (44). Therefore these ECM molecules could be used to coat silk fibres in order to establish a natural human ECM as guiding structure for regenerating axons (45). Covalently bound to the silk fibroin fibres we expect these ECM proteins to improve Schwann cell adhesion to the fibres and therefore less heterogenicity in cell distribution after seeding *in vitro*, and to enhance neurite outgrowth and therefore functional recovery *in vivo*.

Chapter I

Extracorporeal Shockwave Treatment to Improve Schwann Cells and Schwann Cell-like Cell Differentiation

In vitro Extracorporeal Shockwave Treatment Enhances Stemness and Preserves Multipotency of Rat- and Human Adipose derived Stem Cells

Christina M.A.P. Schuh[1,2,3], Philipp Heher[1,2], Anna M. Weihs[2,3],
Asmita Banerjee[1,2], Christiane Fuchs[2,3], Christian Gabriel[4],
Susanne Wolbank[1,2], Rainer Mittermayr[1,2], Heinz Redl[1,2], Dominik Rünzler[2,3],
Andreas H. Teuschl[2,3]

[1]Ludwig Boltzmann Institute for Experimental and Clinical Traumatology, AUVA Research Center, Donaueschingenstraße 13, A-1200 Vienna, Austria
[2]Austrian Cluster for Tissue Regeneration, Austria
[3]University of Applied Sciences Technikum Wien – Department of Biochemical Engineering, Vienna, Austria
[4]Red Cross Blood Transfusion Service for Upper Austria, Linz, Austria

Abstract

Adipose derived progenitor/stem cells (ASCs) are discussed as a promising candidate for various tissue engineering approaches. However, its applicability for the clinic is still difficult due to intra- and inter-donor heterogeneity and limited life span *in vitro*, influencing differentiation capacity as a consequence to decreased multipotency. Extracorporeal shockwave treatment has been proven to be a suitable clinical tool to improve regeneration of a variety of tissues for several decades, while the mechanisms underlying these beneficial effects remain widely unknown. In this study we show that human and rat adipose derived stem cells respond strongly to repetitive shockwave treatment *in vitro*, resulting not only in maintenance and significant elevation of mesenchymal markers (CD73, CD90, CD105), but also in significantly increased differentiation capacity towards the osteogenic and adipogenic lineage as well as towards Schwann cell-like cells even after extended time *in vitro*, preserving multipotency of ASCs. Hence, ESWT might be a promising tool to improve ASC quality for cell therapy in various tissue engineering and regenerative medicine applications.

INTRODUCTION

Tissue-resident mesenchymal stem cells (MSC) maintain tissue integrity and participate in tissue regeneration, e.g. responding to injury (46). Due to their innate participation in tissue regeneration, MSCs are one of the most promising tools for tissue engineering representing an alternative cell source to human tissue specific cells, which are usually difficult to obtain. There is a great variety of tissues from which MSCs can be isolated from, including bone marrow (47), umbilical cord blood (48) and adipose tissue (49). The cells have shown potential to differentiate *ex vivo* into various mesenchymal cell types such as adipocytes, osteoblasts, chondrocytes or fibroblasts (50–53) but also other lineages including Schwann-like cells (54,55). Moreover, their immunogenic phenotype is lacking major histocompatibility complex class II (MHC II) and hinders T cell stimulation and subsequently immunogenic responses (46,56,57). Furthermore, studies have demonstrated immunosuppressive properties of MSCs (58,59).

A limiting factor for cell therapy using MSCs is the high variation of the isolated cell population (60), due to which functionality of cells influencing targeted therapy cannot be guaranteed. Another factor to be considered is a donor dependent decrease of multipotency after expansion *in vitro* and further influencing the MSC properties including differentiation potential, starting in early passages (60–63). As a consequence there is a clinical need to limit these variations and to take a step closer towards consistent quality of MSCs for cell therapy, which was also defined recently by the IFATS and ISCT (64).

Interestingly, in this regard physical stimuli such as controlled frequency ultrasound (65), shear stress and dynamic compression (66), but also extracorporeal shockwaves (67) have been shown to have positive effects on stem cell isolation and specific differentiations, while only little is known concerning effects on stemness.

Historically, extracorporeal shockwave therapy (ESWT) has its origin in treatment of kidney stones (68), but it has also been proven to be an effective therapeutic tool in the field of regenerative medicine. In clinics beneficial effects of ESWT *in vivo* have been observed in treatment of non-union fractures (69–71), ischemia-induced tissue necrosis (72), peripheral nerve lesions (37), chronic wounds (73,74) and several other fields (75–77).

The basis of a shockwave is a change in local density, caused by expansion and concentration within and medium. The generated shockwave is a sonic pulse characterized by an initial rise, reaching a positive peak of up to 100 MPa within 10 ns, followed by a negative amplitude of up to -10 MPa and a total life cycle of less than 10 µs. The effect resulting from this characteristic is twofold, with the direct generation of mechanical forces as a primary effect,

and the indirect generation of mechanical forces by cavitation as a secondary effect. Biological responses are thought to be triggered by the high initial pressure, followed by a tensile force and the resulting mechanical stimulation (78). Moreover, it has been stated that extracorporeal shockwaves can recruit tissue resident MSCs to the site of injury by inducing the secretion of chemotactic factors from the surrounding tissue (79), while the effect on MSCs itself has not been fully investigated yet, but appears to be a possible tool to direct stem cell fate.

The aim of this study was to investigate *in vitro* the direct effect of ESWT on rat and human MSCs derived from adipose tissue concerning their expression of MSC-typical cell surface markers, proliferation, viability and its impact on differentiation capacity.
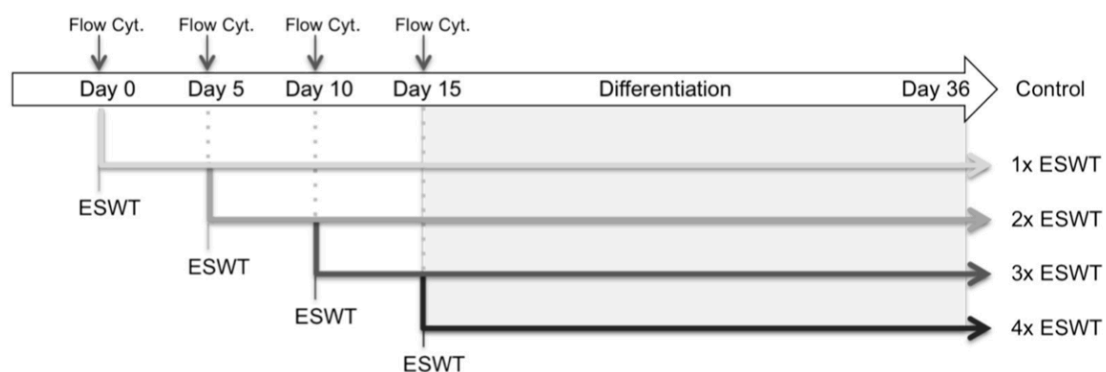
Figure 5: Experimental scheme shows time points for ESWT, evaluation with flow cytometry (Flow cyt.) and respective passage number. Evaluation referred to on day 36 includes differentiation specific stainings, PCR and flow cytometry.

MATERIAL AND METHODS

Isolation of adipose-derived stem cells (ASCs)

For human ASCs (hASCs) liposuction material of male and female patients between 31 and 40 years were used. The collection of human adipose tissue was approved by the local ethical review board and informed, written consent was obtained from each patient prior to the collection of the material. Rat ASCs (rASCs) were isolated from visceral fat pads of adult male Sprague Dawley rats. Rats were euthanized according to established protocols, which were approved by the City Government of Vienna, Austria in accordance with the Austrian law and Guide for the Care and Use of Laboratory Animals as defined by the National Institute of Health. For isolation of human ASCs a protocol described by Wolbank *et al.* (80) was used and adopted for rat fat tissue. Briefly, after mincing the adipose tissue it was digested with Collagenase Type I (Biochrome, Berlin, Germany), filtered through 100 μm cell strainers (BD Bioscience, Franklin Lakes, NJ, USA) and centrifuged at 400xg. Resulting

ASCs separated from adipose tissue were seeded on T75 cell culture flasks (PAA, Pasching, Austria) for expansion.

Cell culture conditions

After isolation, hASC and rASC cells were cultivated using standard cell culture conditions (37°C, 5% CO_2) in Dulbecco's modified Eagles medium (DMEM low glucose; PAA) and Ham's F12 (PAA) supplemented with 10% fetal calf serum (FCS; PAA), 200 μM L-glutamine and 1% (v/v) penicillin-streptomycin (PAA). For expansion, cells were cultivated in cell culture flasks (PAA) with an initial seeding density of 3×10^3 cells/cm^2. At a confluence of 80-90% cells were split with Accutase^{TM} (PAA).

Characterization of adipose-derived stem cells with flow cytometry

hASCs and rASCs were characterized by flow cytometry using mesenchymal stem cell specific markers, as described by Dominici *et al.* 2006 (52). Flow cytometric analysis was performed with a BD FACS Canto II (BD Biosciences). Cells were detached with Accutase^{TM} to minimize influence on cell surface markers and incubated with antibodies on ice and in the dark for 20 minutes. hASCs were incubated with anti-CD14 FITC, anti-CD34 FITC, anti-CD45 PE, anti-CD73 PE, anti-CD90 PE (all mouse monoclonal; BD Bioscience) and anti-CD105 (mouse monoclonal, FITC labeled; Abcam, Cambridge, UK); rASCs were incubated with: anti-CD14 (mouse monoclonal, FITC labeled; Merck Millipore, Billerica, MA, USA) anti-CD34 (rabbit polyclonal; abcam), anti-CD45 (rabbit Polyclonal; abcam), anti-CD73 (rabbit polyclonal; Santa Cruz Biotechnology, Dallas, TX, USA), anti-CD90 (rabbit polyclonal; Santa Cruz Biotechnology) and anti-CD105 (mouse monoclonal; Merck Millipore); and secondary antibody: FITC anti rabbit (goat polyclonal; Dako, Glostrup, Denmark) FITC anti mouse (rabbit polyclonal, Dako);

Schwann cell markers anti-P75 NGFR (goat polyclonal, Santa Cruz Biotechnology, USA), anti- S100b (rabbit polyclonal; Dako) and anti-P0 (rabbit polyclonal, Santa Cruz Biotechnology, USA) for hASCs and rASCs were conjugated with APC (Lynx Rapid Conjugation Kit, ABD Serotec, Kidlington, UK).

Flow cytometry data was evaluated with Flowjo Version 8.8 (Tree Star Inc, Ashland, OR, USA).

In vitro Extracorporeal Shockwave Treatment

For *in vitro* shockwave treatment an unfocused electro-hydraulic device was used (Dermagold 100, MTS Medical, Constance, Germany). The applicator (OP155) was attached to a water bath as described by Holfeld *et al.* 2014 (81) ensuring direct contact to the prewarmed (37°C)

water, allowing reproducible physical propagation and application of shockwaves *in vitro*. hASCs and rASCs detached with Accutase^{TM} were centrifuged, resuspended to a concentration of $1x10^6$ cells/mL with a total volume of 1 mL and transferred into conical 15 mL polypropylene centrifuge tubes (PAA). For shockwave treatment, tubes were placed in front of the applicator inside the water container. Then unfocused shockwaves were applied using the following parameters: 200 pulses at an energy level of 0.09 mJ/mm^2 with a frequency of 3 Hz. These parameters have been chosen according to preliminary experiments, in order to maximise the effect of the ESWT, while concurrently minimizing possible negative effects. Both, treated and untreated cells were immediately plated after treatment. Scheme for experimental setup (timeline) is shown in Figure 5. All cell culture experiments were performed as quadruplicates from four different donors.

In vitro differentiation of hASC and rASC into adipogenic lineage

hASCs and rASCs were differentiated into adipogenic lineage using adipogenic differentiation medium composed of Dulbecco's modified Eagle's medium (high glucose; PAA) containing 10% FCS (v/v), 200 μM L-glutamine and 1% (v/v) penicillin-streptomycin and supplemented with dexamethasone (1 μM; Sigma Aldrich, St. Louis, MO, USA), IBMX (0.5 mM; Sigma Aldrich), hydrocortisone (0.5 μM; Sigma Aldrich) and indomethacin (60 μM; Sigma Aldrich). Cells were plated at an initial cell seeding density of $7x10^3$ cells/cm^2. Control cells were seeded at a density of $1x10^3$ cells/cm^2 and maintained in stem cell medium. Medium was changed every second day for a total culture period of 21 days.

Evaluation of adipogenic phenotype

Adipogenic potential was evaluated by staining intracellular lipid accumulations with common Oil Red O staining. Briefly, cells were washed with PBS and fixed with 10% neutral formalin solution (Sigma Aldrich) for 30 minutes. After rinsing with distilled water and 70% ethanol, cells were stained with Oil Red O in isopropanol (Sigma Aldrich) for 15 minutes. Cells were then washed with water, counterstained with Mayer's hematoxilin solution (Sigma Aldrich) and blued with tap water. Stained samples were examined using a Leica DMI6000B microscope (Leica, Solms, Germany).

In vitro differentiation of hASC and rASC into osteogenic lineage

hASCs and rASCs were differentiated into osteogenic lineage using osteogenic differentiation medium composed of Dulbecco's modified Eagle's medium (low glucose; PAA) containing 10% FCS (v/v), 200 μM L-glutamine and 1% (v/v) penicillin-streptomycin (PAA)

supplemented with dexamethasone (0.01 μM, Sigma Aldrich), ascorbat-2-phosphate (150 μM; Sigma Aldrich) and β-glycerophosphate (10 mM; Stemcell Technologies, Vancouver, Canada). Cells were plated with an inititial cell seeding density of 1×10^3 cells/cm^2. Control cells were seeded at a density of 1×10^3 cells/cm^2 and maintained with stem cell medium. Medium was changed every second day for 21 days.

Evaluation of osteogenic phenotype

Calcification was assessed by common von Kossa staining. Cells were rinsed with PBS twice, fixed with 10% formalin solution for 30 minutes, rinsed with distilled water and incubated with 5% (w/v) silver nitrate (Sigma Aldrich) for 25 minutes, developed with 5% sodium carbonate (w/v) (Sigma Aldrich) and finally fixed with sodium thiosulfate (Sigma Aldrich). Stained samples were examined using a Leica DMI6000B microscope (Leica).

PCR- Evaluation of osteogenic markers

Osteogenic gene expression (Osteocalcin, Biglycan) was evaluated with semiquantitative PCR. Total RNA was isolated from control and differentiated cells using GenElute^{TM} Mammalian Total RNA kit (Sigma Aldrich) according to manufacturer's instructions. Amplification of cDNA was done with DyNAmo cDNA Synthesis Kit (Biozym, Hessisch Oldendorf, Germany).

PCR amplification was performed with 1 μg cDNA in 29 μl DEPC treated water (Sigma Aldrich), 10 μl Enhancer 5x, 5 μl Reaction Buffer Y 10x, 1 μl MgCl$_2$ 25 mM, 2 μl dNTPs 10 mM, 0.2 μl Taq Polymerase (all PeqLab, Erlangen, Germany) and 0.5 μl forward and reverse primer at a final concentration of 100 mM. Temperature scheme and primer design are depicted in table 1. PCR products were evaluated on a 1.5% (w/v) agarose gel containing 1 μl/10 mL GelGreen (10000X; Biotium, Hayward, CA, USA), visualized in a MultiImageTM Light Cabinet (Biozym) using AlphaEaseFC software (Version 3.2.1; Alpha Innotech, San Leandro, CA, USA) for densitometrical analysis.

		Sequence	fragment size	PCR scheme
GAPDH	fwd:	5'-ATGGGGAAGGTGAAGGTCGG-3'		94°C – 53°C – 72°C
	rev:	5'-AGGGATGATGTTCTGGAGAG-3'		
biglycan	fwd:	5'-CGGACACACCGGACAGATAGAC-3'	103 bp	94°C - 60°C – 72°C
	rev:	5'-ACATGGCGGATGGACCTGGAG-3'		
osteocalcin	fwd:	5'-TTGGCTGACCACATCGGCTTTC-3'	142 bp	94°C - 60°C – 72°C
	rev:	5'-AGGGCAAGGGCAAGGGGAAG-3'		

Table 1: Primer sequences, fragment size and PCR scheme for RT PCR

In vitro differentiation of hASC and rASC into Schwann-like Cells

hASCs and rASCs were plated at 0.5×10^3 cells/cm^2 and grown for 36 hours in Dulbecco's modified Eagles medium (high glucose; PAA) supplemented with 10% FCS (v/v), 200 μM L-glutamine and 1% (v/v) penicillin-streptomycin (PAA). All media used during the differentiation process differed only in supplements. Differentiation into Schwann-like Cells was performed in a three step procedure modified from Dezawa *et al.* 2001 (54). Briefly, cells were prepared for differentiation into neural lineage by a 24 hour incubation with 1 mM β-mercaptoethanol (Sigma Aldrich), followed by washing with PBS and a 60 hour incubation with 50 ng/mL *all-trans* retinoic acid (Sigma Aldrich). After washing with PBS, cell culture medium was changed to final differentiation medium containing 5 ng/mL recombinant human platelet-derived growth factor (PDGF-AA, R&D systems; Minneapolis, MN, USA), 10 ng/mL recombinant human basic fibroblast growth factor (bFGF, R&D systems), 200 ng/mL human recombinant heregulin-β1 (Peprotech, Hamburg, Germany) and 15 μM forskolin (Sigma Aldrich). Medium was completely changed on day three and day six, and 60% changed every third day for the next 12 days. Differentiation into SCL was evaluated by measuring specific cell surface marker using flow cytometry. S100b was used to determine differentiation into Schwann cell phenotype, while P75 and P0 distinguish between different activation states. P75 indicates a proliferative/regenerative phenotype, while P0 is typically expressed during myelination.

Proliferation

Proliferation of hASC and rASC after shockwave treatment was determined using a 5-bromo-2-deoxyuridine (BrdU) uptake assay (Cell Proliferation ELISA assay Kit; Roche Diagnostics, Basel, Switzerland) according to manufacturer's instructions. Briefly, 48 hours after cell seeding, medium was changed to stem cell medium containing 100 μM BrdU and cells were incubated for 12 hours at standard cell culture conditions (37°C and 5% CO_2). The culture plates were airdried and fixated with FixDenat® solution and subsequently incubated with anti-BrdU POD antibody solution for 60 minutes at room temperature. After washing the plates with PBS, tetramethyl benzidine was added for 30 minutes as a substrate. The reaction was stopped with 1 M H_2SO_4 and absorption was measured at 450 nm with 690 nm as reference wavelength on an automatic microplate reader (Tecan Sunrise; Tecan, Maennedorf, Switzerland).

Cell viability

Cell viability of hASC and rASC after shockwave treatment was determined using common

MTT assay. Briefly, cells were incubated with stem cell medium containing 650 μg/ml MTT [3-(4,5- dimethylthiazol-2-yl)-2,5-diphenyltetrazolium] bromide (Sigma Aldrich) for 1 hour at standard cell culture conditions (37°C and 5%). Medium was discarded and MTT formazan precipitate was dissolved in DMSO (Sigma Aldrich) by shaking in dark for 20 minutes. Aliquots of 100 μl were transferred to 96-well plates. Light absorbance at 540 nm was measured immediately and optical density (OD) values were corrected for an unspecific background on an automatic microplate reader (Tecan Sunrise; Tecan).

Statistics

Statistical difference was analysed using one-way ANOVA (analysis of variance) followed by Tukey range test for significant differences between the means. Significance was considered for $P<0.05$. For statistical calculations GraphPad Prism 5 for Mac OS X, Version 5.0b (GraphPad Software, Inc., La Jolla, CA, USA) was used. All data in this study are shown as mean ± standard deviation (SD).

RESULTS

ESWT influences mesenchymal marker expression in hASCs

To gain insight into the effect of ESWT on the expression of mesenchymal marker expression, flow cytometry using MSC specific surface markers was performed, which is shown in Figure 6. At P4 (day 0) untreated hASCs did not express endothelial marker CD14 and hematopoietic markers CD34 and CD45. The levels of these markers did not change throughout the whole culture period (until passage 8; data not shown). At day 0 (passage 4) expression levels of mesenchymal markers CD73 and CD105 were lower than 50% while expression of CD90 was around 90%. Five days after the first shockwave treatment (day 5), untreated control cells showed a significantly reduced marker expression (CD73 <15%, CD90 <40%, CD105 <5%) compared to the shockwave treated group (CD73 >60%, CD90 >80%, CD105 >30%). Ten days after shockwave treatment (day 10), no significant difference in marker expression could be observed between untreated control group (Control) and cells receiving single shockwave treatment (1x ESWT) (CD73 <40%, CD90 <55%, CD105 <15%) while cells receiving a second shockwave treatment at day 5 (2x ESWT) showed a significantly higher expression of all three mesenchymal markers (CD73 >85%, CD90 >85%, CD105 >40%). On day 15, levels of mesenchymal markers further decreased in the control group and the single shockwave treatment group (CD73 <20%, CD90 <30%, CD105 <10%). Cells receiving repetitive treatment (2x ESWT, 3x ESWT) showed a significantly higher marker expression (CD73 >80%, CD90 >75%, CD105 >35%) compared to cells in the control

group (CD73 <10%, CD90 <20%, CD105 <5%) and cells receiving single shockwave treatment (CD73 <20%, CD90 <30%, CD105 <10%). On day 36 (P8), 21 days after the last treatment and cell seeding, expression of all three mesenchymal markers was almost absent in the control group (CD73 <5%, CD90 <5%, CD105 <5%). In contrast to all other treatment groups, single ESWT increased only CD90 levels significantly (CD90 >45%, CD73, CD105 <10%). hASCs receiving repetitive treatment showed an increased marker expression concerning all three mesenchymal markers. Significant increases on day 36 (P8) compared to control group (CD73 <5%, CD90 <5%, CD105 <5%) could be observed for CD73 in the following groups 2x ESWT (>25%), 3x ESWT (>50%) and 4x ESWT (>90%), for CD90 1x EWST (>45%), 2x ESWT, 3x ESWT and 4x ESWT (all >90%) and CD105 3x ESWT (>40%) and 4x ESWT (>70%) (Figure 6).
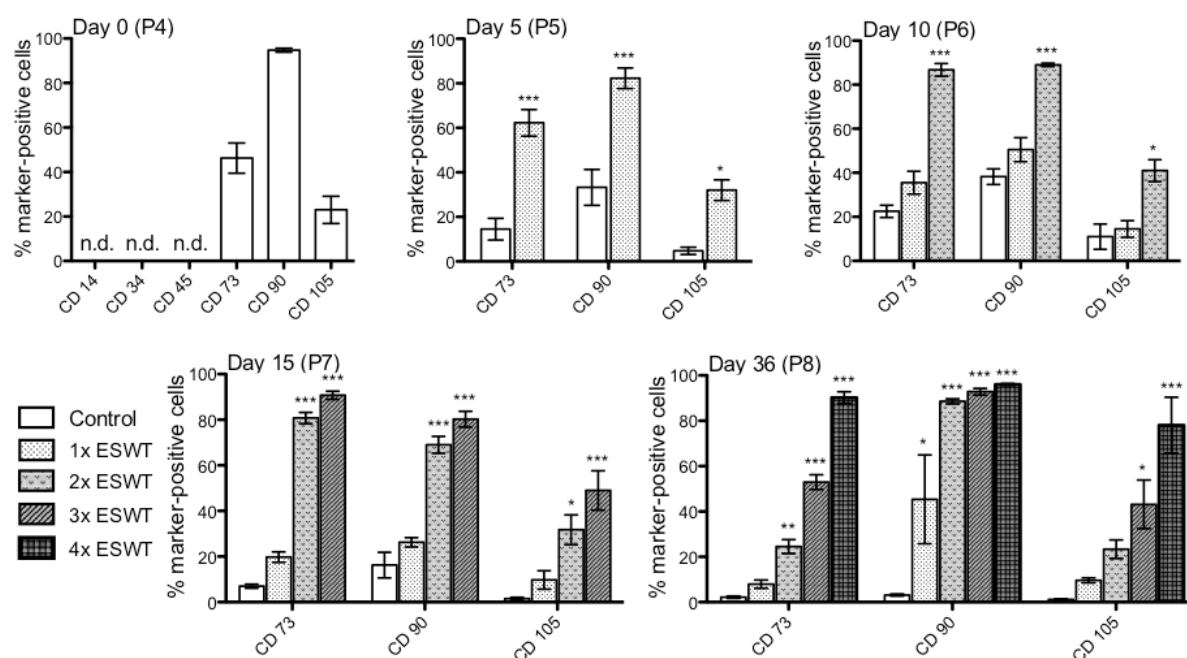
Figure 6: Flow cytometry results of hASCs on day 0 (P4) and hASC treated with ESWT compared to untreated control on day 5 (P5), 10 (P6), 15 (P7) for hematopoietic markers (CD14, CD34, CD45) and mesenchymal markers (CD73, CD90 CD105) and on day 36 (P8) for mesenchymal markers, (CD73, CD90 CD105); statistical significance was tested with 1- way ANOVA and Tukey range test; data is presented as Mean ± SD; *P<0.05, **P<0.01, ***P<0.0001; n =4;

ESWT influences mesenchymal marker expression in rASCs

Additionally, the same experiment as mentioned above using hASCs was performed in rASCs to prove that the effect of ESWT is host-independent. Flow cytometry characterization of rASCs in P4 revealed expression of mesenchymal markers CD73, CD90, CD105 > 55%, but also a considerable percentage of hematopoietic marker-positive cells (CD34> 20%, CD45> 25%) (Figure 7). While expression of CD34 declined with P5, CD45 remained at a level of

20% until P7 in the untreated control group. On day 5 after single shockwave treatment (1x ESWT), cells receiving shockwave treatment showed no expression of hematopoietic markers (CD14 <2%, CD24 <2%, CD45 <2%) and a significant increase in expression of mesenchymal markers (CD73 >65%, CD90 >65%, CD105 >65%) compared to control group (CD14 <2%, CD34 <5%, CD45 >10%, CD73 <20%, CD90 <20%, CD105 <20%). On day 10, cells receiving repetitive shockwave treatment (2x ESWT) showed increased percentages of mesenchymal marker expression (CD73, CD90, CD105> 85%), while cells receiving single shockwave treatment had only CD105 significantly upregulated (CD73 < 40%, CD90 < 35%, CD105 >50%) compared to control group (CD45 >15%, CD73 <20%, CD90 <20%, CD105 <15%). On day 15, levels of mesenchymal markers further decreased in the control group (CD45 <5%, CD73 <5%, CD105 <10%) as well as in the group 1x ESWT (CD73 <15%, CD90 <15%, CD105 <15%). In rASCs treated twice with shockwaves, mesenchymal marker expression decreased as well (CD73 <40%, CD90 <50%, CD105 <40%), but not to the same extent as in the control group or 1x ESWT.
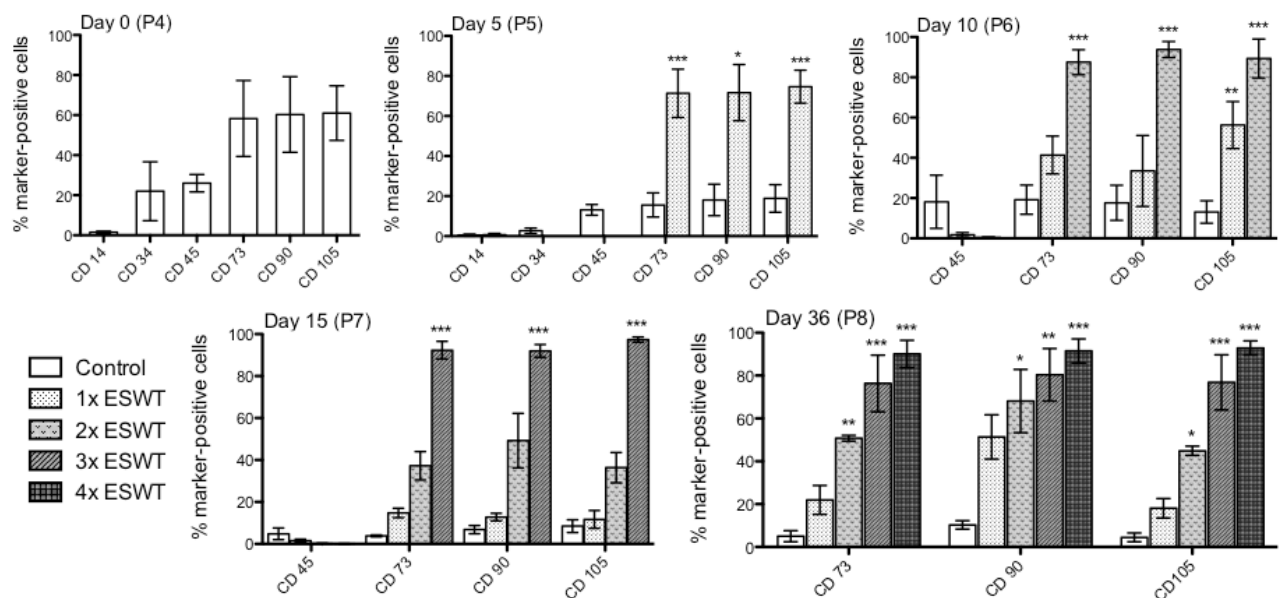

Figure 7: Flow cytometry results of rASCs on day 0 (P4) and day 5 (P5) and rASC treated with ESWT compared to untreated control on day 5 (P5), 10 (P6), 15 (P7) for hematopoietic markers (CD14, CD34, CD45) and mesenchymal markers (CD73, CD90 CD105) and on day 36 (P8) for mesenchymal markers, (CD73, CD90 CD105); statistical significance was tested with 1- way ANOVA and Tukey range test; data is presented as Mean ± SD; *P<0.05, **P<0.01, ***P<0.0001; n =4

In rASCs receiving three shockwave treatments all three mesenchymal markers were significantly increased (> 90%). 21 days after final shockwave treatment (day 36, P8) marker expression levels of control group were <10%, while - depending on number of treatments - all samples of shockwave groups showed elevated marker expression levels. A significant increase was observed for 2x ESWT (CD73 >50%, CD90 >60%, CD105 >40%), 3x ESWT

(CD73 >75%, CD 90 >75%, CD105 > 75%) and 4x ESWT (CD73 >90%, CD90>90%, CD105 >90%) (Figure 7).

ESWT influence on cell proliferation and viability

We wanted to know if ESWT has any effect, whether beneficial or inhibiting, on proliferation and viability of those cells. Therefore a BrdU ELISA - to measure proliferation - and a MTT assay for viability was performed.

BrdU assay revealed a significant decrease in new synthesis of DNA in hASCs groups 2-4x ESWT (Figure 8) compared to untreated control, while in rASCs no significant differences in proliferation could be detected. MTT showed a tendential decrease in mitochondrial activity in hASCs after shockwave treatment and an increase in rASCs. However, in both hASCs and rASCs these findings did not significantly differ from the untreated control group.
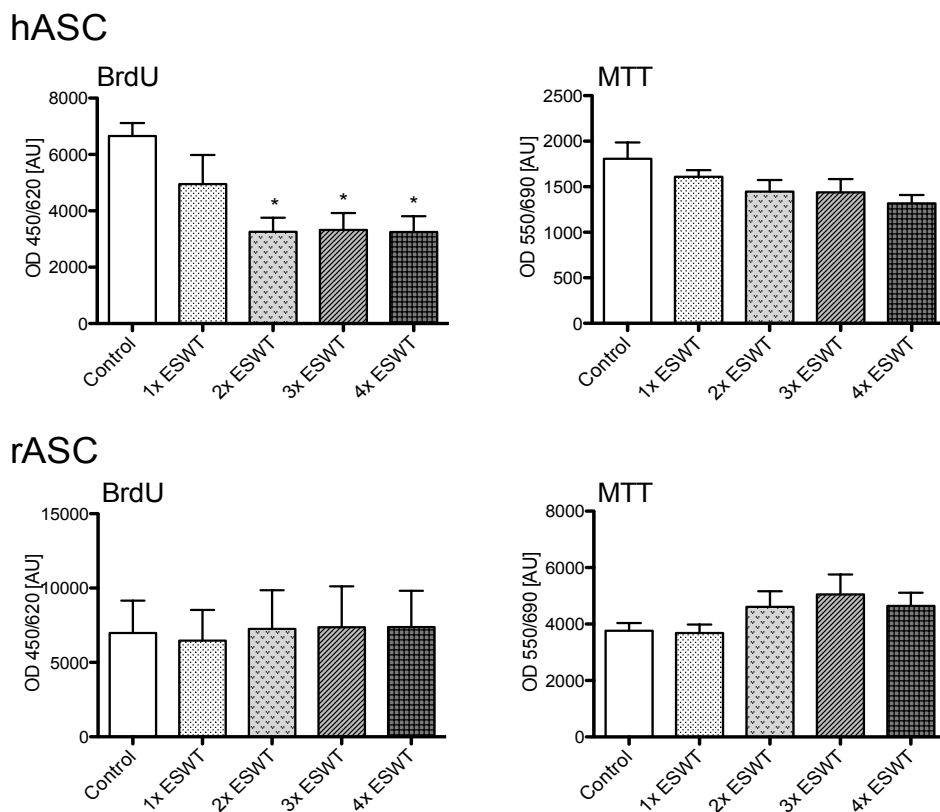
Figure 8: BrdU and MTT assay for hASCs and rASCs after 1-4x ESWT compared to untreated control group. Data is presented as Mean + SD; significance tested with 1-way ANOVA and Tukey range test; *P<0.05; n =4;

ESWT influences differentiation potential of ASCs

The potential influence of ESWT on the mesenchymal differentiation potential of hASCs and rASCs was determined by differentiation into adipogenic and osteogenic lineage, as well as by transdifferentiation into Schwann-like cells (SCLs).
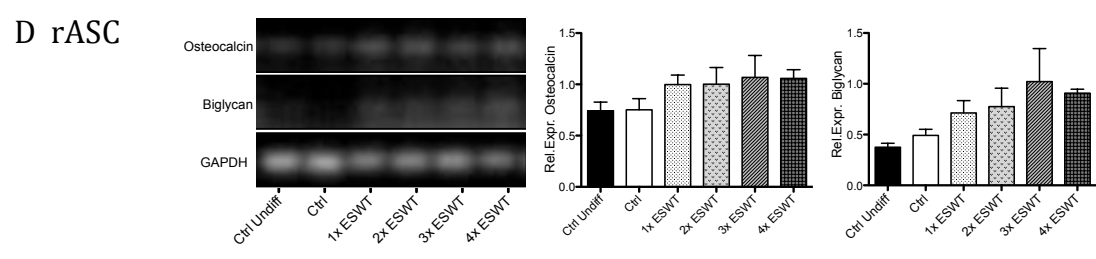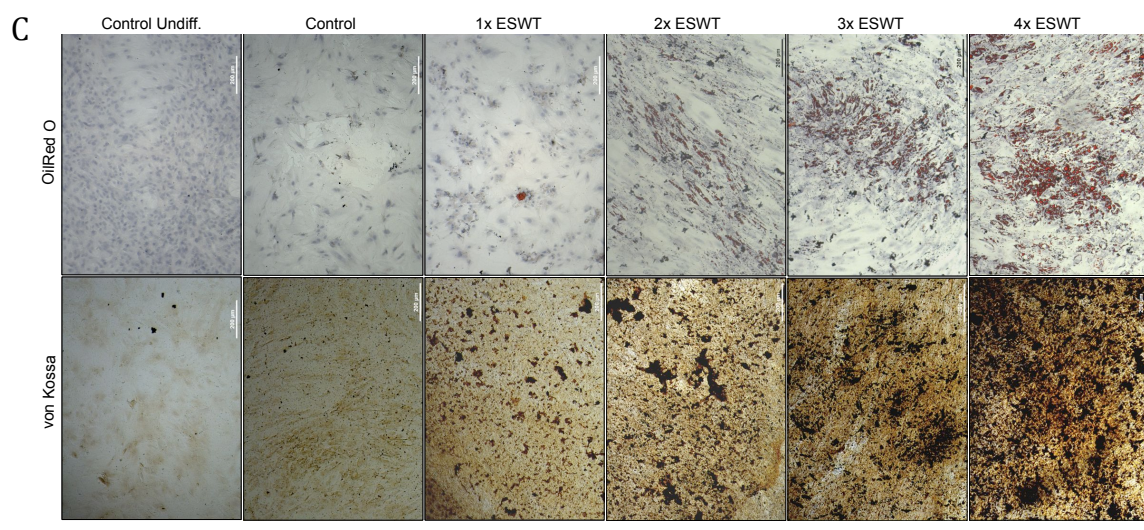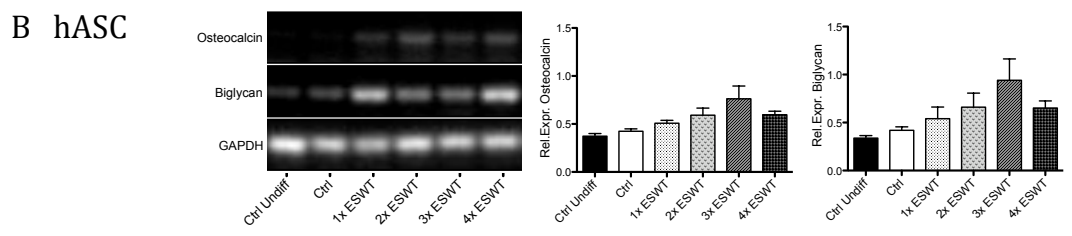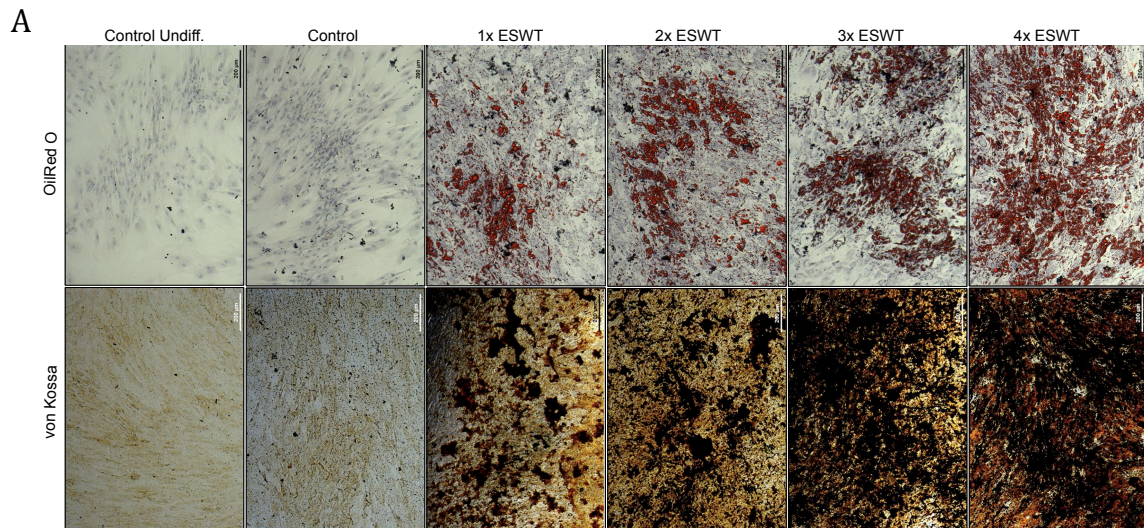
Figure 9: Differentiaton specific stainings of hASCs (A) and rASCs (C) to exhibit either adipogenic differentiation by staining lipid accumulations (Oil Red O) or osteogenic differentiation by staining calcium phosphate (von Kossa) after 20 days in differentiation medium and 1-4x ESWT compared to untreated, undifferentiated control (Control undiff.) and untreated, differentiated control (Control). Scale bar represents 200 µm; B, D: PCR and densitometric analysis of osteogenic markers osteocalcin and biglycan of hASCs (B) and rASCs (D) after 20 days in differentiation medium; data is presented as Mean + SD, normalized on housekeeping gene GAPDH; significance tested with 1-way ANOVA and Tukey range test; *P<0.05 to untreated, undifferentiated control (Control undiff); n=4;

Adipogenic differentiation

After 20 days in adipogenic differentiation medium no lipid accumulations could be observed in untreated control cells of both, hASCs and rASCs. While a single ESWT in hASCs resulted a prominent amount of intracellular lipids (Figure 9 A; 1x ESWT), this effect was not seen in rASCs before two (2x ESWT) shockwave treatments (Figure 9 C). In both hASCs and rASCs an increase of Oil Red O positive cells in the ASC cultures could be observed with number of shockwave treatments (Figure 9 A, C).

Osteogenic differentiation

Intensity of osteogenic differentiation was assessed 21 days after change to osteogenic differentiation medium by staining mineralized nodules (von Kossa staining). Positive staining could be observed in hASC and rASC cultures after single shockwave treatment and the amount of stained mineralized calcium phosphate increased with number of shockwave treatments (Figure 9 A, C).

In addition to the von Kossa staining, semi-quantitative PCR was performed to get an insight in the expression profile of the osteogenic markers osteocalcin and biglycan. In hASCs and rASCs only minor differences between the undifferented, untreated control (Ctrl undiff) and the differentiated, untreated control (Ctrl) could be observed in both expression profiles, osteocalcin and biglycan. The relative expression increased in both tested markers with the number of shockwave treatments resulting in a peak at three treatments (Figure 9 B, D).

Transdifferentiation into Schwann-like cells

Additionally, potential to differentiate into Schwann-like cells was evaluated with flow cytometry analysis and for Schwann cell specific markers S100b, P75 and P0. Figure 10 shows that both, hASCs and rASCs significantly increase S100b and P75 expression after single shockwave treatment compared to undifferentiated control and untreated, differentiated control. In hASCs >95% of the cells were found positive for both markers in the group 4x ESWT, while in rASCs single shockwave treatment led to an increase of P75 to >80% and S100b > 85%. rASCs treated with 4x ESWT showed expression levels of P75 and S100b > 98%. Expression levels of P0 were below 10% in all groups. Schwann cell morphology, characterized by a prominent nucleus and an elongated, bipolar cell body, could not be found in control groups, but was prominent in ESWT treatment groups (Figure 10).
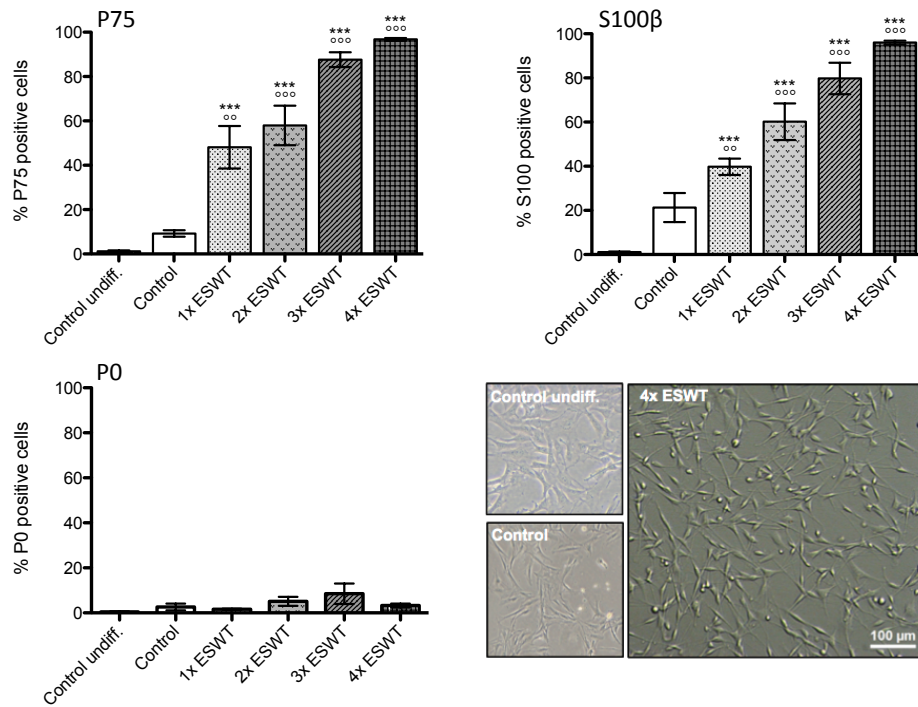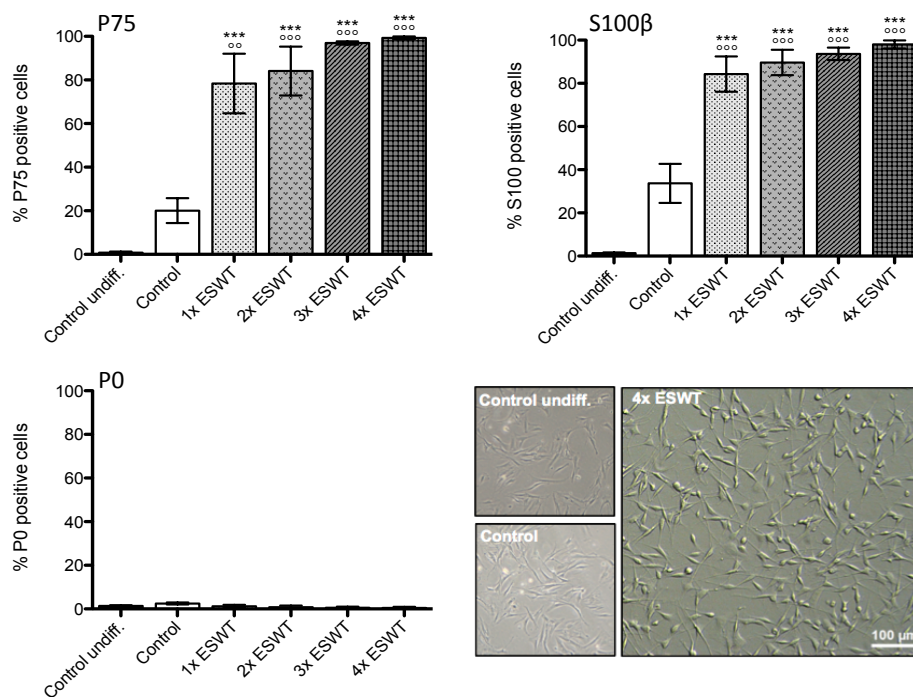
Figure 10: ASCs differentiated towards SCLs express Schwann cell specific markers dependent on number of ESWT; Flow Cytometry results (P75, S100b, P0) for hASCs (A) and rASCs (B) differentiated into Schwann-like cells on day 36 (P8), treated with ESWT compared to untreated control and undifferentiated control; statistical significance was tested with 1-way ANOVA and Tukey range test; data is presented as Mean ± SD; *P<0.05, **P<0.01, ***P<0.0001 to untreated, undifferentiated control (Control undiff); °P<0.05, °°P<0.01, °°°P<0.0001 to untreated, differentiated control (control); n = 4; Light microscopy pictures of undifferentiated (control undiff), differentiated, untreated (control) and differentiated hASCs (A) and rASCs (B) after shockwave treatment (4x ESWT);

DISCUSSION

ASCs could be a useful tool for tissue engineering approaches due to their easy accessibility and versatility. Several studies have shown that these cells are capable of differentiating into numerous cell types and differentiation is not restricted to their initial tissue type (54,82,83). One of the major downsides of ASCs represents their high variability and loss of differentiation capacity at higher passage numbers after expansion *in vitro* (60,84,85). To address these limitations retention of marker expression and differentiation potential has been of interest in previous studies. For instance, Tsutsumi, *et al.* (86) described a positive effect of fibroblast growth factor 2, which has an effect in maintaining multilineage differentiation potential *in vitro,* while Lai, *et al.* (87) describe the opposite. Shahdadfar, *et al.* (88) observed that the choice of serum, (autologous serum or fetal bovine serum), is a crucial factor in proliferation and gene expression, concluding that autologous serum leads to a rapid expansion with stable gene expression, but fetal bovine serum induces more differentiated but less stable transcriptional profiles. Stolzing *et al.* (89) showed that lower glucose concentrations in culture medium have an inhibiting effect on replicative senescene.

Physical stimuli have shown to have beneficial effects on isolation of hASCs (radio electric asymmetric conveyed fields (65)) and differentiation into osteoblasts (controlled frequency ultrasound; (66)) , or chondrocytes (combination of shear and dynamic compression; (90)). The advantageous effects of *in vivo* extracorporeal shockwave therapy in several fields of regenerative medicine are known for more than one decade, whereas *in vitro* effects have not been studied extensively yet. To our best knowledge, so far no study has investigated the effects of extracorporeal shockwave treatment on human or rat mesenchymal stem cells evaluating mesenchymal marker expression and multi-lineage differentiation potential after treatment. However, Raabe, *et al.* (67) showed that equine mesenchymal stem cells maintain their multilineage differentiation capacity in low passages (P1-4) after treatment with focused shockwaves.

In our study, human and rat ASC cultures were randomly chosen and did not meet the standards and defined minimal requirements for mesenchymal stem cells concerning marker expression (Figure 6, Figure 7) and purity (Figure 7; CD34, CD45 > 20%) (52,64) before treatment with ESWT. Treated with ESWT, cells not only maintained but also increased their expression of mesenchymal markers (Figure 6, Figure 7), to a level >95% (except hASC CD105: 80%), which meets the defined minimal requirements for mesenchymal stem cells (52), while the amount of marker-positive cells further decreased in the control group. After approximately 55 days of continuous culture (P8), expression of CD73, CD90 and CD105

was diminished to <5% (except CD90 in rASC: 10%), in untreated cells of both, hASCs and rASCs.

Considering expression of these stem cell defining markers, rASCs reacted stronger to single shockwave treatment than hASCs. These findings are strengthened by the results of SCL differentiation, where difference between 1x ESWT and 4x ESWT is less than 20% in S100b and P75. In hASCs, S100b expression increased stepwise (20% per treatment) from undifferentiated control to 4x ESWT. S100b is known as a common Schwann cell marker while the expression of P75 and P0 are restricted to one of the two activation states of Schwann cells: proliferating/regenerative (P75) and myelinating (P0) (26,91,92). Elevated levels of S100b and P75 indicate a differentiation into proliferating/regenerative Schwann cell phenotype, reaching a peak in marker expression at almost 95% positive cells by repeated ESWT.

To evaluate effects of the ESWT treatments on cell proliferation the amount of newly synthesized DNA in hASCs was determined by BrdU ELISA and was found to be significantly lower in groups 2-4x ESWT compared to 1x ESWT and control group. However, it has been previously described that a decrease of proliferation can have an advantageous effect on differentiation (93,94), which is in accordance with our findings (Figure 9 A) for osteogenic and adipogenic differentiation. In contrast to the results for hASCs, rASCs synthesis of new DNA was not significantly affected and results of osteogenic and adipogenic differentiation (Figure 9 C) showed a less clear (but still evident) difference between untreated control and treatment groups. In contrast to our findings, Raabe, *et al.* (67) observed a significant increase in proliferation in early passages. This could indicate that the hASCs and rASCs used in our study are pushed towards the end of their *in vitro* life span resulting in a decreased proliferation, but not in a diminished multilineage differentiation potential.

It has been stated that, over passages, mesenchymal stem cells may either lose their potential to differentiate into adipogenic lineage, while maintaining potential for osteogenic differentiation (60,63,95,96) or vice versa (61,97). In this study, we could show that ESWT allowed the cells to maintain their differentiation capacity for both, adipogenic and osteogenic differentiation, and additionally the capacity for differentiation into Schwann-like cells.

In rASCs a high amount of cells expressing hematopoietic marker CD34 and CD45 could be observed, indicating a highly heterogeneous ASC culture. Five days after first shockwave treatment (P5), no CD34 or CD45 positive cells were present in the shockwave group, but still in untreated control (until P7). These findings indicate that already a single shockwave treatment leads to higher purity of heterogeneous ASC cultures. It has been described that the

presence of cells expressing hematopoietic markers decreases over subsequent expansion (98). However, our findings suggest that hematopoietic cells not only undergo a subsequent overgrowth by ASCs, but also potentially react more sensitive to ESWT.

Extracorporeal shockwave treatment, independent of number of treatments, had a favourable and no adverse effects in all treatment groups compared to control group. Overall, concerning evaluated parameters in this study, treatment groups in all experiments were superior to control group. However, the presented study is purely descriptive and does not deal with the specific cellular response of MSCs to ESWT. Attempts to describe the cellular response in literature include eliciting mechanotransduction (99,100) or transient membrane permeability (101), but further studies have to be performed to clarify how these known effects influence MSC behaviour in terms of stemness and differentiation capacity.

CONCLUSION

The observed effect of ESWT on ASCs was twofold: not only did repetitive shockwave treatment improve expression of mesenchymal markers, but also multipotency in high passages was preserved after extensive expansion, resulting in a higher capacity to differentiate into adipogenic and osteogenic lineage as well as Schwann-like cells, with only minor changes in cell proliferation and viability.

However, planned follow up studies *in vivo* have to verify whether these findings are an *in vitro* effect or represent part of the observed positive effects of the extracorporeal shockwave therapy *in vivo.*

Extracorporeal Shockwave Treatment: a Novel Tool to Improve Schwann Cell Isolation and Culture

Christina M. A. P. Schuh[1,2]*; David Hercher[1,2]; Michaela Stainer[1,2],
Rudolf Hopf[1,2], Andreas H. Teuschl[2,3], Robert Schmidhammer[1,2], Heinz Redl[1,2]

[1] Ludwig Boltzmann Institute for Experimental and Clinical Traumatology / AUVA Research Center, Vienna, Austria
[2] Austrian Cluster for Tissue Regeneration, Vienna, Austria
[3] University of Applied Sciences Technikum Wien – Department of Biochemical Engineering, Vienna, Austria

ABSTRACT

As new approaches for peripheral nerve regeneration are sought, there is an increasing demand for native Schwann cells for *in vitro* testing and/or reimplantation. Extracorporeal shockwave treatment (ESWT) is an emergent technology in the field of regenerative medicine, which recently has also been shown to improve peripheral nerve regeneration. In this study we elucidate the effects of ESWT on Schwann cell isolation and culture. Rat sciatic nerves were dissected, treated with ESWT and Schwann cells were isolated and cultured for 15 passages. Single treatment of the whole nerve *ex vivo* led to significantly increased extracellular ATP as an immediate consequence, and subsequently a number of effects on the culture were observed, starting with a significantly increased Schwann cell yield after isolation. In the ESWT the group quality of culture, reflected in consistently higher purity (S100b, morphology), proliferation rate (BrdU, population doublings per passage) and expression of regenerative phenotype-associated markers (P75, GFAP, c-Jun), was significantly improved. In contrast, the control group exhibited progressively senescent behaviour, reflected in a decrease of proliferation, loss of specific markers and increase in P16^{INK4A} expression. Concluding, extracorporeal shockwave treatment has beneficial effects on Schwann cell isolation and culture.

INTRODUCTION

Peripheral nerve lesions occur with an incidence of approximately 300.000 cases annually in Europe, representing a frequent cause of hospitalization and displaying a major burden to patients and social health-care (102).

Although the peripheral nerve system has a remarkable regenerative potential, regeneration over nerve gaps or over long distances, for example after very proximal lesions, faces several difficulties. In this regard, nerve autografts are the gold standard to treat peripheral nerve injuries with tissue loss, but often do not result in a satisfactory outcome (3). Especially long distance gaps or severe injuries affecting several nerves push autografting to its limits regarding the availability of donor material. Alternatives to facilitate nerve regeneration, such as artificial nerve guidance tubes or other types of scaffolds, application of neurotrophic substances, etc are sought. Some of these approaches are currently used in clinical nerve repair, though there is an ongoing debate as concerns their appropriate use, effectiveness and side-effects (103,104). One of the major reasons for the unsatisfactory outcome after repair of long distance gaps is the limited proliferative capacity of Schwann cells (105). Schwann cells play a key role in peripheral nerve regeneration: they participate in the removal of myelin and axonal remnants, start proliferating and align to build the so called bands of Büngner (106). After the axon has elongated along these bands of Büngner, the Schwann cells start to remyelinate the newly formed axon to complete the regenerative process.

A novel strategy to improve the functional outcome of peripheral nerve regeneration is the therapy of injured nerves with extracorporeal shockwave treatment (ESWT). Historically, ESWT has its origin in the field of urology with destroying kidney stones (68), but it has also been proven to be an effective therapeutic tool in the field of regenerative medicine. In clinics and pre-clinics, beneficial effects have been reported in treatment of various medical indications such as non-union fractures (69–71), ischemia-induced tissue necrosis (72), or chronic wounds (73,74). The shockwave generated is a sonic pulse and is characterized by an initial rise, reaching a positive peak of up to 100 MPa within 10 ns, followed by a negative amplitude of up to - 10 MPa and a total life cycle of less than 10 µs. Biological responses are thought to be triggered by the high initial pressure, followed by a tensile force and the resulting mechanical stimulation (78).

Recently, Hausner *et al.* (37) showed a novel approach of accelerating regeneration after peripheral nerve injury, bridged with an autologous nerve graft. After dissecting and bridging the sciatic nerve of a Sprague Dawley rat, extracorporeal shockwaves were applied at the site

of injury. Six weeks after surgery animals of the ESWT group exhibited a significantly improved functional recovery relative to the controls. Based on this study we investigated *in vitro* Schwann cell behavior after ESWT treatment with focus on their regenerative capacity.

MATERIAL AND METHODS

Shockwave treatment of nerve tissue and Schwann cell isolation

All animals were euthanized according to established protocols, which were approved by the City Government of Vienna, Austria in accordance with the Austrian Law and Guide for the Care and Use of Laboratory Animals as defined by the National Institute of Health. Animals and treatment/control groups were randomly chosen and analysed without pre- or post selection of the respective nerves or cultures.

For *ex vivo* shockwave treatment an unfocused electro-hydraulic device was used (Dermagold 100, MTS Medical, Germany). The applicator was attached to a water bath as described in other studies (38,81,107) ensuring direct contact to the prewarmed (37°C) water, allowing reproducible physical propagation and application of shockwaves *in vitro*. Sciatic nerves of adult male Sprague Dawley rats were dissected and each nerve was transferred into a 15 mL conical centrifuge tube (PAA, Austria) containing phosphate buffered saline (PBS; PAA, Austria) pre-chilled on ice. Nerves were kept on ice until further use but not longer than one hour. For ESWT application, tubes were placed 5 cm in front of the applicator inside the water container. Subsequently, unfocused shockwaves were applied using the parameters chosen according to previous experiments (37) in order to maximize the effect of the ESWT treatment, while minimizing possible negative effects: 300 pulses at an energy level of 0.10 mJ/mm^2 with a frequency of 3 Hz. The corresponding second nerve from the same animal served as control and was placed in a water bath (37°C) for the time of treatment to avoid the creation of artefacts due to different sample treatments.

After ESWT treatment, Schwann cells were isolated from the treated and non-treated sciatic nerve tissues according to a method adapted from (108). Briefly, the epineurium was removed and nerves were weighed on a fine scale to assess nerve wet weight (Sartorius, Austria). Subsequently nerves were strained and minced. Nerve fragments were incubated with 0.05% collagenase (Sigma-Aldrich, UK) for 1 hour at 37°C subsequently filtered through a 40 μm cell strainer and centrifuged at 400 x g for 6 minutes. After washing the cell pellet with Dulbecco's Modified Eagle Medium (DMEM; PAA, Austria) containing 10% fetal calf serum

(FCS; PAA, Austria), the pellet was resuspended in DMEM-D-valine (PAA, Austria), supplemented with 10% FCS, 2 mM L-Glutamine (PAA, Austria), 1% antibiotics (PAA, Austria), N_2 supplement (Invitrogen, Germany), 10 µg/mL bovine pituitary extract (Sigma-Aldrich), 5 µM forskolin (Sigma-Aldrich). This medium is further referred to as "Schwann cell medium". Cell suspension was seeded on 6-well plates (PAA, Austria) coated with poly-L-lysin (Sigma-Aldrich) and laminin (Sigma-Aldrich).

Cell culture and experimental set up

Cells were subcultured for the first time after 19 days, to establish a proliferative phenotype and keep them in a proliferative state. Schwann cell medium was added on day 5 after isolation (1 mL), and was partially (50%) changed on day 9, 13 and 17. Subsequent splitting of cells was performed for 15 passages as follows: cells were detached with a cell scraper, centrifuged at 1200 rpm for 5 minutes and seeded at a density of $4x10^4$ cells/cm^2 on plates previously coated with poly-L-lysin. Residual cells were used for flow cytometric analysis, BrdU assay and protein isolation. Medium was partially (50%) changed every third day and cells were split every sixth day. Scheme of analysis performed is shown in Figure 11.

	Isolation	P0	P1	P2	P3	P4	P5	P6	P7	P8	P9	P10	P11	P12	P13	P14	P15	n=
ATP release	x																	5
LDH release	x																	5
Cell yield		x																12
Flow cytometry			x	x	x	x	x	x	x	x	x	x	x	x	x	x	x	10
BrdU assay			x			x			x			x			x		x	8
Western Blot				x						x							x	6
Activation switch						x					x						x	6

Figure 11: Diagram illustrating the schematic setup of the experiments and assays performed; Abbreviation P0-P15: passage 0 to passage 15;

Evaluation of cell yield

To evaluate cell yield, representative phase contrast pictures were taken from each culture using a Leica DMI6000B microscope (Leica, Solms, Germany), and cells were counted using a Bio-Rad TC20^{TM} automated cell counter (Bio-Rad Laboratories Inc., US). Non-viable cells were identified and excluded by trypan blue staining. Cell count was normalized to 10 mg nerve wet weight assessed before isolation.

Proliferation assay

Proliferation assay using a 5- bromo-2-deoxyuridine uptake (BrdU; Cell Proliferation ELISA assay Kit; Roche Diagnostics, Switzerland) for quantitative evaluation of Schwann cell proliferation was performed according to manufacturer's instructions. Briefly, poly-L-lysine coated 96 well plates were seeded with cells at a density of $2.5x10^4$ cells/cm^2. After 48 hours medium was changed to Schwann cell medium containing 100 μM BrdU and cells were incubated for 24 hours at standard cell culture conditions (37°C and 5% CO_2). The culture plates were fixated with FixDenat® solution and subsequently incubated with anti-BrdU POD antibody solution for 60 minutes at room temperature. After washing the plate with PBS, tetramethyl benzidine was added for 30 minutes as a substrate. The reaction was stopped with 1 M H_2SO_4 and absorption was measured at 450 nm with 690 nm as reference wavelength on an automatic microplate reader (Tecan Sunrise; Tecan, Switzerland).

Flow cytometric analysis

Purity of the Schwann cell cultures was evaluated with flow cytometry for common Schwann cell markers: anti-S100b (rabbit polyclonal; Dako, Denmark), anti-P75 NGFR (goat polyclonal; Santa Cruz Biotechnology, USA), and anti-P0 (rabbit polyclonal; Santa Cruz Biotechnology, USA). Antibodies were labeled with Allophycocyanin (APC) (Lynx Rapid Conjugation Kit, ABD Serotec, UK). For analysis, cells were detached with a cell scraper and incubated with the antibodies (1:200) on ice and in the dark for 20 minutes. Cell pellets were washed twice and resuspended in 200 µl PBS. Flow cytometric analysis (10.000 events) was performed with a BD FACS Canto II (Becton Dickinson, USA) and data was evaluated with Flowjo Version 8.8 (Tree Star Inc, USA).

Immunoblotting

Total protein of cells was extracted using Trizol (peqGold TriFast, Peqlab, Austria) according to manufacturer's instructions. Briefly, proteins were precipitated from organic phase with ethanol and pelleted by centrifugation (12.000xg, 10 min, 4°C). Protein pellet was washed three times with 0.3 M guanidine hydrochloride (Sigma Aldrich, UK) in 95% ethanol and once with 100% ethanol (Merck, Germany), each washing step followed by centrifugation (7500xg, 5 min, 4°C). Supernatants were discarded and dry protein pellets solubilized in 1% SDS (Sigma Aldrich, UK) in analytical grade water.

Equal amounts of protein (up to 3 µg/lane; one donor per gel: passage 2, passage 7, passage 15) were separated on a 12% SDS-polyacrylamide gel and blotted onto a nitrocellulose

membrane. Membranes were blocked with 5% skim milk in Tris buffered saline containing 1% Triton-X100 (Sigma Aldrich, UK) (TBS-T) for 120 min, and incubated with primary antibodies S100b (Dako, Netherlands), c-Jun (abcam, UK), GFAP (Bioss USA, USA), P16^{INK4A} (abcam, UK), α-Tubulin (Calbiochem, USA) diluted in 5% bovine serum albumin (Sigma Aldrich, UK) (BSA) in TBS-T at 4°C on a roll mixer for 12 hours. Membranes were washed twice with TBS-T and incubated with the secondary antibody in 5% milk-TBS-T. Signals were detected using an Odyssey Fc infrared imaging system (LI-COR Biosciences; US). After membranes were incubated in 1x NewBlot IR Stripping Buffer (LI-COR Biosciences) on a shaker at room temperature for 5 min and washed three times in PBS, membranes were re-probed with total antibodies. Ratio of analysed protein to housekeeping gene α-tubulin was densitometrically analysed using Image Studio Version 5.0.21 (LI-COR Biosciences).

Activation switch

In passage 4, 9 and 15, the activation status and the capacity to switch activation status (proliferating to pro-myelinating) were assessed. Cells were split ($2x10^4$ cells/cm^2, 24 hours adherence time) in two groups: one was cultured in Schwann cell medium, and the other one in basic medium (DMEM-D-valine (PAA, Austria), supplemented with 10% FCS, 2 mM L-Glutamine, 1% antibiotics) without supplements favouring the proliferating or the pro-myelinating status, respectively. Proliferation behaviour (BrdU ELISA) and marker expression (flow cytometry) were assessed 5 days after medium switch.

ATP Release and Lactate Dehydrogenase (LDH) Release

The amount of ATP released into the supernatant from nerve tissue treated with ESWT was determined using the CellTiter-Glo assay (Promega, Germany). Sciatic nerves were dissected and kept in PBS on ice until further treatment. After removing the epineurium and teasing of the nerve fibres with a mounted needle (15 times in fibre direction), remaining nerve tissue was placed in 500 µl DMEM. Shockwave treatment was performed at 37°C and with following parameters: 300 pulses with 3 Hz and 0.03 mJ/mm^2, 0.10 mJ/mm^2 or 0.19 mJ/mm^2. Control group was placed in a water bath (37°C). Nerve tissue was incubated for 5 min on ice and subsequently centrifuged at 1500 rpm for 5 min at 4°C. Supernatant was transferred to a micronic tube (150 µl) for LDH measurement (Cobas C111- Roche Diagnostics, Switzerland), and 96-well plate (triplicate, 100 µl) for ATP measurement. An equal amount of CellTiter-Glo reagent was added, the plate was horizontally shaken for 2 min, and after

incubation for 10 min at room temperature, the resulting luminescence was measured. ATP standards were used for calibration of the measured luminescence. After sampling of the initial supernatant, fresh, ice-chilled DMEM was added on nerve tissue and was incubated on ice for another 30 min. ATP and LDH concentration in supernatants was quantified as before.

Statistics

All data in this study are shown as mean ± standard deviation (S.D.) and were tested for normal distribution. Statistical analysis was performed using –depending on groups analysed- student t test or one-way ANOVA (analysis of variance) followed by Tukey range test for significant differences between the means. Significance was considered for $P<0.05$. For statistical calculations GraphPad Prism 5 for Mac OS X, Version 5.0b (GraphPad Software, Inc., USA) was used.

RESULTS

Increased cell yield by incorporation of ESWT in the isolation process

To evaluate effects on the isolation efficacy, cells were counted after 19 days in culture, and cell number was normalized to 100 mg nerve wet weight. Sciatic nerve weights ranged between 66.2 and 88.5 mg and there was no significant difference between the groups (Figure 12B).

As shown in Figure 12A, cell yield after 19 days was significantly increased in the ESW treated group. While initial cell count revealed $1.62 \times 10^6 \pm 9.3\%$ cells per 100 mg nerve wet weight in the control group, cell yield in the ESW treated group was on average 52.3% higher ($3.10 \times 10^6 \pm 8.2\%$ cells per 100 mg nerve wet weight). Furthermore, Figure 12A illustrates a consistent improvement of the cell yield for every culture assessed.
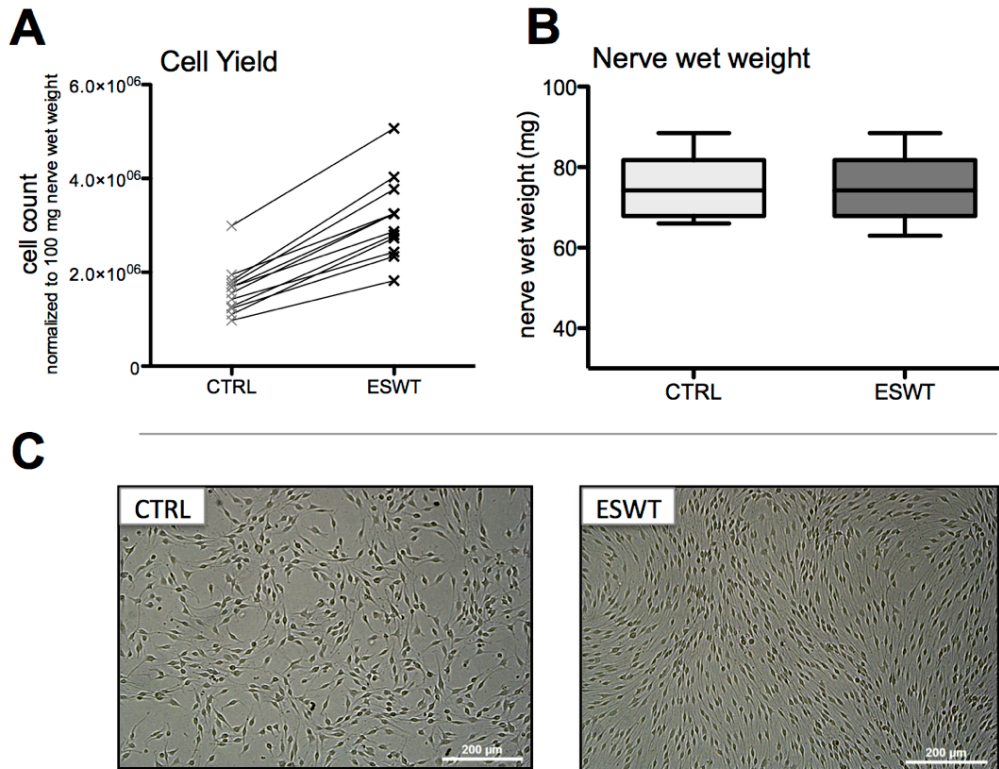
Figure 12: ESWT resulted in an increased cell yield; A) Intra-animal comparison of Schwann cells counted after 19 days in culture, normalized on 100 mg nerve wet weight, n=12; B) nerve wet of the respective nerves, assessed with a fine scale before isolation; n=12; C) phase contrast micrographs of SCs in passage 0, untreated (CTRL) and treated with extracorporeal shockwaves (ESWT);

BrdU assay and population doublings per passage reveal a significantly higher proliferation after ESWT for 15 passages

The cell proliferation was quantified using a BrdU assay and assessment of population doublings per passage. In all passages examined (passage 1, 4, 7, 10, 13 and 15), Schwann cells treated with ESWT showed a higher proliferative behaviour than the Schwann cells in the control group, respectively (Figure 13). Furthermore proliferation decreased steadily in the control group starting in passage 4, while proliferation in the ESWT group further increased until passage 7 and remained at a similar level until passage 15. Western Blot analysis in passage 2, 7 and 15 also exhibited a steady increase in the cell-cycle-arrest/senescence marker P16^{INK4a} in the control group, while ESWT group remained at the same low level for the tested passages (Figure 15).
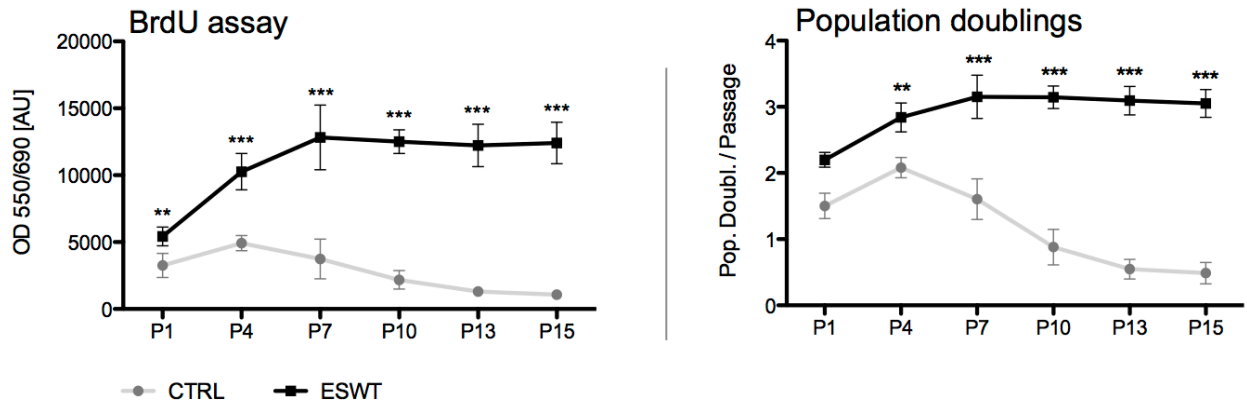
Figure 13: BrdU assay and population doublings per passage revealed a significantly higher proliferation of the ESW treated Schwann cells over 15 passages; BrdU: n=6 rats, values were obtained in quadruplicates in passage 1, 4, 7, 10, 13 and 15; Population doublings per passage: population doublings were obtained by cell count in passage 1, 4, 7, 10, 13 and 15; n=6 rats; data is shown as mean ± SD, and significance was tested with student t test; *P < 0.05; **P < 0.01; ***P < 0.001;

Sustained purity and P75 expression after ESWT for extended culture period

In order to determine purity and phenotype of these cultivated cells, expression of Schwann cell specific marker S100b, as well as the markers P75 (proliferative/regenerative phenotype) and P0 (myelinating phenotype) were assessed *in vitro* over 15 passages with flow cytometry (Figure 14).
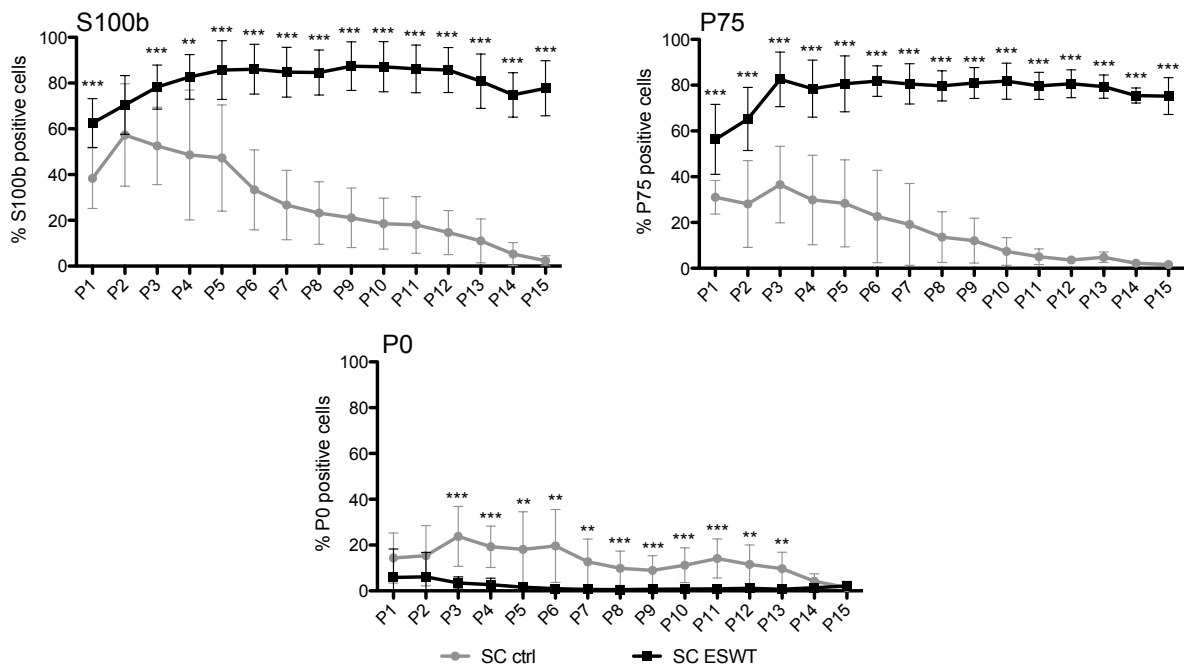
Figure 14: Schwann cells treated with ESW show an increased purity (100b) over 15 passages, along with increased expression of proliferation associated marker P75 and a decreased expression of myelin marker P0; Flow cytometric immunophenotype analysis (S100b, P75, P0) of Schwann cells treated with ESWT (black), compared to control (grey) over 15 passages (P1-P15); one passage represents the detachment, counting, and

seeding of the cells with $4*10^4$ cells/cm^2 for 5 days; n=10 rats; data is shown as mean of percentage marker positive cells ± SD and significance was tested with student t test; *P < 0.05; **P < 0.01; ***P < 0.001;

In passage 1 24.2% more cells expressed S100b in the ESW treated group compared to the control group (62.6% compared to 38.4%). In both groups Schwann cell purity increased in passage 2 to 70.0% (ESWT) and 57.3% (CTRL). However, starting in passage 3, S100b expression in the control group decreased steadily over the following passages. In contrast, in the ESW treated group expression increased until passage 5 (85.3%) and remained at this level until passage 15 (Figure 14 S100b). A similar temporal pattern applied to the expression of the proliferation-associated marker P75, briefly: while control group reached a peak expression of 36.7% in passage 3, steadily decreasing over time, ESW treated cells increased from 57.4% P75 expression to 83.1% positive cells and remained at this level until passage 15 (Figure 14 P75). Myelin marker P0 was downregulated in both groups, however stronger in the ESWT treated group, exhibiting a significant difference in passage 3 where control group showed an increase of 9.0% compared to passage 2 (Figure 14 P0).

Protein expression levels using Western Blot densitometric analysis revealed a similar difference between the groups in the expression of S100b as found with flow cytometry in the respective passages passage 2, 7 and 15 (Figure 15, S100b). Further analysis of the markers c-Jun and GFAP - both associated with the proliferative Schwann cell phenotype- exhibited an increase of both markers in the ESWT group and a decrease in the control group (Figure 15).
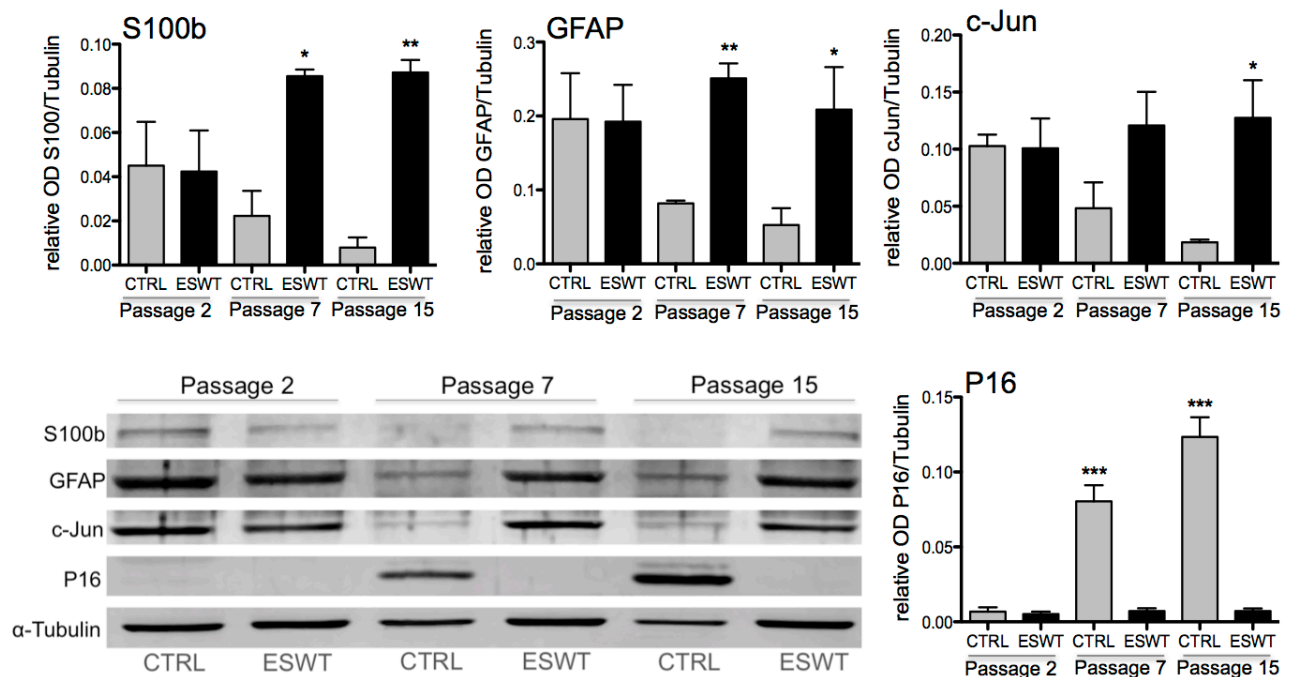

Figure 15: Western Blot analysis of Schwann cell protein lysate demonstrates a decrease of Schwann cell markers in the control group along with a simultaneous increase of senescence marker P16; Western Blot analysis of Schwann cells in passage 2, passage 7 and passage 15, treated with ESW compared to untreated

control. Blots were densitometrically analysed and data is presented as mean ± SD (n=6), statistical significance was tested with 1-way ANOVA and Tukey range test; *P<0.05, **P<0.01, ***P<0.001;

Schwann cells treated with ESWT display a consistent morphology

Schwann cell morphology was assessed in passage 0, 5, 9 and 15 using phase contrast microscopy (Figure 16). Schwann cells of both groups showed a spindle or tripolar shape in passage 0. Starting in passage 5, a second cell morphology was found in the control group, similar to the classic fibroblastic phenotype. Cells exhibiting this morphology increased in number from passage 5 to passage 15 in the control group (Figure 16, indicated with arrows), while the ESWT treated group revealed a homogenous Schwann cell morphology over 15 passages.
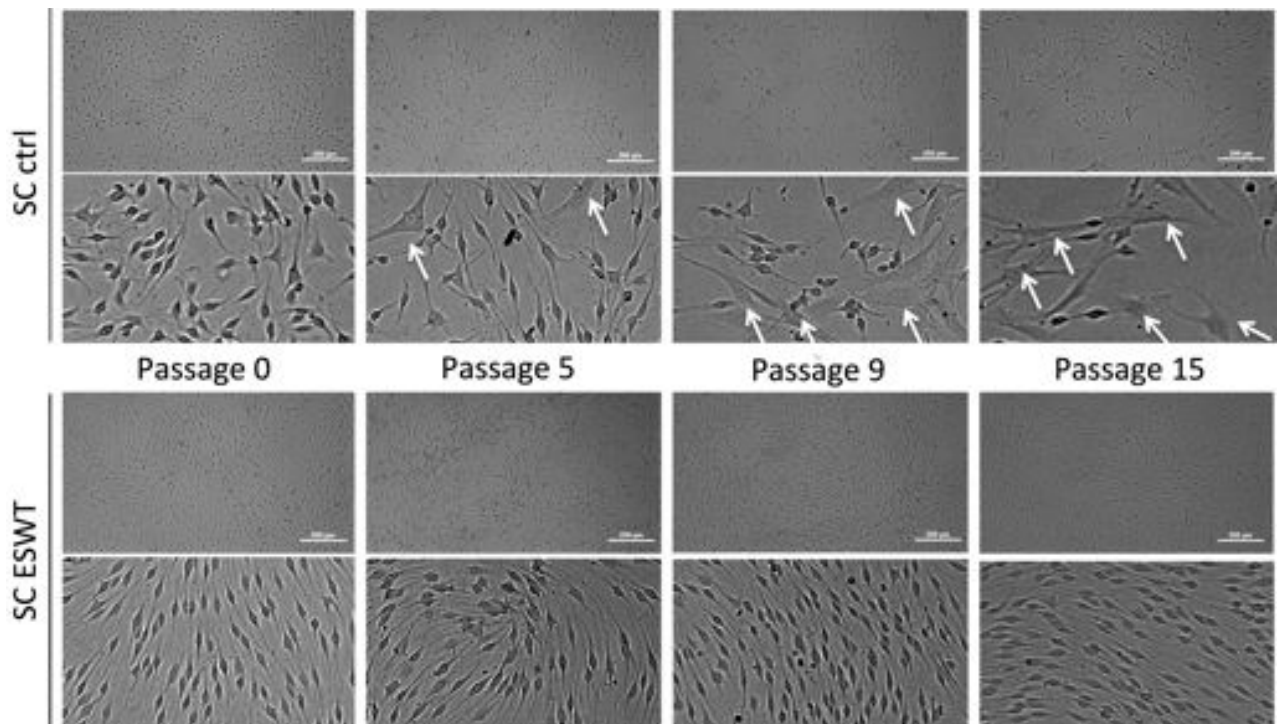
Figure 16: Morphology of Schwann cells changes over time in the control group, while it remained consistent in the group treated with extracorporeal shockwaves (ESWT); Phase contrast micrographs depicting Schwann cells in passage 0, 5, 9 and 15 of control group (CTRL, upper bar) and ESW treated group (lower bar); arrows mark cells displaying non-typical morphology (tripolar, fibroblast-like); size bar indicates 200 μm.

Schwann cells revert faster to myelinating phenotype after ESWT

To demonstrate that the proliferative activation of SCs is not permanent and reversible the Schwann cell ability to switch phenotype from proliferating to pro-myelinating was tested. Therefore in passage 4, 9 and 15, medium was changed to medium lacking pro-proliferative

growth factors - giving the cells a minimal stimulus to change their phenotype. Flow cytometry revealed no change in expression of S100b between the cells cultured in the different mediums in the respective passages (Figure 17). In passage 4 cells of the control group and the ESWT group were able to perform the switch, as it can be seen in Figure 17: P75 was significantly down-regulated while P0 was strongly upregulated. Expression of P0, however, was significantly higher in the ESW treated group. In passage 9 and 15 only cells of the ESWT group reacted to the stimulus by significant down-regulation of P75 together with up-regulating P0. BrdU assay confirmed a significantly decreased proliferation in the ESW treated group cultured in pro-myelination medium compared to proliferation medium (Figure 17, lower panel).
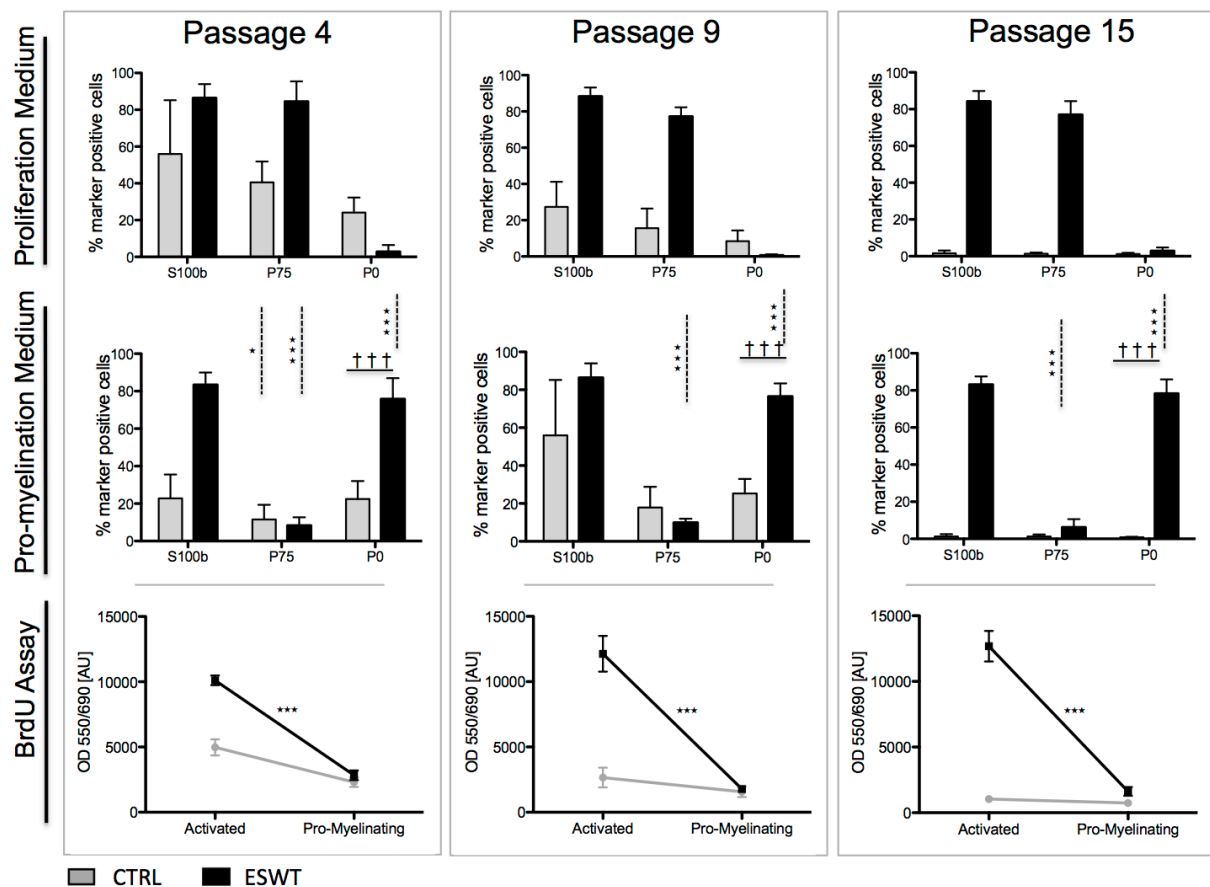
Figure 17: Schwann cells treated with ESWT can express both phenotypes (regenerative and pro-myelinating) dependent on culture medium, but independent of passage number; Flow cytometry analysis concerning expression of Schwann cell markers S100b, P75 and P0 of Schwann cells in activation medium and pro-myelinating medium (day 5 after medium switch); control group is shown in grey, ESWT group in black; statistical significance was tested with 1-way ANOVA and Tukey range test; data is presented as mean ± SD; *P<0.05, **P<0.01, ***P<0.001: comparison of activation to pro-myelination medium of the respective groups; †P<0.05, ††P<0.01, †††P<0.001: comparison between CTRL and ESWT group; BrdU ELISA of Schwann cells in activation medium and pro-myelination medium; statistical significance was tested with 1-way ANOVA and Tukey range test; data is presented as mean ± SD; *P<0.05, **P<0.01, ***P<0.001; n=6;

ESWT induces immediate and sustained ATP release

Purinergic signalling is capable of inducing enhanced proliferation after ESWT treatment, associated with ATP release (38). Therefore, we assessed ATP release of the *ex vivo* treated sciatic nerves. Extracellular concentration of ATP was enhanced depending on the applied energy flux densities. The "minimal" setting with the lowest energy level (0.03 mJ/mm^2) did not result in any initial increase whereas application of ESW with treatment (0.1 mJ/mm^2) as well as the "maximal" setting (0.19 mJ/mm^2) had a significant increase in initial extracellular ATP as a consequence (Figure 18 ATP 5 min). Nerve tissue was incubated in freshly added DMEM for 30 min on ice to assess sustained ATP release. These supernatants showed a generally lower concentration of ATP in all groups, however treatment (0.1 mJ/mm^2) and maximal setting (0.19 mJ/mm^2) showed again higher levels than control and minimal setting (0.03 mJ/mm^2) (Figure 18, ATP 30 min). Among other triggers, ATP can be released into the extracellular space due to cell membrane damage. In order to exclude membrane damage as the reason for increased extracellular ATP after ESW treatment we assessed extracellular lactate dehydrogenase (LDH) concentration as an indicator for cell damage. As seen in Figure 18 (LDH), supernatants of nerve tissue that received the highest energy (0.19 mJ/mm^2), were the only ones that showed significantly enhanced LDH concentrations. At both time points, our selected treatment setting (0.1 mJ/mm^2) did not increase levels of extracellular LDH when compared to the control group.
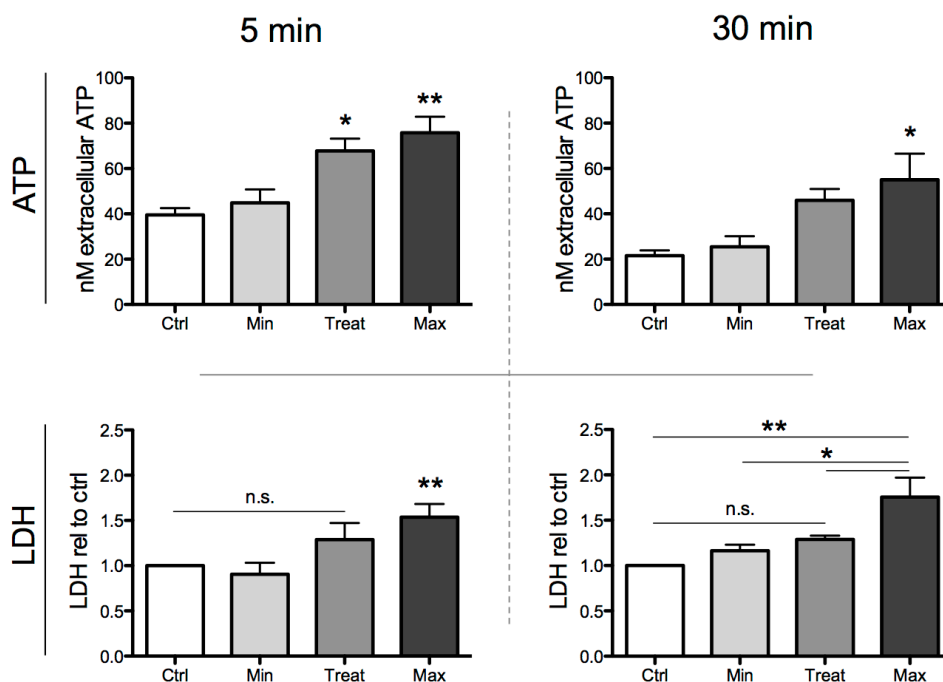

Figure 18: Extracellular ATP was significantly increased in nerves treated with 0.1 mJ/mm^2 (Treat) over a period of 30 minutes, with no increase in cell damage (LDH); whole nerves without epineurium were treated with ESW of different energy levels: 0.03 (Min), 0.10 (Treat) and 0.19 mJ/mm^2 (Max) and compared to the untreated

control; ATP concentration in the supernatant was determined after 5 min and 30 min on ice with luminescence, alongside with assessment of LDH; amount of ATP was calculated using ATP standards; LDH was normalized to untreated control; n=5; statistical significance was tested with 1-way ANOVA and Tukey range test; *P<0.05, **P<0.01, ***P<0.001;

DISCUSSION

After peripheral nerve injury, Schwann cells are triggered to change their phenotype from myelinating to activated, proliferating, building Bands of Büngner- the substrate for outgrowing axons. There is a myriad of studies describing the importance of Schwann cells during peripheral nerve regeneration (eg Frostick *et al.*, 1998; Bhatheja and Field, 2006; Toy and Namgung, 2013), but the difficulties and issues associated are also well-known (112–114). Especially in long-distance injuries, the demand for supportive Schwann cells expanded *in vitro* (e.g. seeded on a tubular graft) would be high, as autologous Schwann cells lack the proliferative capacity to provide bands of Büngner throughout a tube longer than 40 mm (105). This limited proliferative capacity is also reflected *in vitro*, displaying together with insufficient purity the main issue of Schwann cell cultures. To our knowledge, we are the first to demonstrate an increase in proliferation, proliferative capacity and purity in *in vitro* Schwann cell cultures with ESWT.

The basis for our study was found in two preceding shockwave studies. Hausner *et al.* (37) showed that shockwave treatment after nerve dissection leads to significantly accelerated regeneration in a rat model. It was hypothesized that this effect may result from improved macrophage infiltration and an earlier onset of regeneration. However, Weihs *et al.* (38) elucidate in their study how ESWT stimulates cell proliferation in several cell types (e.g. mesenchymal stem cells) by ATP release-coupled extracellular signal-regulated kinase (ERK) activation. Applying ESWT on the whole nerve before isolation of Schwann cells, our results demonstrate that ESWT is capable of enhancing the extracellular levels of ATP without causing any cell membrane damage. Furthermore, the sustained release over 30 minutes suggests an active mechanism of ATP release.

Analysing the cultures in passage 0 we assessed a significantly higher cell yield in all cultures treated with ESWT (Figure 12), alongside a significantly increased proliferation rate in passage 1 (Figure 13). In the shockwave treated group quality of culture, reflected in purity and proliferation rate, improved over the first passages: S100b, a marker indicating purity of Schwann cells, increased over the first five passages and remained at the level for the period

of analysis; this purity was also observed in morphology of Schwann cells (Figure 15); moreover P75 increased over time, while P0 in the same manner decreased until passage 4 and subsequently was not expressed (Figure 14); P0 and P75 are known to counteract each other (115): P0 is a myelin component and therefore solely expressed in myelinating Schwann cells (116), while P75 is a marker associated with the regenerative, proliferating phenotype of Schwann cells (26,35). Western blot analysis at three time points throughout the culture period revealed a similar expression pattern for S100b, acting as a control marker between the methods (Figure 15, compared to Figure 14 S100b). GFAP and c-Jun were also upregulated in passage 7 (compared to passage 2) and showed a comparable expression in passage 15. Both markers are associated with the regenerative phenotype. GFAP is suppressed in myelinated axons and becomes upregulated after injury, initiating proliferation by binding of integrin $\alpha v \beta 8$ (117). The transcription factor c-Jun however is an antagonist to Krox20, a protein controlling the myelination in the peripheral nervous system, and displays one of the key regulators to initiate and maintain the regenerative phenotype (30,118). Together with the strongly increased proliferation (assessed with BrdU assay and population doubling per passage), the Schwann cells treated with ESWT represent a highly regenerative phenotype for an extended culture period of 15 passages (103 days).

As the sum of these observations leads inevitably to the question whether hyper-proliferating Schwann cells may lead to adverse effects such as post-stimulus proliferation and subsequently Schwannoma formation, we conducted a functionality experiment. Schwann cells were cultured for five days in basic medium lacking any kind of proliferation stimulating growth factors (forskolin, PEX). Schwann cells treated with ESWT reacted even more to the change of stimulus, independent of the passage: they not only stopped proliferating (Figure 17- BrdU), but also significantly downregulated the proliferation-associated marker P75 and upregulated the myelin component P0. This prompt and consistent reaction to the absence of mitogenic growth factors demonstrates their capacity to switch to the myelinating phenotype. However, the functionality of the SCs in an *in vivo* defect model has to be shown.

In contrast to the ESWT group, the untreated Schwann cells did not display a consistent Schwann cell phenotype over the culture period of 15 passages. Starting with passage 5 to 7, purity and proliferation significantly decreased. Abated purity was observed in lower expression of S100b (Figure 14/Figure 17), as well as in increased appearance of cells displaying an atypical morphology (Figure 16). Reduced proliferation was primarily assessed in a decline of population doublings and additionally by reduced BrdU OD values. The entire

marker expression levels associated with the regenerative phenotype (P75, GFAP, c-Jun) diminished over time, while the senescence marker P16 significantly increased. Therefore, our *in vitro* study reflects the before mentioned *in vivo* problem and represents a possible solution: the limited proliferative capacity of Schwann cells can be improved with ESWT. With treated Schwann cells building a growth substrate faster and for a longer period of time, the *in vivo* effect can be twofold: not only results ESWT in an acceleration of regeneration by activating autologous Schwann cells – as it has been shown by Hausner *et al.* (37)- but would also allow reimplantation of a high number of autologous Schwann cells expanded *ex vivo,* in a decidedly regenerative state.

A partial explanation for the underlying mechanisms of the observed effects could be the sustained ATP release. A wide range of mechanisms from vesicular release over connexins/pannexins to ABC transporters are thought to conduct an active release of ATP (119–121). Subsequent purinergic signalling plays a crucial role not only as a danger associated molecular pattern but also in a variety of cellular functions such as proliferation, chemotaxis, differentiation and amplification of other signals (38,122). This includes Schwann cell – axon interactions. Especially immature/unmyelinating Schwann cells signal via extracellular ATP in a paracrine manner with axons (123,124). It was proposed that ATP and glutamate are building a positive feedback loop enhancing their activities (125). The fate of Schwann cells is influenced by neuronal activity, by the activation of purinergic metabotropic P_2Y receptors and direct actions of ATP and its metabolite adenosine (126–128) as well as the activation of metabotropic glutamate receptors (129). Furthermore, purinergic signalling is thought to be both an autocrine and a paracrine amplifier for other signalling inputs. This is a further explanation for the enhanced proliferative activity of ESWT treated Schwann cells in medium containing proliferation-inducing factors such as Forskolin and PEX. Adenosine, a metabolic product of ATP hydrolization, is hypothesized to play a role in learning by affecting histone modifying proteins resulting in epigenetic changes (130). Therefore, the prolonged phenotypic stability and increased susceptibility to external stimuli as observed in the phenotype switch experiments in this study may be explained by epigenetic changes.

Concluding, we observed a higher proliferative activity without phenotype commitment, increased purity of the culture as well as reduced expression of senescence associated markers even after long cultivation periods. These positive effects of ESWT on Schwann cell isolation and cultivation may partly be explained by the actions of extracellular ATP. However, in

order to gain a deeper understanding of the effects of ESWT on Schwann cells and their natural habitat, the nerve, further studies *in vitro* as well as *in vivo* focusing on purinergic signalling, mechanotransduction and epigenetic processes have to be performed.

CHAPTER II

Fibrin and activated Schwann cells as a potential luminal filler for nerve guidance conduits

Activated Schwann cell-like cells on aligned fibrin/PGLA structures: a novel construct for application in peripheral nerve regeneration

Christina M. A. P. Schuh[1,2], Tatjana J. Morton[1,2], Asmita Banerjee[1,2], Christian Grasl[3,4], Heinrich Schima[3,4], Robert Schmidhammer[1,2], Heinz Redl[1,2], Dominik Ruenzler[2,5]

[1] Ludwig Boltzmann Institute for Experimental and Clinical Traumatology / AUVA Research Center, Vienna, Austria

[2] Austrian Cluster for Tissue Regeneration, Vienna, Austria

[3] Center for Medical Physics and Biomedical Engineering, Medical University of Vienna

[4] Ludwig Boltzmann Cluster for Cardiovascular Research, Vienna, Austria

[5] University of Applied Sciences Technikum Wien – Department of Biochemical Engineering, Vienna, Austria

ABSTRACT

Tissue engineering approaches in nerve regeneration search for ways to support gold standard therapy (autologous nerve grafts) and to improve results by bridging nerve defects with different kinds of conduits. In this study, we describe electrospinning of aligned fibrin/PGLA fibres in an attempt to create a biomimicking tissue-like material seeded with Schwann cell-like cells (SCLs) *in vitro* for potential use as an *in vivo* scaffold.

Rat adipose-derived stem cells (rASCs) were differentiated into SCLs and evaluated with flow cytometry concerning their differentiation and activation status (S100b, P75, MAG, P0). After receiving the proliferation stimulus forskolin, SCLs expressed S100b and P75; comparable to native, activated Schwann cells, while cultured without forskolin cells switched to a pro-myelinating phenotype and expressed S100b, MAG and P0.

Human fibrinogen and thrombin, blended with Poly Lactic-co-Glycolic Acid (PGLA), were electrospun and the alignment and homogeneity of the fibres were proven by scanning electron microscopy (SEM). Electrospun scaffolds were seeded with SCLs and the formation of Büngner-like structures in SCLs was evaluated with phalloidin/propidiumiodide staining. Carrier fibrin gels containing rASCs acted as a self-shaping matrix to form a tubular structure.

In this study we could show that rASCs can be differentiated into activated, proliferating SCLs and that these cells react to minimal changes in stimulus, switching to a pro-myelinating phenotype. Aligned electrospun fibrin-PGLA fibres promoted the formation of Büngner-like structures in SCLs, which also rolled the fibrin-PGLA matrix into a tubular scaffold. These *in vitro* findings favour further *in vivo* testing.

Keywords: peripheral nerve regeneration; Schwann cell-like cells; electrospinning; fibrin;

INTRODUCTION

Lesions of peripheral nerves occur with a prevalence of about 5% in traumatic injuries. The gold standard treatment of peripheral nerve defects with loss of nerve tissue is still the autologous nerve transplant. In autologous nerve transplants, an exclusively sensitive nerve (e. g. sural nerve) is transplanted to the defect site, providing guiding structures and Schwann cells to augment axonal regeneration. Major drawbacks in the use of autografts are limited availability and loss of a healthy donor nerve, as well as donor site morbidity. (9,102,131,132) New approaches in tissue engineering look at ways to support autologous nerve grafts and to improve the results by bridging nerve defects with different kinds of conduits (9). Promising results are found in conduits seeded with Schwann cells (131,132), which again require a second incision site to isolate the Schwann cells, potentially leading to donor site morbidity (102).

To address the issue of sacrificing a healthy donor nerve, alternative sources for Schwann cells were sought. Tissue-resident mesenchymal stem cells (MSCs) are a key component in maintaining tissue integrity and have been shown to participate in tissue regeneration, e. g. responding to injury (46). Due to their role in tissue regeneration, MSCs are thought to be a promising tool for tissue engineering, representing an alternative cell source to tissue specific cells, such as Schwann cells, which are usually difficult to obtain. In contrast, there is a variety of easily accessible tissues MSCs can be isolated from, including adipose tissue (49), bone marrow (47) or umbilical cord blood (48). These cells have shown potential to differentiate ex vivo into various mesenchymal cell types such as adipocytes, osteoblasts, chondrocytes or fibroblasts (50–53), but also other lineages including Schwann cell-like cells (54,55). Moreover, their immunogenic phenotype lacks major histocompatibility complex class II (MHC II) and hinders T cell stimulation and subsequently immunogenic responses (46,56,57). Some studies even demonstrated immunosuppressive properties of MSCs (58,59).

A crucial factor when utilizing therapeutic cells in the field of nerve tissue engineering is the form of application. It was shown that Schwann cells align along orientated fibres, forming Bands of Büngner and enhancing axonal regeneration (133,134). An effective method to fabricate aligned fibres is electrospinning, in which electrostatic forces are utilized to create micro- or nanofibres from a solution of polymers (135,136). The efficiency of this process, as well as the quality of the final fibre product, are influenced by a variety of factors, including polymer concentration, viscosity of the solution, voltage between solution and ground electrode, the distance between the Taylor cone and the ground electrode, and environmental

conditions (137,138). The electrospinning method offers the possibility to obtain a standardized fibrous scaffold from a variety of polymers.

The formation and controlled degradation of fibrin is one of the major components in natural wound healing. It is not only important for hemostasis, but also acts as a provisional growth matrix for tissue-specific cells (139). Fibrin sealants are used in several surgical applications and have become a versatile scaffold in the field of tissue engineering, augmenting regeneration in a variety of tissues such as bone (140–142), skin (143,144) or cartilage (145,146). Fibrin is an especially important factor in nerve regeneration: after an injury, nerve stumps leak fibrin plasma exudate into the affected area, forming fibrin cables that enable Schwann cells to migrate towards the distal stump and form Bands of Büngner (1,39). Fibrin is a key regulator to myelin formation. As long as fibrin is present, Schwann cells cannot switch to their myelinating phenotype, and continue proliferating. Moreover, fibrin induces the production of P75 low-affinity NGF receptor. (147)

In this study, we describe electrospinning of aligned fibrin fibres in an attempt to create a biomimicking tissue-like material seeded with well-characterized Schwann cell-like cells (SCLs) *in vitro* for a potential use as scaffold *in vivo* to treat peripheral nerve defects.

MATERIAL AND METHODS

Isolation and culture of cells from rat tissue

Isolation of mesenchymal stem cells from adipose tissue (rASCs)

Rats were euthanized according to established protocols, which were approved by the City Government of Vienna, Austria in accordance with the Austrian law and the Guide for the Care and Use of Laboratory Animals as defined by the National Institute of Health. Fat pads of 4 - 10 male rats (Sprague-Dawley) were minced and incubated in 2% collagenase (Biochrom, Germany). Digestion was stopped by addition of culture medium (PAA, Austria) containing 10% FCS. The digested tissue was filtered through 100 μm cell strainers (BD Falcon, Germany) and centrifuged for seven minutes at 400 x g. The supernatant, containing mature adipocytes, was discarded and the pellet with pre-adipocytes, mesenchymal stem cells and stromal cells was washed with phosphate buffered saline (PBS) (PAA, Austria) and centrifuged at 400 x g. The resulting rASCs separated from adipose tissue were seeded on T75 cell culture flasks (PAA, Austria) for expansion.

After isolation, rASCs were cultivated using standard cell culture conditions (37°C, 5% CO_2) in Dulbecco's modified Eagles medium (low glucose, PAA, Austria) and Ham's F12 (PAA, Austria) supplemented with 10% fetal calf serum (FCS; PAA, Austria), 200 µM L-glutamine and 1% antibiotics (PAA, Austria). For expansion, cells were cultivated in cell culture flasks (PAA, Austria) with an initial seeding density of 3 x 10^3 cells/cm^2. At a confluence of 80-90%, cells were split with Accutase™ (PAA, Austria).

Isolation of native Schwann cells

Schwann cells from rat sciatic nerves were isolated as described by (108). Briefly, sciatic nerves of adult male Sprague Dawley rats were dissected and minced after removing the epineurium. Nerve fragments were incubated with 0.05% collagenase for 1 hour at 37°C, subsequently filtered through a 40 µm cell strainer and centrifuged at 400 x g for 6 minutes. After washing the cell pellet with DMEM containing 10% FCS, the pellet was resuspended in DMEM-D-valine (PAA, Austria), supplemented with 10% FCS, 2 mM L-glutamine, 1% antibiotics, N_2 supplement (Sigma Aldrich, UK), 10 µg/mL bovine pituitary extract (Sigma Aldrich, UK), 5 µM forskolin. Cell suspension was seeded on 6-well plates (PAA, Austria) coated with poly-L-lysine (Sigma Aldrich, UK) and laminin (Sigma Aldrich, UK). Cells were evaluated 19 days after isolation.

Differentiation and Characterization of cells

In vitro differentiation of rASCs into SCLs

Differentiation into SCLs was performed in a three-step procedure as modified from (54). Briefly, rASCs in P1 were plated at a density of 0.5 x 10^3 cells/cm^2 and after 36 hours of reattachment in DMEM (high glucose; PAA, Austria) supplemented with 10% FCS, 200 µM L-glutamine and 1% antibiotics (PAA, Austria), cells were prepared for differentiation into neural lineage by incubation with 1 mM β-mercaptoethanol (Sigma Aldrich, UK) for 24 hours, followed by washing with PBS and 60 hour incubation with 50 ng/mL all-*trans*-retinoic acid (Sigma Aldrich, UK). The residual medium was removed by washing with PBS and cell culture medium was changed to "SCL medium" containing 5 ng/mL recombinant human platelet-derived growth factor (PDGF-AA, R&D systems, Germany), 10 ng/mL recombinant human basic fibroblast growth factor (bFGF, R&D systems, Germany), 200 ng/mL human recombinant heregulin-β1 (Peprotec, Germany) and 15 µM forskolin (Sigma Aldrich, UK). SCL medium was changed every third day for 22 days. Samples for evaluation with flow cytometry were taken on day 0, 7, 14, and 21.

Flow cytometry of surface antigens

rASC specific markers as described by (52) were used in flow cytometry analysis to characterize rASCs in P2: anti-CD14 (mouse monoclonal, FITC labeled, Merck Millipore, USA) anti-CD34 (rabbit polyclonal, Abcam, UK), anti-CD45 (rabbit polyclonal, Abcam, UK), anti-CD73 (rabbit polyclonal, Santa Cruz Biotechnology, USA), anti-CD90 (rabbit polyclonal, Santa Cruz Biotechnology, USA) and anti-CD105 (mouse monoclonal, Merck Millipore, USA); and secondary antibody: FITC (goat polyclonal, Dako, Denmark). Expression of Schwann cell specific markers of SCLs and native Schwann cells was evaluated with following markers: anti-S100b (rabbit polyclonal; Dako, Denmark), anti-P75 NGFR (goat polyclonal; Santa Cruz Biotechnology, USA), anti-MAG (rabbit monoclonal; Abcam, UK) and anti-p0 (rabbit polyclonal; Santa Cruz Biotechnology, USA). Antibodies were labeled with APC (Lynx Rapid Conjugation Kit, ABD Serotec, UK) according to manufacturer's instructions.

Cells were detached with Accutase™ and incubated with the antibodies on ice and in the dark for 20 minutes. Cell pellets were washed twice and resuspended in 200 µl PBS. Cell incubated with an unlabeled primary antibody were incubated with a secondary antibody for 20 min, washed twice and then resuspended in 200 µl PBS. Flow cytometric analysis (10 000 events) was performed with BD FACS Canto II (Becton Dickinson, USA) and data was evaluated with Flowjo Version 8.8 (Tree Star Inc., USA).

Activation status of SCLs

SCLs were cultured for two weeks in SCL medium and then split into two groups: one was further cultured with SCL medium ("activated", favouring proliferation), while cells of the other group were cultured in SCL medium not containing the pro-proliferating factor forskolin ("pro-myelinating", favouring myelination). Native Schwann cells served as a control and were tested concerning activation-switch capacity as well. Samples of both groups were evaluated on day 0, 7, 14 and 21 for the expression of common Schwann cell markers S100b, P75, MAG and P0 with flow cytometry, as well as for proliferation with BrdU ELISA, and cell viability with MTT assay.

Proliferation assay

Proliferation of SCLs in medium favouring proliferation and medium favouring myelination was determined on day 0, 7, 14 and 21, using a 5- bromo-2-deoxyuridine (BrdU) uptake assay (Cell Proliferation ELISA assay Kit, Roche Diagnostics, Switzerland) according to

manufacturer's instructions. Briefly, medium was changed 48 hours after cell seeding to the respective medium containing 100 μM BrdU, and cells were incubated for 12 hours at standard cell culture conditions (37°C and 5% CO_2). The culture plates were fixated with FixDenat® solution and subsequently incubated with anti-BrdU POD antibody solution for 60 minutes at room temperature. After washing the plates with PBS, tetramethyl benzidine was added for 30 minutes as a substrate. The reaction was stopped with 1 M H_2SO_4 and absorption was measured at 450 nm with 690 nm as reference wavelength on an automatic microplate reader (Spectra Thermo, Tecan Austria GmbH, Austria).

Cell viability

Cell viability of SCLs in medium favouring proliferation and medium favouring myelination was determined on day 0, 7, 14 and 21 using MTT assay. Cells were incubated with the respective medium containing 650 μg/mL MTT [3-(4,5-dimethylthiazol-2-yl)-2,5-diphenyltetrazolium] bromide (Sigma Aldrich, Austria) for 60 minutes at standard cell culture conditions (37°C and 5% CO_2). Medium was discarded and MTT formazan precipitate was dissolved in DMSO (Sigma Aldrich, UK) by shaking in the dark for 20 minutes. Aliquots of 100 μl were transferred to 96-well plates. Light absorbance at 540 nm was measured immediately and optical density (OD) values were corrected for an unspecific background on an automatic microplate reader (Tecan Sunrise, Tecan Austria GmbH, Austria).

Electrospun Fibrin-PGLA scaffolds

Poly(Lactic-co-Glycolic Acid) (PGLA) (0.1 g/mL; Purasorb® PLG 8523, Purac, Netherlands) and pre-warmed lyophilized thrombin (500 IU; TISSEEL Lyo Two-Component Fibrin Sealant, Baxter, Austria) were dissolved in hexafluoroisopropanol (HFP) (Sigma Aldrich, UK). Fibrinogen (TISSEEL Lyo Two-Component Fibrin Sealant, Baxter) was dissolved in HFP containing 10% DMEM high glucose (10x; PAA, Austria) and components were mixed at a ratio of 2:1:1 fibrinogen:thrombin:PGLA.

Electrospinning was performed in three different ambient conditions: A) 28°C and 28% humidity; B) 26°C and 28% humidity; C) 24°C and 35% humidity.

Polymer solution was placed in the electrospinning apparatus (described by Arras *et al.*, 2012 (148)) in a 2 mL syringe (Terumo, Japan, 19562) with a 20 gauge needle (Terumo, Japan, NN-2050R). Distance between needle and collector was 9 cm. The voltage applied to the needle was -14.7 kV and fibres were collected on a grounded rotating wheel at a circumferential speed of 16 m/s. The rotating wheel collector was accelerated to a speed of 16

m/s. The process of electrospinning was performed continuously in a Faraday cage over a time period of 45 minutes, in order to apply 750 µl of a fibrin-PGLA solution to the rotating wheel collector. After removing the electrospun sheets from the collector, they were kept at room temperature for at least 1 hour to remove solvent residues. Electrospun sheets were stored at 4°C for up to 14 days.

Scanning electron microscopy

Electrospun scaffolds were sputter coated with gold-palladium (Emitech SC7620, Quorum Technologies, UK) and were observed by scanning electron microscopy (JEOL 6500, Japan) at an accelerating voltage of 10 kV.

Cell-scaffold interaction

Electrospun scaffolds obtained under condition C (see 2.3) were tested for compatibility with SCLs in cell culture. After sterilization under UV light, SCLs were seeded on fibrin-PGLA scaffolds at a density of 1 x 10^4 cells/cm^2 and evaluated on day 1, 3 and 7 with phalloidin/propidium iodide (PI) staining concerning orientation along the fibres. As a control, undifferentiated rASCs, SCLs and native Schwann cells were seeded with the same concentration into a cell culture-treated 24-well plate (PAA, Austria). For phalloidin/PI staining, cells were fixated with 1% paraformaldehyde (Riedel de Haen, Germany) for 10 minutes and subsequently washed with PBS twice. Cell membranes were permeabilized with 0.1% Triton X-100 (Sigma Aldrich, UK) in PBS for 5 minutes, and again washed twice with PBS. Unspecific background fluorescence was blocked with 1% bovine serum albumin (BSA; Sigma Aldrich, UK) in PBS for 15 minutes. Subsequently, cells were incubated with AlexaFluor 488 Phalloidin (Invitrogen, USA), diluted 1:400 in PBS, containing 1% BSA, at room temperature, in the dark for 25 minutes and washed twice with PBS. PI (Sigma Aldrich, UK) was diluted 1:40 in PBS and cells were incubated with PI solution in the dark for 10 minutes and washed twice with PBS. Scaffolds were then mounted on a coverslip with fluorescence mounting medium (Dako, USA) and observed with a Leica DMI6000B.

Self shaping fibrin tubular structures

The method was adapted from (149). Prior to fibrin gel formation, 6-well plates (PAA, Austria) were coated with 2.5 mL polydimethylsiloxane (Sylgard® Dow Corning, USA). Plates were stored for one week to allow solvent evaporation and UV sterilized for 30 minutes before use.

Pre-warmed fibrinogen ("TISSEEL", Baxter, Austria) was reconstituted with aprotinin and thrombin 4 IU ("TISSEEL", Baxter, Austria) with calcium chloride, according to the manufacturer's instructions. Fibrinogen was diluted 1:2, thrombin 1:4 with DMEM high glucose.

rASCs were detached with Accutase™ and resuspended with thrombin at a concentration of 1.2×10^6 cells/mL. 350 µl thrombin-cell-suspension was distributed homogenously throughout the wells of the 6-well plate by agitation. The same amount of fibrinogen-solution was added, distributed homogenously and placed in the incubator for 20 minutes. After fibrin polymerization, the UV-sterilized 8x6 mm electrospun fibrin-PGLA scaffolds were placed centrally on the fibrin gel. Stainless steel minutien pins (Austerlitz Insect Pins, Czech Republic) were placed at 1 mm distance from the scaffold, as shown in Figure 24D. Schwann cell-like cells were detached with Accutase™ and seeded on the scaffold at a volume of 50 µl at a concentration of 2×10^5 cells/mL. Constructs were placed in the incubator for cell attachment for 90 minutes and subsequently 2 mL rASC growth medium containing 2% FCS, 14 µM forskolin and 1% aprotinin were added. Medium was changed every second day for two weeks.

Statistics

Statistical analysis was performed using one-way ANOVA (analysis of variance) followed by Tukey's range test for significant differences between the means. Significance was considered to be at $P < 0.05$. For statistical calculations GraphPad Prism 5 for Mac OS X, Version 5.0b (GraphPad Software, Inc., USA) was used. All data in this study are shown as mean ± standard deviation (SD).

RESULTS

Characterization of rASCs

To evaluate whether or not cells isolated from adipose tissue show properties of mesenchymal stem cells, they were analysed with flow cytometry and cell surface markers suggested by the IFATS (52) (Figure 19A). While the hematopoietic markers CD14, CD34 and CD45 could not be detected, mesenchymal stem cell markers CD73, CD90 and CD105 were present in P2 (Figure 19A).

Cells were also treated with agents known to favour differentiation into adipogenic and osteogenic lineage. Adipogenic differentiation was confirmed by formation of lipid droplets detected with Oil Red O (Figure 19B) and osteogenic differentiation by production of calcium deposits, evaluated with von Kossa staining (Figure 19C).
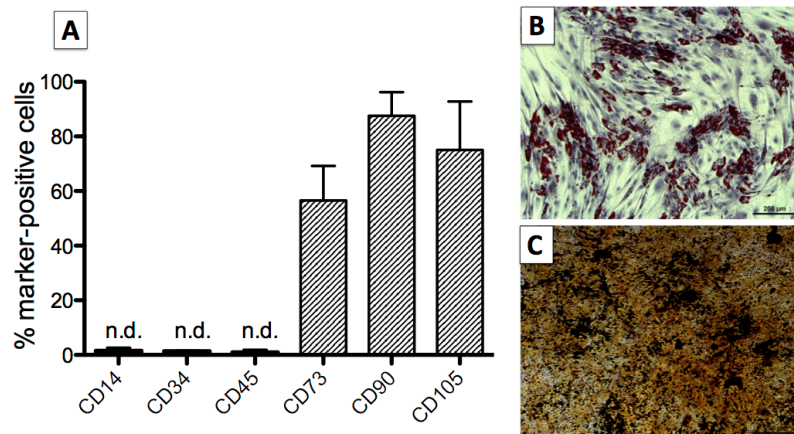
Figure 19: A: Flow cytometry results of rASCs in P2 for hematopoietic markers (CD14, CD34, CD45) and mesenchymal markers (CD73, CD90 CD105); statistical significance was tested with 1-way ANOVA and Tukey range test; data is presented as mean ± SD; *P<0.05, **P<0.01, ***P<0.0001; n=4; B,C: Differentiation-specific stainings of rASCs to exhibit either adipogenic differentiation (B) by staining lipid accumulations (Oil Red O) or osteogenic differentiation (C) by staining calcium phosphate (von Kossa) after 20 days in differentiation medium. (Detailed multilineage differentiation protocol in the supplement);

Differentiation of SCLs

Samples were taken during the differentiation procedure and evaluated with flow cytometry on day 6, day 12 and day 18 (SCL day 6 – day 18) after addition of the SCL medium. Statistical analysis (ANOVA and Tukey's range test) was performed using data from 4 independent differentiation procedures and the significance of change in marker expression was tested against the untreated sample (rASCs).

Expressions of mesenchymal stem cell markers during the differentiation procedure are shown in Figure 20B. CD73 was expressed by 56% of undifferentiated rASCs and decreased

significantly within the first 6 days to <30% and up until day 18 decreassed further to <10%. Expression of CD90, shown in Figure 20B, was not significantly down-regulated from day 0 to day 6, remaining at >80%. A reaction to the growth factor mixture can be seen in a significant decrease of CD90 on day 12 in SCL medium, followed by a further decrease until day 18. The amount of CD90 positive cells then remained at approximately 40%. CD105 was expressed by 75% of untreated rASCs, which decreased in SCL medium on day 6 and showed further down-regulation on day 12 and day 18 to show expression comparable to CD73 (<10%), shown in Figure 20B.

Expressions of Schwann cell markers during the differentiation procedure are shown in Figure 20C. Less than 5 % of untreated rASCs showed an expression of Schwann cell markers. Stimulation with growth factors led to a prompt and significant up-regulation of S100b to 60% marker-positive cells. Expression of S100b increased throughout the differentiation procedure to 80%, comparable to isolated native Schwann cells. Low affinity nerve growth factor receptor P75 (P75) showed an increase of marker-positive cells to almost 45% on day 6. Throughout the differentiation procedure, marker expression further increased to a percentage of marker-positive cells of 80% on day 18 (Figure 20C). Myelin-associated glycoprotein (MAG) was significantly up-regulated on day 12 to a percentage of marker-positive cells of approximately 25%. Expression of MAG did not further increase during the differentiation procedure and showed a slight decrease to 20% marker-positive cells on day 18 (Figure 20C).

An indicator for compact myelin, protein 0 (P0) did not show a significant up-regulation during the differentiation procedure and remained within a range of 10-15%. (Figure 20C).

An important factor in the differentiation of mesenchymal stem cells is also the transformation of stem cell form to a morphology similar to the cell type the differentiation is aimed at.

Characteristic morphology of mesenchymal stem cells is shown in Figure 20D1, where cells display a flattened, fibroblast-like shape with a larger nucleus, while in contrast, Schwann cells reveal a bipolar, elongated shape, displaying less matrix, but a prominent nucleus (Figure 20D4).

Figure 20D shows the change in morphology during differentiation, from mesenchymal stem cell specific (D1-D3) to Schwann cell specific forms (D4). While the expression of Schwann cell specific markers S100b, P75 and MAG starts as early as day 6 in the differentiation process (Figure 20C), a significant change in morphology cannot be observed until day 18.
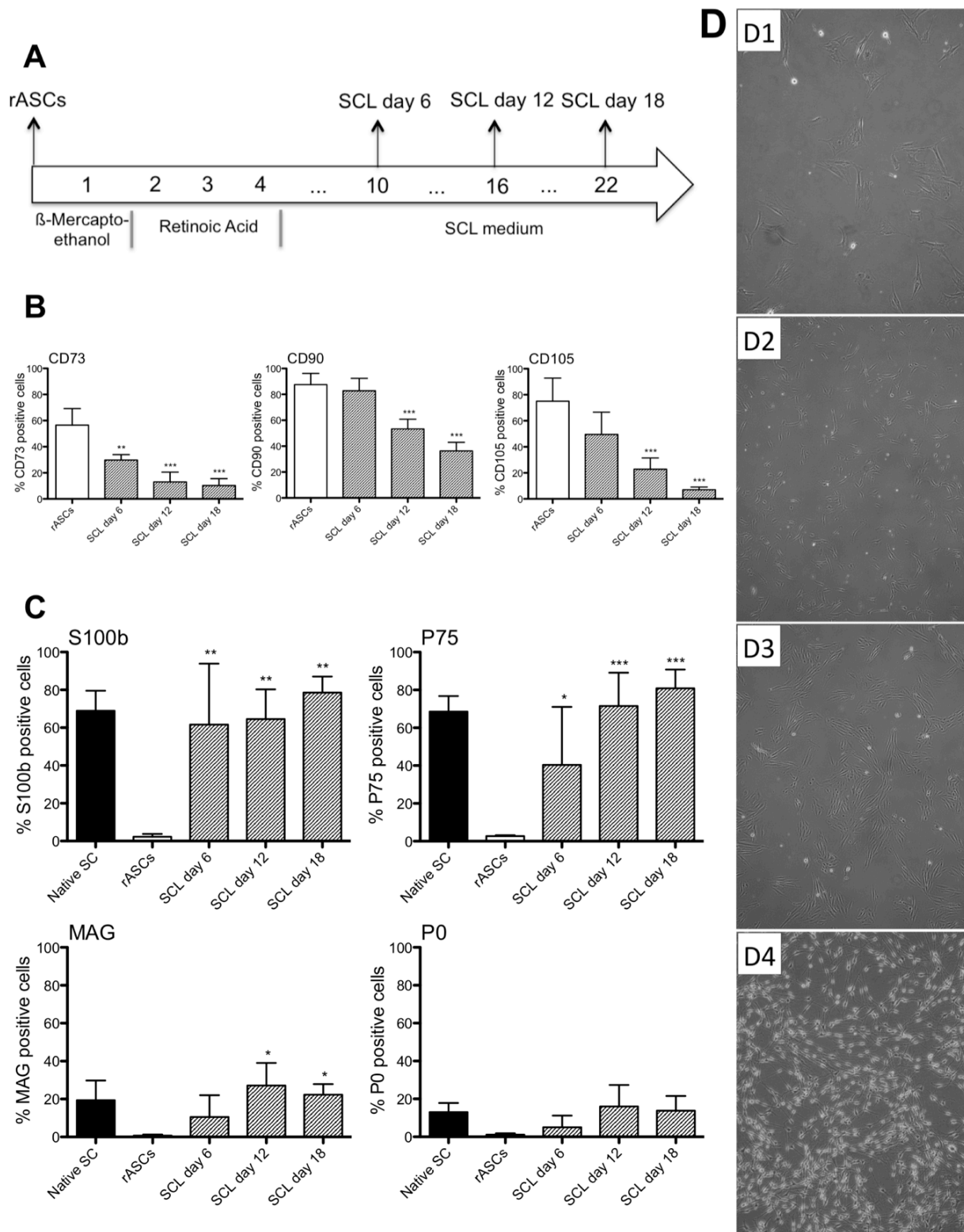
Figure 20: A: Experimental scheme depicting differentiation procedure from rASCs to SCLs and time points of evaluation with flow cytometry (marker expression) and light microscopy (morphology); B: Evaluation of SCLs with flow cytometry and stem cell specific markers (CD73, CD90, CD105) during the differentiation process, compared to undifferentiated rASCs; C: Evaluation of SCLs with flow cytometry and Schwann cell specific markers (S100b, P75, MAG, P0) compared to native Schwann cells and undifferentiated rASCs; statistical significance was tested with 1-way ANOVA and Tukey range test; data is presented as mean ± SD; *P<0.05, **P<0.01, ***P<0.0001; n=4; D: phase contrast microscopy pictures of rASCs (D1) and SCLs during the differentiation process on day 6 (D2), day 12 (D3) and day 18 (D4); scale bar indicates 200 μm.

Activation status of SCLs

To assess activation status, differentiated SCLs cultured in medium containing forskolin ("activated") and medium without forskolin (pro-myelinating) were evaluated with flow cytometry on day 0, 7, 14 and 21 after medium switch, and compared to SCs cultured with the same conditions.

7 days after medium switch native SCs showed a decrease of P75 expression from around 75-80% to less than 10%, while MAG increased from less than 20% to 55% and P0 to 70%, with S100b remaining at a comparable level in both groups (Figure 21A).

Expression of S100b is shown in Figure 21B. Cultured with or without forskolin, expression of S100b remained between 60% and 75%, showing no significant difference, increasing or decreasing between the two groups, comparable to S100b expression of native SCs.

When cultured with forskolin, P75 is expressed by SCLs on day 0 to a percentage of around 70% marker positive cells and steadily increases up to 90% on day 21. SCLs cultured without forskolin showed a decrease in P75 expression on day 7 to approximately 40% marker positive cells and decreased further to 25% on day 21. Differences in P75 expression between the two groups were significant on day 14 and day 21 (Figure 21B).

Percentage of P0 positive cells on day 0 was less than 10%, but showed an increase to 15% on day 7 when cultured with forskolin, followed by a steady decrease to again less than 10%. Cultured without forskolin, P0 was significantly up-regulated on day 7 to a percentage of approximately 65%, followed by a further increase in expression on day 14 (70%) and a decrease to 60% on day 21. Differences between the two groups were significant on day 7, day 14, and day 21.

Percentage of MAG positive cells on day 0 was, like P0, less than 10%. Cultured without forskolin, up-regulation of MAG resulted in 55% marker-positive cells on day 7, followed by a decrease to 45% on day 14 and again an increase to almost 60% on day 21. Cultured with forskolin, MAG expression in SCLs also increased on day 7 (15% MAG positive), but steadily decreased to a percentage of marker positive cells of less than 5% on day 21. Differences between the two groups were significant on day 7, day 14, and day 21.

Additionally, a change in proliferation was evaluated by measurement of 5-bromodeoxyuridine incorporation (BrdU assay). SCLs cultured without forskolin decreased their proliferation rate initially between day 0 and day 7, but remained at a comparable level and did not decrease further after this time point, while SCLs treated with forskolin showed no significant change in proliferation. Over time, mitochondrial activity (measured with MTT

assay) in both groups also remained at a level comparable to day 0 and showed no significant changes (Figure 21C).
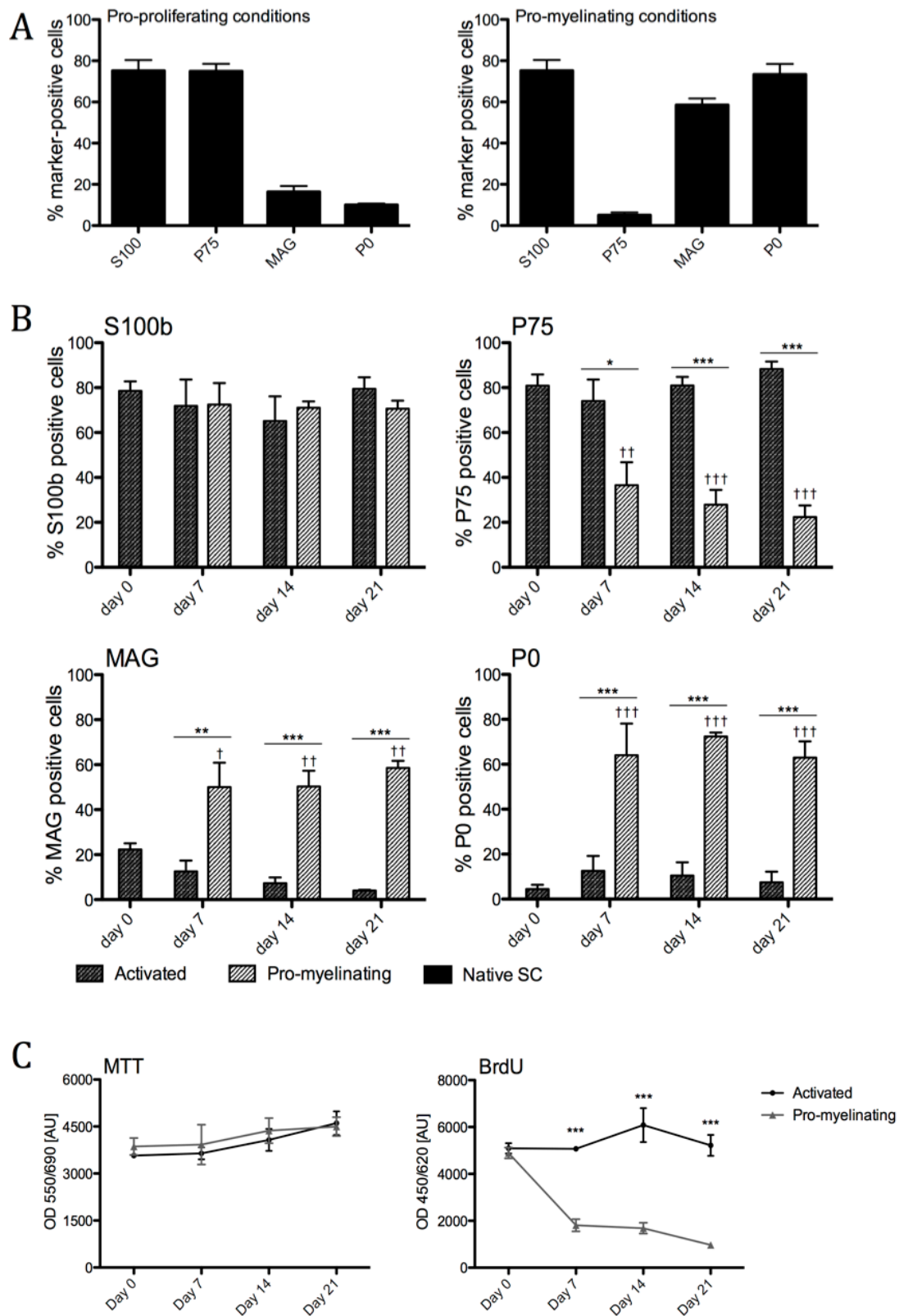

Figure 21: Flow cytometry analysis concerning expression of Schwann cell markers S100b, P75, MAG and P0 of A) SCs in activation medium and pro-myelinating medium (day 7 after medium switch) and B) SCLs in activation medium (dark grey bars) and pro-myelination medium (light grey bars) on day 0, 7,15 and 21 after

medium switch; statistical significance was tested with 1-way ANOVA and Tukey range test; data is presented as mean ± SD; *P<0.05, **P<0.01, ***P<0.0001, compared to control group on respective day; †P<0.05, ††P<0.01, †††P<0.0001, compared to day 0; C) MTT assay and BrdU ELISA of SCLs in activation medium (dark grey bar) and pro-myelination medium (light grey bar) on day 0, 7, 14 and 21; statistical significance was tested with t-test; data is presented as mean ± SD; n=4.

Electrospun Fibrin-PGLA scaffolds

Fibrous fibrin-PGLA scaffolds with parallel fibre orientation were produced using electrospinning. A high voltage (-14,7 kV) was applied to the fibrin-PGLA solution and fibres were collected on a grounded rotating wheel (16 m/s) at different ambient parameters.

Electrospinning of fibrin solution without PGLA was not possible under conditions A (28°C and 28% humidity) and B (26°C and 28% humidity) because viscosity and cohesion were not high enough to form a Taylor cone and subsequently a polymer-jet. Under condition C (24°C and 35% humidity) Taylor cone and jet formation was possible, but led to brittle, inhomogeneous fibres with poor parallel orientation (Figure 22A). Electrospinning of fibrin-PGLA solution was possible under condition A, B and C, but led to differing results. Fibrin-PGLA fibres spun under condition A (28°C and 28% humidity), shown in Figure 22B, were orientated to a certain extent, but were brittle and inhomogeneous in diameter with a range of 0.4 to 9 μm. Bead and droplet formation were observed as well. Electrospinning condition B (26°C and 28% humidity) led to highly inhomogeneous fibrin-PGLA fibres with a range in diameter of 0.4 to 11 μm. Fibres showed poor orientation and a high amount of curved fibres. Beads and droplets could be observed as well (Figure 22C). Under condition C (24°C and 35% humidity), electrospun fibrin-PGLA fibres were homogenous with a range in diameter of 500 to 900 nm. No beads or droplets were observed and to a certain extent, fibres showed parallel orientation. A small amount of curved, non-orientated fibres can be seen in Figure 22D, resulting from minor bead formation.
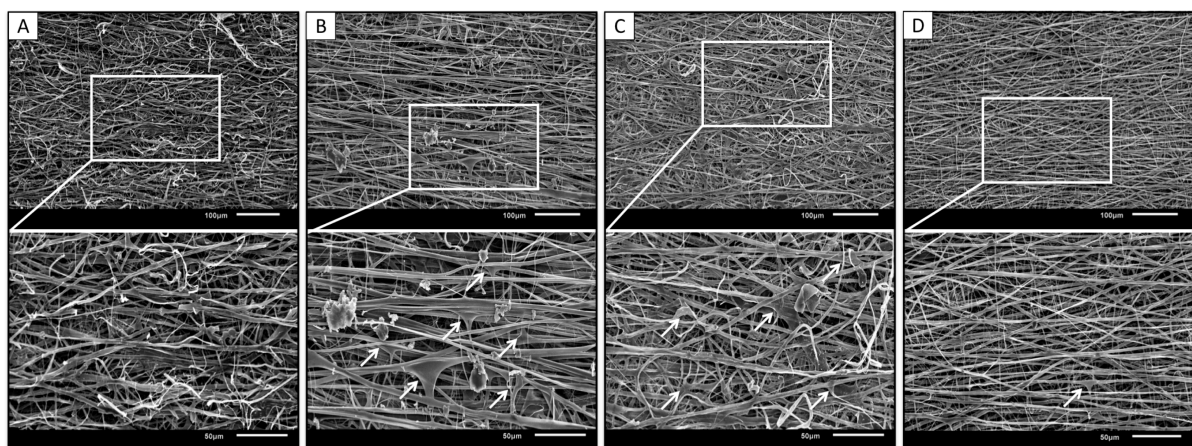

Figure 22: Scanning electron micrographs of electrospun fibres; fibrin fibres obtained at an ambient temperature of 24°C and humidity of 35% (A); fibrin-PGLA fibres obtained at an ambient temperature of 28°C and humidity of 28% (B), 26°C and 28% (C) and 24°C and 35%; arrows indicate beads (D).

Cell-scaffold interaction

Schwann cell-like cells seeded on electrospun fibrin-PGLA scaffold attached to the scaffold and oriented along the direction of the fibres (Figure 23A-C). On day 3 (Figure 23B), and day 7, (Figure 23C) proliferation along the fibres can be observed, while undifferentiated rASCs (Figure 23D), SCLs (Figure 23E) and Schwann cells (Figure 23F) cultivated in culture plates did not show directed cell growth.
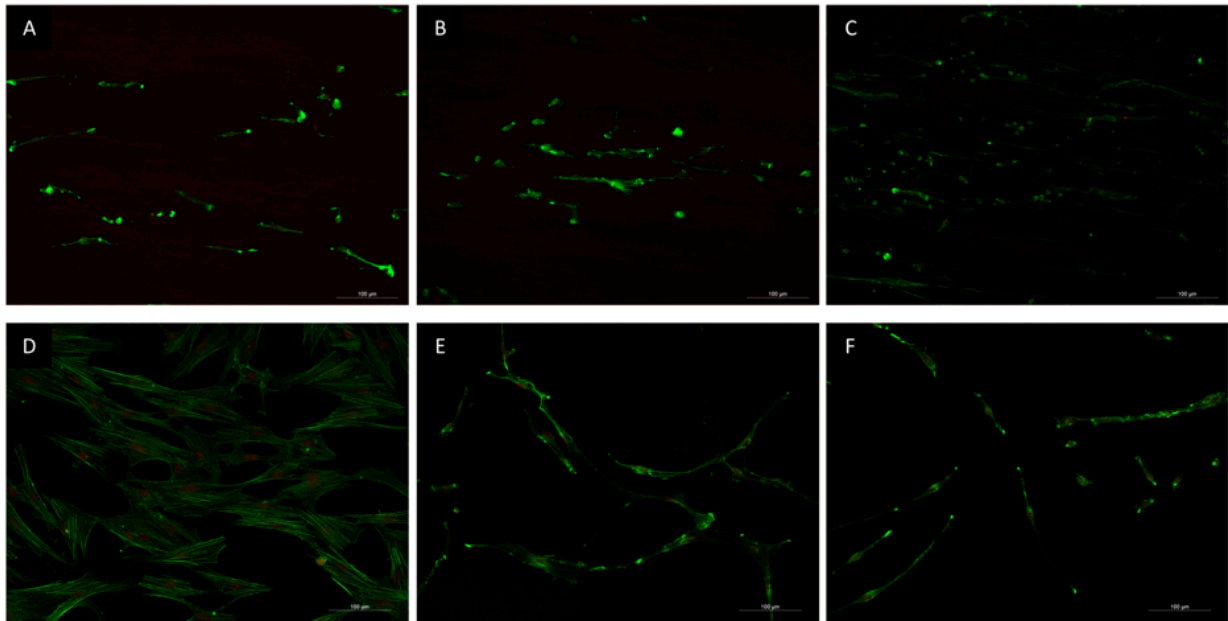
Figure 23: Fluorescence micrographs of SCLs seeded on electrospun fibrin-PGLA scaffold, stained with AlexaFluor 488 phalloidin (green) and propidium iodide (red) on day 1 (A), day 3 (B) and day 7 (C) after cell seeding; undifferentiated rASCs (D), SCLs (E) and native Schwann cells (F) seeded on a cell culture dish (control); scale bar indicates 100 μm.

Self-shaping fibrin tubular structures

For further *in vivo* use, it is necessary to place the fibrin-PGLA scaffold seeded with Schwann cell-like cells inside a protective silicone tube without damaging the cells. Therefore a self-shaping fibrin gel containing rASCs was used as supportive structure.

Figure 24 depicts the self-shaping process of the fibrin gel containing the scaffold and SCLs to a tube-like structure from day 0 (Figure 24 A) to day 14 (Figure 24 C). First contractions of the gel are visible after 7 days in culture (Figure 24 B), when the gel folds up rather than rolls up. Fully contracted, fibrin gel covers scaffold and cells (Figure 24 C) inside a folded roll.
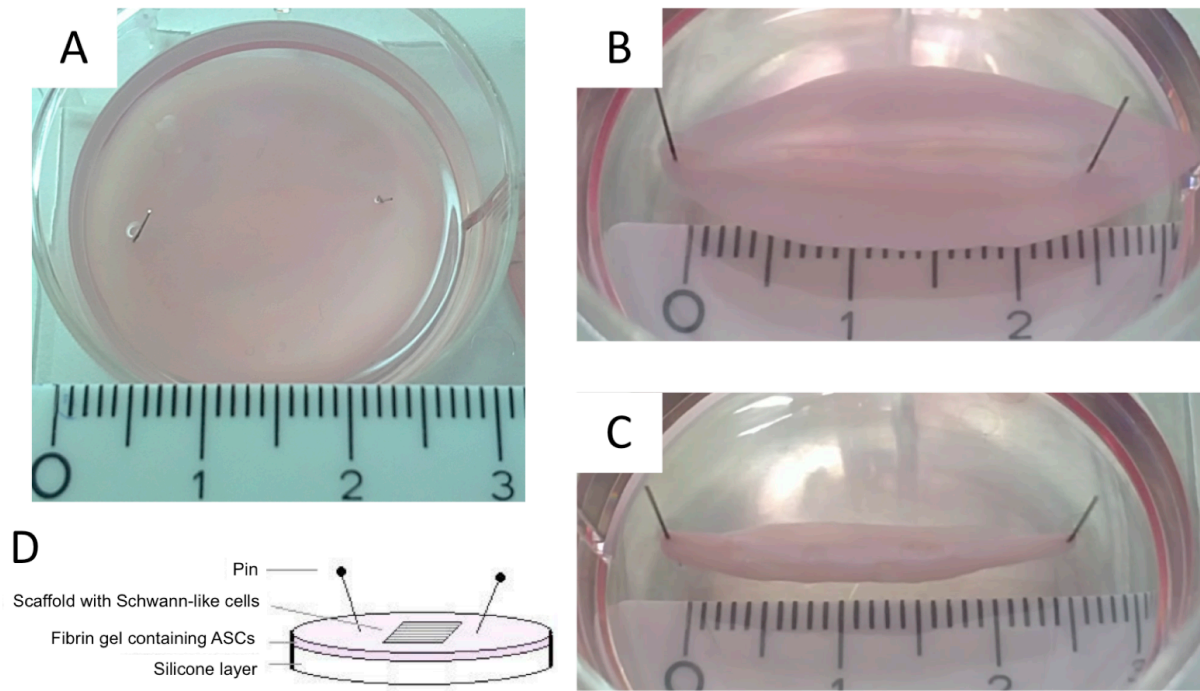
Figure 24: Fibrin gel-scaffold construct with SCLs seeded on the electrospun scaffold on day 0 (A), day 7 (B) and day 14 (C) after cell seeding; D: Scheme of fibrin gel-scaffold construct.

DISCUSSION

Differentiation of rat rASCs into SCLs

Schwann cells have a strong supporting role in peripheral nerve regeneration (150), which suggests a transplantation to defect sites to enhance axonal regeneration. Culturing Schwann cells *in vitro* is a tightrope act between high costs and dedifferentiation. Autologous Schwann cells might not result in sufficient numbers for large gaps and require a second incision site, while allogenic Schwann cells show immunogenic reactions, enhanced by their ability to modulate immune response, present antigens and secret cytokines (151).

rASCs isolated from adipose tissue expressed stem cell markers to a moderate extent. Dominici *et al.* (52) stated, as one of three minimal criteria, that stem cell cultures must show a minimal percentage of 95% of CD73, CD90 and CD105 positive cells. In our cultures, flow cytometry revealed percentages of marker positive cells that are below this 95% limit, especially regarding CD73. Nevertheless, isolated cells were positive for plastic adherence under standard conditions and could be differentiated into osteogenic and adipogenic lineages (Figure 19), indicating a stem cell-enriched culture.

During the differentiation procedure, stem cell markers CD73, CD90 and CD105 decreased significantly from day 6 to day 18 (Figure 20B). Differentiating rASCs show a prompt reaction to growth factors by expression of Schwann cell markers S100b and P75 at comparable levels to native Schwann cells (Figure 20C). MAG and P0 are expressed to a lesser extent (Figure 20C), which does not diminish the differentiation results, as P75 and the myelin components P0 and MAG are, to a certain extent, antagonists, and it is known that these molecules inhibit axonal outgrowth and regeneration (152).

Even though there is no significant change in S100b and P75 expression between day 6 and day 18, the constant decrease in stem cell marker expression over the time period of 18 days indicates a progressive loss of multipotency and therefore slow manifestation of differentiation. This progress can also be seen in the slow morphological change from mesenchymal stem cell-typical morphology (Figure 20 D1-D4), with flattened and fibroblast-like cells, to Schwann cell-typical morphology, with bipolar, elongated cells and a prominent nucleus, comparable to Schwann cell morphology shown in the literature (108,153). Expression of Schwann cell markers and changes to Schwann cell morphology indicate a differentiation into "Schwann cell-like cells".

Activation status of SCLs

Since Schwann cells appear in several phenotypes and two activation states, evaluation of SCLs for status-specific markers is of utmost importance, especially when used for augmenting regeneration in the treatment of nerve defects. It is desirable that SCLs can be transformed from a proliferating phenotype into a pro-myelinating or myelinating phenotype. While the expression of P0 in the proliferating phase of nerve regeneration might inhibit regeneration, the failure to express P0 and MAG, and therefore the failure to remyelinate after a change of stimulus, would impair saltatoric conduction. (92,154,155) Furthermore, continued *in vivo* proliferation of SCLs after the axon has grown through the tube can result in undesirable neuroma formation. Therefore, SCLs were treated with different growth factor mixtures (with and without forskolin), creating a minimal change of stimulus to resemble the switch from pro-proliferating and pro-myelinating environments.

When cultured with forskolin, flow cytometry results showed a high and stable expression of P75 and S100b, while MAG and P0 were expressed to a moderate extent (< 20%) and continued proliferating over the following passages at levels similar to native Schwann cells. This indicates a proliferating, non-myelinating status. Cultured without forskolin, MAG and

P0 showed a prompt and significant increase within 7 days, while P75 significantly decreased. Proliferation was also significantly decreased, indicating a change in activation status towards myelination.

These findings prove our hypothesis that Schwann cell-like cells differentiated from rat adipose-derived mesenchymal stem cells cultured with forskolin can be called "*Activated Schwann cell-like cells*", due to proliferation as well as S100b and P75 expression, while cultured without forskolin they can be called "*Pro-myelinating Schwann cell-like cells*", due to their MAG, P0 and decreased proliferation. (26,91)

In studies of peripheral nerve regeneration, hollow tubes as nerve grafts have been shown to neither inhibit nor enhance axon outgrowth in non-critical gaps. In over-critical gaps (> 3 cm), hollow tubes are unfavourable due to the lack of autologous matrix inside the tube. The benefits of guiding structures inside a tube, whether single fibres, pores or fibrous scaffolds, are evident. (156)

Electrospinning on a rotating wheel collector allows the formation of fibrous scaffold sheets, which can then be seeded with cells and roll-folded, and placed inside a protective tube.

Important factors affecting spinning quality are not only the choice of polymer solution (fibrin or fibrin-PGLA), but also the ambient parameters temperature and humidity. (157)

Ambient parameters affect viscosity and cohesion of the polymer solution, altering the jet behaviour (droplet formation and second jets) and influencing the homogeneity of the fibres. Furthermore, it also leads to an overly rapid solvent evaporation, resulting in brittle fibres with low internal scaffold stability.

Fibrin-PGLA spun at 24°C and 35% humidity could be characterized as smooth in handling, with highly aligned, homogenous fibres and was used for further experiments.

Morphological changes due to surface patterns are known in other cell types, including fibroblasts (158) or smooth muscle cells (159) and are especially important in Schwann cells. The formation of Bands of Büngner *in vitro* prior to implantation has a promoting effect on axon sprouting *in vivo*. (160)

The attachment, orientation and proliferation of Schwann cell-like cells seeded on fibrin-PGLA fibres were analyzed. A distinct orientation of elongated, bipolar Schwann cells along the fibres was visible when actin filaments were stained with Alexa-Fluor 488 phalloidin, indicating the initial formation of aligned and directional Büngner-like structures. It was possible to adapt the method from Huang *et* al. (149) to create a tubular structure by a self-shaping hydrogel. With this method we could address the issue of standardizing the folding process of the aligned electrospun fibres containing SCLs.

CONCLUSION

In this study we showed that rASCs can be differentiated into activated, proliferating Schwann cell-like cells and that these cells react to a minimal change in stimulus, switching to a pro-myelinating phenotype. Highly aligned electrospun fibrin-PGLA fibres promote the formation of Büngner-like structures of the SCLs and rolled into a folded tubular structure. These *in vitro* findings favour further *in vivo* studies.

ACKNOWLEDGEMENTS

CHAPTER III

Functionalizing silk fibroin to serve as an improved biomaterial for nerve regeneration

A new preparation method for anisotropic silk fibroin nerve guidance conduits and its evaluation *in vitro* and in a rat sciatic nerve defect model

Andreas Teuschl[1,2,3], Christina M.A.P. Schuh[1,2,3], Robert Halbweis[2,3], Gábor Márton[4], Krisztián Pajer[4], Rudolf Hopf[2,3], Shorena Mosia[2,3], Dominik Rünzler[1,2], Heinz Redl[2,3], Antal Nógrádi[2,3,4], Thomas Hausner[2,3,5,6],

[1]University of Applied Sciences Technikum Wien, Department of Biochemical Engineering, Vienna, Austria
[2]The Austrian Cluster for Tissue Regeneration, Vienna, Austria
[3]Ludwig Boltzmann Institute for Experimental and Clinical Traumatology / AUVA Research Center, Vienna, Austria
[4]Department of Anatomy, Histology and Embryology, Faculty of Medicine, University of Szeged, Hungary
[5]Department of Traumatology, Lorenz Böhler Hospital, Austrian Workers' Compensation Board, Vienna, Austria
[6]Department for Trauma Surgery and Sports Traumatology, Paracelsus Medical University, Salzburg, Austria

ABSTRACT

Over the last decade, silk fibroin has been emergently used in peripheral nerve tissue engineering. Current approaches aiming to produce silk fibroin based nerve guidance conduits (SF-NGCs) used dissolved silk either based on aqueous solutions or organic solvents. In this study, we describe a novel procedure to produce SF-NGCs: a braided tubular structure of raw Bombyx mori silk is subsequently processed with the ternary solvent $CaCl_2/H_2O$/ethanol, formic acid and methanol to improve its mechanical and topographical characteristics.

Topographically, the combination of the treatments results in a fusion of the outer single silk fibres to a closed layer with a thickness ranging from about 40 to 75 μm. In contrast to the outer wall, the inner lumen (not treated with processing solvents), still represents the braided structure of single fibres. Mechanical stability, elasticity and kink characteristics were evaluated with a custom-made test system. The here described modification procedure drastically improved the elastic properties of our tubular raw scaffold favouring its use as a NGC. A cell migration assay with NIH/3T3-fibroblasts revealed the impermeability of the SF-NGC wall for possible invading and scar-forming cells. Moreover, the potential of the SF-NGC to serve as substratum for Schwann cells has been demonstrated by cytotoxicity tests and live-dead stainings of Schwann cells grown on the inner surface of the SF-NGC.

In vivo, the SF-NGC was tested in a rat sciatic nerve injury model. In short term *in vivo* studies it was proven that SF-NGCs are not triggering host inflammatory reactions. After 12 weeks we could demonstrate morphological and functional reinnervation of the distal targets. Filled with collagen, a higher number of axons could be found in the distal to the graft (1678±303), compared to the empty SF-NGC (1274±146).

The novel SF-NGC presented here shows promising results for the treatment of peripheral nerve injuries. The modification of braided structures to adapt its mechanical and topographical characteristics may support the translation of SF-based scaffolds into the clinical setting. However, further improvements and the use of extracellular matrix molecules and Schwann cells are suggested to enable silk tube based conduits to bridge long distance nerve gaps.

Key words: silk fibroin, modification, nerve guidance conduit, peripheral nerve regeneration

INTRODUCTION

The incidence of peripheral nerve injury in traumatic wounds of the extremities is approximately 2-5% (2,41,161). Moreover, tumor resection or congenital malformation may also lead to nerve damage. Consequently, these incidences display a major burden on health care expenses, extensive absence from work, and chronic disability (2,41). Direct repair of nerves is one clinical option, however, this direct end-to-end coaptation is limited to short-distance gaps. The current clinical gold standard for the repair of longer nerve gaps is the use of autologous nerve grafts (9,161,162). The main advantage of autografts is their morphologically native structure, which provides an ideal guide for axonal regeneration from the proximal to the distal nerve stump. However, autografting carries several disadvantages such as limited number of donor sites for graft harvesting and associated donor site morbidity, including loss of nerve function, painful neuroma formation and hyperaesthesia (156,163). These negative aspects have led to the search for alternative approaches. Beside nervous tissue, other autologous materials, such as vein grafts (164,165) or muscles (166,167) have been used to bridge nerve gaps. However, the use of these substances is both preclinically and clinically unsatisfactory. Recent advances in tissue engineering (TE) have opened new opportunities in peripheral nerve repair. Artificial nerve guidance conduits (NGCs), composed of synthetic or natural polymers, are currently being investigated for bridging nerve defects (162,168,169). The rationale behind using a NGC is to entubulate the nerve stumps to provide a protective micro-environment for the regenerating peripheral nerve. While numerous synthetic and natural biomaterials have been evaluated, both pre-clinically and clinically, for the bridging of nerve defects, their therapeutic benefits (170,171) still remain unsatisfactory.

In the last few years, silk fibroin (SF) has attracted considerable interest as a biomaterial suitable for applications towards peripheral nerve regeneration. SF has been shown to possess characteristics that favour its use as a NGC, such as mechanical stability, slow degradation rate, biocompatibility and its ability to support nerve regeneration (40,41). Apart from biocompatibility, a NGC should act as a barrier for infiltrating fibroblasts and provide mechanical resistance against compression and kinking by the surrounding tissue. Most of the current approaches to create tubular structures use electrospinning, as this process can be well controlled (41,172–175). Other techniques include dipping (176,177), gel spinning (178,179) or molding (180). All the above-mentioned preparation techniques are based on dissolved SF which is then used to create a tubular construct. For the first time, to our knowledge, our study

attempts to use textile-engineered raw silk constructs as the starting material for bridging a nerve defect. To improve the mechanical properties favouring its use as a NGC these braided tubular structures are further processed by treatment in a ternary solvent system of a CaCl$_2$/H$_2$O/ethanol solution and then re-stabilized with formic acid.

The aim of this study was to develop a novel method to generate a silk fibroin-based NGC with distinct mechanical and anisotropic properties, and to prove its biocompatibility and functionality *in vitro* and *in vivo* in a rat sciatic nerve injury model.

MATERIALS AND METHODS

Unless otherwise noted, all reagents were obtained from Sigma (Vienna, Austria) and are of analytical grade.

Design and preparation of silk conduits

White raw Bombyx mori silkworm fibres of 20/22 den, 250 T/m, were purchased from Testex AG (Zürich, Switzerland). The tubular silk conduit was fabricated in cooperation with a commercial braiding company (Edelrid GmbH, Isny/Allgäu, Germany). Six single silk fibres form a twisted yarn, representing the raw material for the commercial braiding machines. Figure 25 shows the tubular structure designed from six intertwined twisted yarns. The resulting raw silk conduit was degummed by boiling in 0.2 M boric acid in a 0.05 M sodium borate buffer (pH = 9.0) (181). Batches of 2 g of silk conduits were boiled twice in 500 mL of degumming solution for 45 min, with an intermittent exchange of the degumming solution. After degumming, scaffolds were thoroughly washed in double distilled water (ddH$_2$O) and air-dried before further processing (Figure 25).

The degummed SF tubes were placed on an ABS (acrylonitrile butadiene styrene) rod, having a diameter of 2 mm and dipped into a boiling solution of the ternary solvent calcium chloride/distilled water/ethanol (CaCl$_2$/H$_2$O/ethanol) in a molar ratio of 1:2:8 for 20 seconds. Immediately after etching the outer surface, the tubes were dipped in 100% of formic acid (FA) at room temperature for 20 seconds. The tubes were then fixed in methanol for 20 minutes and subsequently washed thoroughly with ddH$_2$O (Figure 25). The tubes were dried under laminar airflow and sterilized by autoclaving prior to use.

Endurance and fatigue tests

To test the elasticity of the SF-NGC in comparison to the unprocessed initial tubular SF-scaffold, a custom-made compression test machine was built (Suppl. Fig. 1). This device was designed for repeated compression of a test specimen with constant maximum pressure. Starting from the top position, a piston is moved downwards by a servo motor (Modelcraft RS2 MG/BB standard servo, Conrad Electronic SE, Hirschau, Germany) at a speed of approximately 5 mm/s linearly until it touches the probe. The piston continually stresses the probe until a predefined force threshold is reached. A force sensitive resistor (Strain gauge FSR 151, Interlink electronics, Camarillo, CA, USA), integrated into the piston, acts as a sensor and is part of a voltage divider. The resistance, and thus the applied force, is constantly sampled at 50 Hz sampling frequency using the built-in 10 bit AD-converter of the microcontroller (Arduino Duemilanove Controller Board with Atmega 328 μC, Atmel Munich GmbH, Garching/Munich, Germany). The system was calibrated using a laboratory scale and operates with a ± 5 g accuracy (corresponding to 0.98 MPa). Once the threshold is reached, the piston is returned to the top position, where it remains for a period of time set by the user.

In order to evaluate the effect of the various treatment components four types of tubes have been evaluated (Figure 26). The first type was produced by degumming of the raw tube followed by methanol treatment. The second and third types were created either by $CaCl_2/H_2O$/ethanol - or formic acid- treatment, both fixed with methanol. The fourth type of tube was produced as described above, combining all sequential treatments (Figure 25).

Prior to testing, respective samples were hydrated in PBS overnight. For testing, the conduits were fixated with cannulas (B.Braun, Austria) in a Sylgard-plated Petri dish (Sylgard® 184, Dow Corning Europe S.A., Seneffe, Belgium) and covered with PBS. The mechanical test regimen consisted of 1000 cycles of compression (300 ms duration and 58.8 MPa load) and release. After testing the tubes were air-dried overnight at room temperature and an approximately 1 mm thick slice was cut out from them at the impression site for morphological analysis. The deformity after the compressions was assessed by scanning electron microscope analysis.

Scanning electron microscope analysis

Samples were fixed in 2.5% glutaraldehyde in cacodylate buffer overnight at room temperature, then washed and dehydrated through graded ethanol changes followed by treatment with hexamethyldisilazane, and allowed to air-dry in a fume hood. Coating with Pd-Au was performed through the use of a Polaron SC7620 sputter coater (Quorum Technologies Ltd. East Grinstead, United Kingdom) and the samples were examined using a JEOL JSM-6510 scanning electron microscope (JEOL Ltd., Tokyo, Japan) operated at 15 kV.

Cell culture experiments

NIH/3T3

NIH/3T3 cell line was purchased from ECACC (European Collection of Cell Cultures, UK). NIH/3T3 cells were cultured in DMEM containing 10% fetal bovine serum (FBS, Lonza Ltd., Basel, Switzerland) supplemented with 2 mM L-glutamine, 100 U/mL penicillin and 0.1 mg/mL streptomycin in plates coated with 0.2 % gelatin solution.

Schwann cells (SCs)

Schwann cells were isolated from rat sciatic nerves as described by Kaekhaw *et al.* (108). All animals were housed in the facilities of the Ludwig Boltzmann Institute for Experimental and Clinical Traumatology in a temperature-controlled environment. Animals were provided with food and water ad libitum. All experimental protocols were approved by the City Government of Vienna, Austria, in accordance with the Austrian law and Guide for the Care and Use of Laboratory Animals as defined by the National Institute of Health.

The sciatic nerves were dissected free of connective tissue and minced after removing the epineurium. Nerve fragments were incubated with 0.05% collagenase for 1 hour at 37°C, subsequently filtered through a 40 μm cell strainer and centrifuged at 400g for 6 minutes. After washing the cell pellet in DMEM containing 10% FCS, the pellet was resuspended in Schwann cell culture medium consisting of DMEM-D-Valine (PAA, Austria) supplemented with 10% FBS, 2 mM L-glutamin, 1% antibiotics, N_2 supplement, 10 μg/ml bovine pituitary extract and 5 μM forskolin. Cell suspension was seeded on 6-well plates coated with poly-L-lysin and laminin.

Schwann cells were seeded on the inner wall of the SF-NGC at a concentration of 105 cells/mL. Three groups were set: in group 1 only degummed (boric acid treatment) silk tubes

were used, in group 2 the silk tubes were further treated with $CaCl_2$ (degumming + $CaCl_2$), whereas group 3 tubes received a full treatment completed with formic acid (degumming + $CaCl_2$ + FA). As a final step all tubes were fixed with methanol. After 2 hours, cells were supplied with Schwann cell culture medium. Schwann cell attachment to the inner wall structure of the SF-NGC and viability was evaluated after 48 hours with Calcein AM/propidium iodide staining (Invitrogen, Vienna, Austria).

Cell permeability

A cell migration assay was designed to verify the cell impermeability of the SF-NGC. A 100 µl fibrin clot (Tisseel, Baxter, Vienna, Austria) containing platelet derived growth factor-AA (PDGF-AA) was used to induce cell migration. Prior to the addition of 250 Units/mL of thrombin to induce polymerization, 10 ng of PDGF-AA (Peprotech Austria, Vienna, Austria) was thoroughly mixed in fibrinogen. The resulting dense fibrin structure provides a slow release of PDGF-AA. This fibrin clot was then placed inside the investigated tubes and the assembled constructs were pinned in silicone-coated (Sylgard® 184, Dow Corning Europe S.A., Seneffe, Belgium) 12-well plates. Besides enabling the fixing of the constructs to a Petri dish, Sylgard® 184 is known to discourage cell adhesion as a result of its hydrophobic character (182) and therefore prevents cell migration from one clot to the other over the surface of the cell culture plate. As a result, the only way for the cell to move from one clot to the other is to pass through the SF-NGC. This thereby permits the assessment, if any, of the NGC's cell permeability. A second 100 µl fibrin clot containing $2.5x10^5$ NIH/3T3 fibroblasts was placed on top of the tube. For this clot, cells were suspended in fibrinogen and then the polymerization was initiated with 2 units/mL thrombin. The generated loose fibrin structure allows fibroblasts to migrate from the clot towards the chemotactic stimulus. As a positive control, the fibrin clot with cells was separated from the clot containing PDGF-AA using the nylon mesh of a cell strainer with a 100 µm pore size. (Becton Dickinson Ltd., Schwechat, Austria). The constructs were completely covered with cell culture medium. On day 6, cell migration was evaluated by staining the PDGF-AA-containing fibrin clot with Calcein AM (Invitrogen, Vienna, Austria).

Cytotoxicity assay

To test cytotoxicity of the prepared SF-NGC, 1 g of the material was immersed in 5 mL cell culture medium for at least 24 h. In parallel, $2 x 10^4$ Schwann cells per well were seeded onto

24-well plates. Then the medium containing leach-out products from the material was filtered (0.22 μm, Rotilabo, Karlsruhe, Germany) and used to change media in the cell cultures. Standard culture medium was used as a negative control. After 72 h, cell culture medium was aspirated and the respective cell culture medium containing 650 μg/mL MTT [3-(4,5-dimethylthiazol-2-yl)-2,5-diphenyltetrazolium] bromide was added to each well. After 1 h of incubation at 37° C and in 5% CO_2, the medium was aspirated and MTT formazan precipitate was dissolved in DMSO by shaking mechanically in the dark for 20 min. Aliquots of 100 μl of each sample were transferred to 96-well plates. The absorbance at 540 nm was read immediately on an automatic microplate reader (Spectra Thermo, TECAN Austria GmbH, Austria). Optical density (OD) values were corrected for unspecific background.

Animals and surgery

All animals were housed in the facilities of the Ludwig Boltzmann Institute for Experimental and Clinical Traumatology in a temperature-controlled environment. Animals were provided with food and water ad libitum. All experimental protocols were approved by the City Government of Vienna, Austria in accordance with the Austrian law and Guide for the Care and Use of Laboratory Animals as defined by the National Institute of Health.

A total of 28 female Sprague-Dawley rats (Animal Research Laboratories, Himberg, Austria), weighing between 250 – 350 g were used in the experiments. Possible adverse effects against the implanted SF-NGCs and the initial axon outgrowth into these tubes were evaluated on day 7, 10 and 21 day (n=2, 6, 2, respectively). Eighteen animals were randomly assigned into three different treatment groups: autologous grafting (n = 6), SF-NGC (n = 6) and collagen-filled SF-NGC (n = 6) for 12 weeks observation. The animals were weighed and anesthetized in a fume box with 3.5% isoflurane (Forane®, Abbott, Vienna, Austria) at a flow rate of 800 mL/min. Subsequent anesthesia throughout the surgical procedure was maintained using 2.5% isoflurane via a nosepiece. The right lower limb in each animal was shaved and disinfected with povidone-iodine (Betaisodona®, Mundipharma, Vienna, Austria) at the mid-thigh level. All the following surgical procedures were carried out under an operating microscope (Leica M651, Leica Microsystems, Vienna, Austria). The sciatic nerve was exposed and an 8 mm segment of the sciatic nerve was excised resulting in a 10 mm gap due to elastic retraction. In the autologous grafting group, the excised 8 mm segment of the sciatic nerve was rotated 180° and then sutured to the proximal and distal stumps using Ethilon 8/0 epineurial sutures (Ethicon-Johnson & Johnson, Brussels, Belgium). In both SF-NGC groups, the conduit was

82

implanted by insertion of the proximal and distal nerve stumps into the 12 mm tube and coaptated to the conduit by two epineurial sutures. In the SF-NGC-collagen group, the lumen of the SF-NGCs was filled with 8 microliters of collagen solution (Type I, 2.5 mg/ml, Millipore, Vienna, Austria). Afterwards the wound was closed in anatomical layers. The analgesic treatment was administered in form of 0.75 mg/kg bodyweight (BW) meloxicam (Metacam®, Boehringer Ingelheim, Ingelheim/Rhein, Germany) and 1.25 mg/kg BW butorphanol (Butamidor®, Richter Pharma AG, Wels, Austria) immediately before the surgical procedure and for two days thereafter.

Tissue sampling, perfusion and immunohistochemistry

Twelve weeks after surgery the animals were deeply anesthetized by inhalation of 3.5% isoflurane and euthanized with 110 mg/kg BW ketamine hydrochloride (Ketasol®; Dr. E. Graeub AG, Berne, Suisse) and 12 mg/kg BW xylazine (Rompun® 2 %, Bayer AG, Vienna, Austria) intraperitoneally. Animals were perfused transcardially with 4% paraformaldehyde in a 0.1 M phosphate buffer (pH 7.4). The autologous transplants or the implanted SF-NGC were harvested under the operating microscope along with the proximal and distal nerve stumps.

The nerve grafts or conduits (n=6 per group), removed from perfusion-fixed animals, were immersion-fixed for 6 h in 4 % paraformaldehyde and then cryoprotected in 30% sucrose in PBS. Parallel cryostat sections were cut on a Leica 1850 cryostat (Leica Microsystems, Vienna, Austria) and sections were either stained with cresyl violet or processed for 200 kD neurofilament immunohistochemistry. Section were treated with a 1% milk powder solution and incubated with an anti-200 kD rabbit neurofilament antibody overnight at 4°C (Abcam Ltd, UK, Lot. No.: ab8135, rabbit, 1:1000). Subsequently, sections were treated with an anti-rabbit Alexa 546 secondary antibody for 2 h at room temperature, protected with a coverslip and investigated under an epifluorescence microscope (Olympus FX-50, Olympus Ltd, Tokyo, Japan).

The sciatic nerve segment distal to the graft was transferred into a 2.5% phosphate-buffered glutaraldehyde solution after perfusion and immersion fixed for 24 h. Remnants of fixative were carefully washed out from the nerve, and the tissue was treated in 1% OsO_4 in PBS (Agar Scientific, Stansted, UK) for 1 h, dehydrated in a graded ethanol series and propylene oxide and then embedded in Durcupan (Fluka, Switzerland). Semithin sections (0.4 μm thick)

were cut 2 mm distal to the graft on a Leica Ultracut-R ultramicrotome and stained according to Rüdeberg (183).

Locomotor tests - Gait analysis (CatWalk™)

To evaluate the functional recovery of the animals Catwalk gait analysis system (version 7.1, Noldus, Wageningen, The Netherlands) was used. This method allows an objective quantification of multiple static and dynamic gait parameters (184,185). The animals were trained to use the runway before the surgery for a period of 3 weeks. Postoperatively, animals were evaluated once a week from week 4 to week 12. Various parameters for locomotor functional recovery including print area, maximum intensity, stance time and duty cycle were determined. The intensity of the right hind paw was expressed as a percentage of the contra-lateral left hind paw. The Catwalk experiments were performed in a blinded fashion.

Electrophysiology

At the end of the defined regeneration period (12 weeks), electrophysiological analysis (NeuroMax-XLTEK, Oakville, ON, Canada) was carried out before sacrificing the animals. Stimulation electrodes were placed 2 mm proximal and 2 mm distal to the graft for calculation of the nerve conduction velocity. A needle electrode was placed as a recording electrode into the tibialis anterior muscle, and the sciatic nerve was stimulated for 0.05 ms first proximally and then distally to the graft, so as to achieve the supramaximal stimulation amplitude. The compound action potential, the amplitude and the nerve conduction velocity were determined. All measurements were carried out at a temperature between 38 and 39° C.

Statistical analysis

Statistical analysis was performed using Graph Pad Prism software (Graph Pad Software Inc., San Diego, CA, USA). Normal distribution of data was tested with the Kolmogorov-Smirnov test. One-way ANOVA followed by Tukey´s post hoc test was used to assess statistical significance and p-values below 0.05 were considered statistically significant. All graphs in this study are shown as mean ± standard deviation (SD).

RESULTS

Structural changes during processing of silk tubes

Figure 25 A-C shows the raw SF-NGC consisting of braided single silk fibres. After degumming, the SF-NGC was subsequently treated with $CaCl_2/H_2O$/ethanol and FA for 20 seconds each, followed by fixation with methanol (Figure 25A). This treatment resulted in a fusion of the outer single silk fibres to a closed layer with a varying thickness ranging from 40 to 75 μm (Figure 25 D-F). Treatment with $CaCl_2/H_2O$/ethanol for less than 20 seconds resulted in thinner outer layer (Figure 25 G). In contrast, the luminal wall of the tube which was not treated with the various solvents, preserved its original braided structure (Figure 25 F). Figure 26 shows the time-dependent effects of $CaCl_2/H_2O$/ethanol and FA on the SF fibres. SF fibres solely treated with $CaCl_2/H_2O$/ethanol dissolve and precipitate, especially after 40 seconds. In contrast, FA-treatment alone disorganizes the original braided structure in a time-dependent manner.
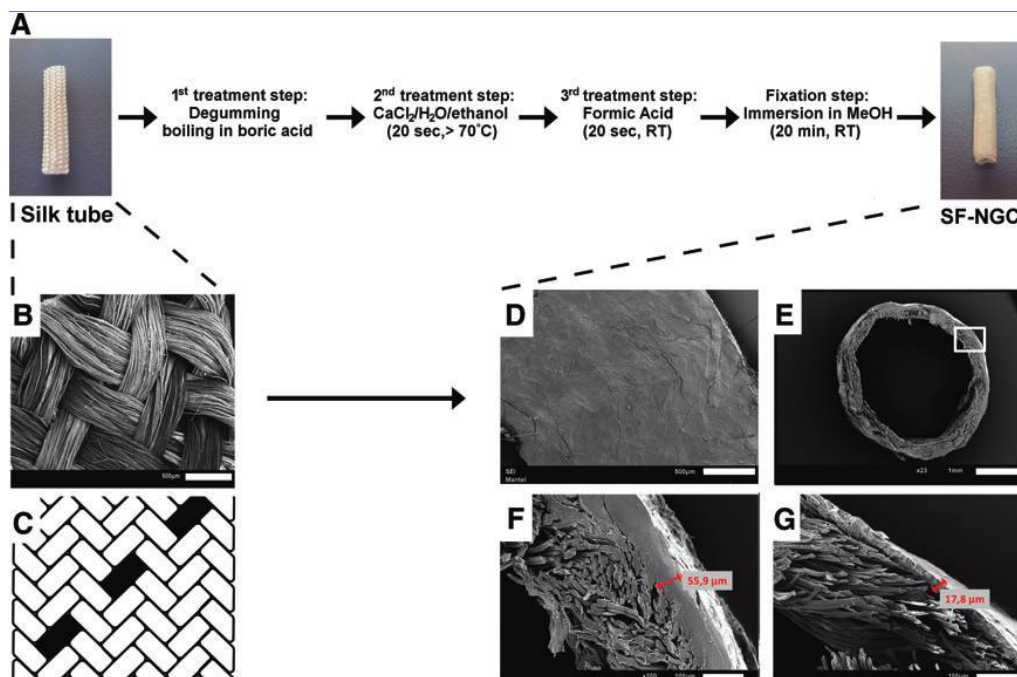
Figure 25: Overview of the preparation method of the silk fibroin (SF) nerve guidance conduit (NGC). (A) shows a scheme of the treatment steps modifying a tubular braided structure based on SF fibres and generating a NGC. Scanning electron micrograph of the raw tubular structure of SF-based NGCs are shown before (B) and after (D-F) subsequent treatment with a ternary solvent of calcium chloride, ethanol and water in a molar ratio of 1:2:8 (1st treatment step: in $CaCl_2/H_2O$/ethanol for 20 sec, >70°C), formic acid (2nd treatment step: Formic Acid (FA), for 20 sec at room temperature (RT)) and a final fixation step with Methanol (MeOH, for 20 min at room temperature). E: cross-sectional view of SF-NGC, D) Lateral view of SF-NGC, F) enlarged view of the framed area in E). C indicates the initial braiding design of the raw unprocessed NGC. In G) the SF structure was only treated for 10 sec in $CaCl_2/H_2O$/ethanol and FA, resulting in a thinner outer layer.
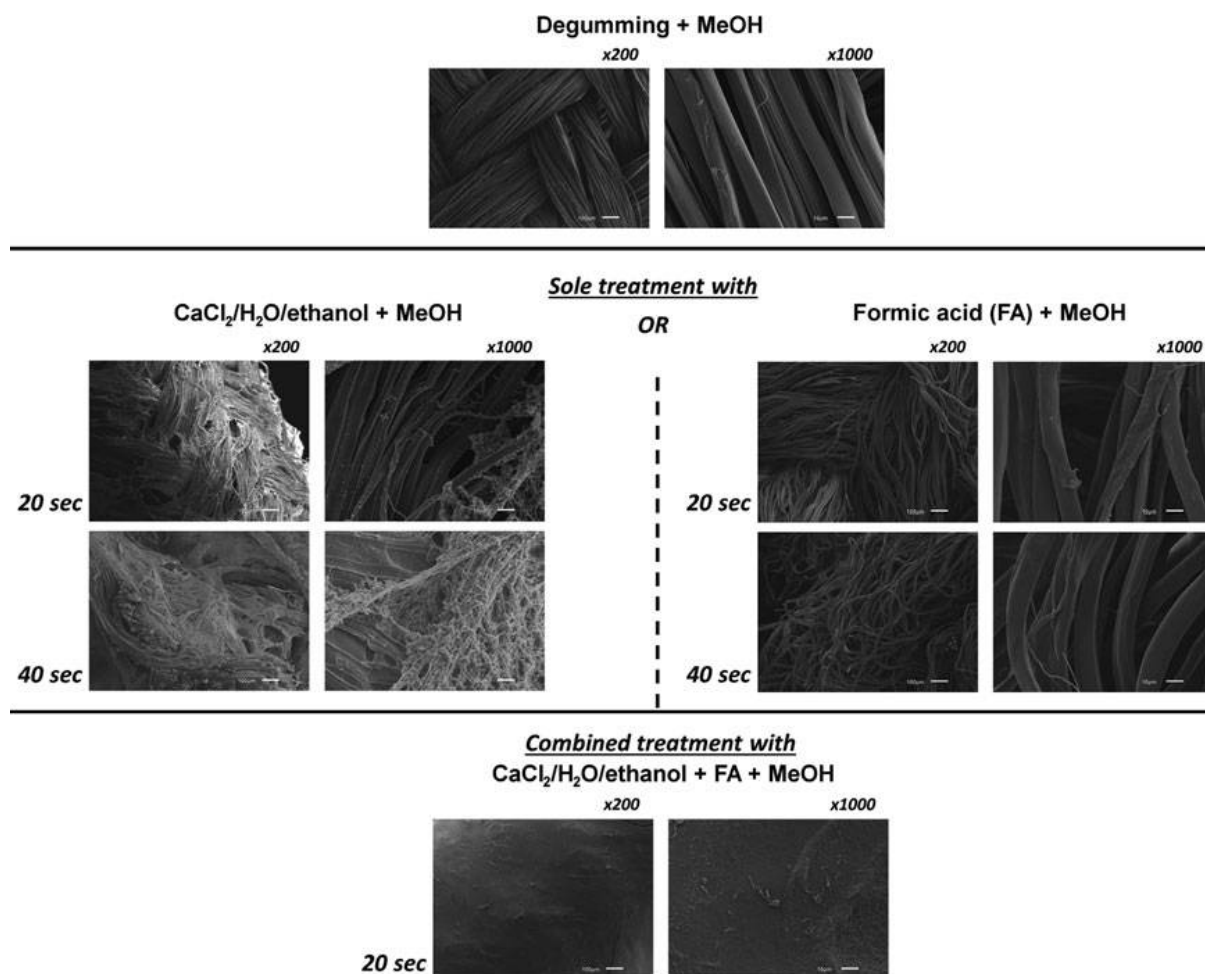
Figure 26: Effects of the treatment steps on the surface of the silk fibroin (SF) fibre based nerve guidance conduits (NGC). Panels show scanning electron micrographs of the single treatments with calcium chloride, ethanol and water in a molar ratio of 1:2:8 (1st treatment step CaCl$_2$/H$_2$O/ethanol), formic acid (2nd treatment step: Formic Acid (FA) and the combined treatment (CaCl$_2$/H$_2$O/ethanol + FA), respectively. In the combined treatment, SF constructs were treated with CaCl$_2$/H$_2$O/ethanol and FA subsequently for 20 sec each, resulting in a total treatment time of 40 sec. For comparison the single steps have also been performed for a total time of 40 sec.

Cytocompatibility assays

To investigate whether cytotoxic residuals were left in the SF-NGCs during the preparation procedure a MTT assay was performed. Dissected material from the SF-NGC and the unprocessed raw silk scaffold were incubated in cell culture media, to collect substances that may leach out of the constructs. Treatment of cultured Schwann cells with these leach-out media resulted in no significant difference in the cell viability of Schwann cells in any treatment group (Figure 27 A). Viability and adhesion pattern of Schwann cells cultured on the luminal surface of the silk tubes processed to various extent during the SF-NGC preparation procedure were tested with Calcein AM/propidium iodide staining. Treatment with CaCl$_2$/H$_2$O/ethanol and the full treatment procedure including incubation with FA induced significantly more Schwann cells to adhere to the luminal surface of the silk tubes

86

than degumming only (Figure 27 B-E). On the other hand, propidium iodide staining did not reveal any non-viable Schwann cells on the luminal surface of these cultured silk tubes (Figure 27 F).
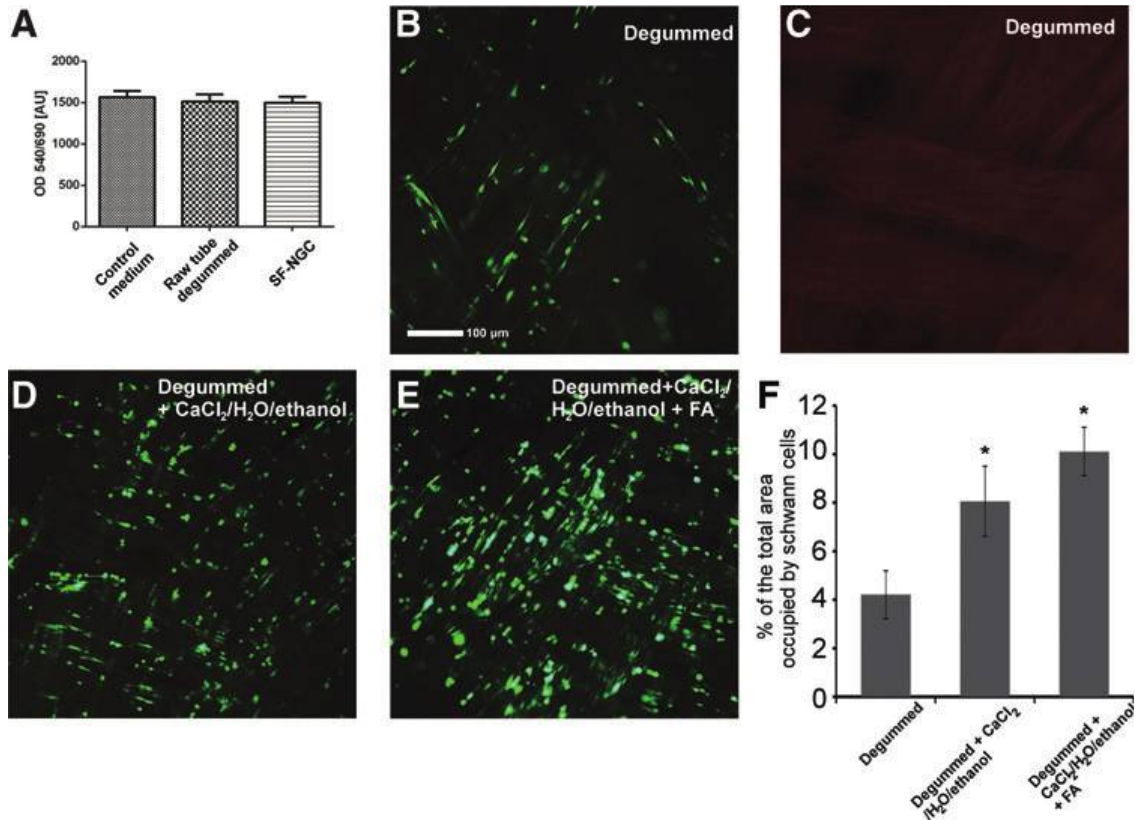

Figure 27: Results of the cytotoxicity, Schwann cell viability, and compression tests of the various conduits. (A) The primary Schwann cells cultured in the leach-out medium of either fully treated or degummed silk structures did not show signs of cytotoxic damage. (All data are means – standard deviation [SD] of eight independent experiments) (B–E) Fluorescent micrographs of Schwann cells showed good adherence and viability on the inside of the SF NGCs, where the propidium iodide staining [in (C)] revealed no dead cells on the internal wall of the tubes. (F) Schwann cell densities (cellular area occupied on the total surface) on the luminal surface of tubes were treated to vari- ous extents. Note the increasing attachment with the treatment steps. Asterisks indicate significant ($p < 0.005$) difference between the tubes receiving degumming and the tubes treated further.

Endurance test

To verify the required elasticity of the SF-NGC, mechanical endurance tests were performed with a custom-made system (see Supplemental Figure 1). Degummed tubes were remained compressed and flat after 1000 cycles of compression (Figure 28 G). FA or $CaCl_2/H_2O$/ethanol improved the elastic properties of the SF-NGCs resulting in partial preservation of the lumen; however, substantial deformation was still present. On their own, none of these treatments were able to provide the SF-NGC with elastic properties to withstand external pressure, whereas full treatment (degumming, $CaCl_2/H_2O$/ethanol followed by FA

treatment) helped improving the elastic properties of these SF-NGCs to become resistant to external forces (Figure 28 G).
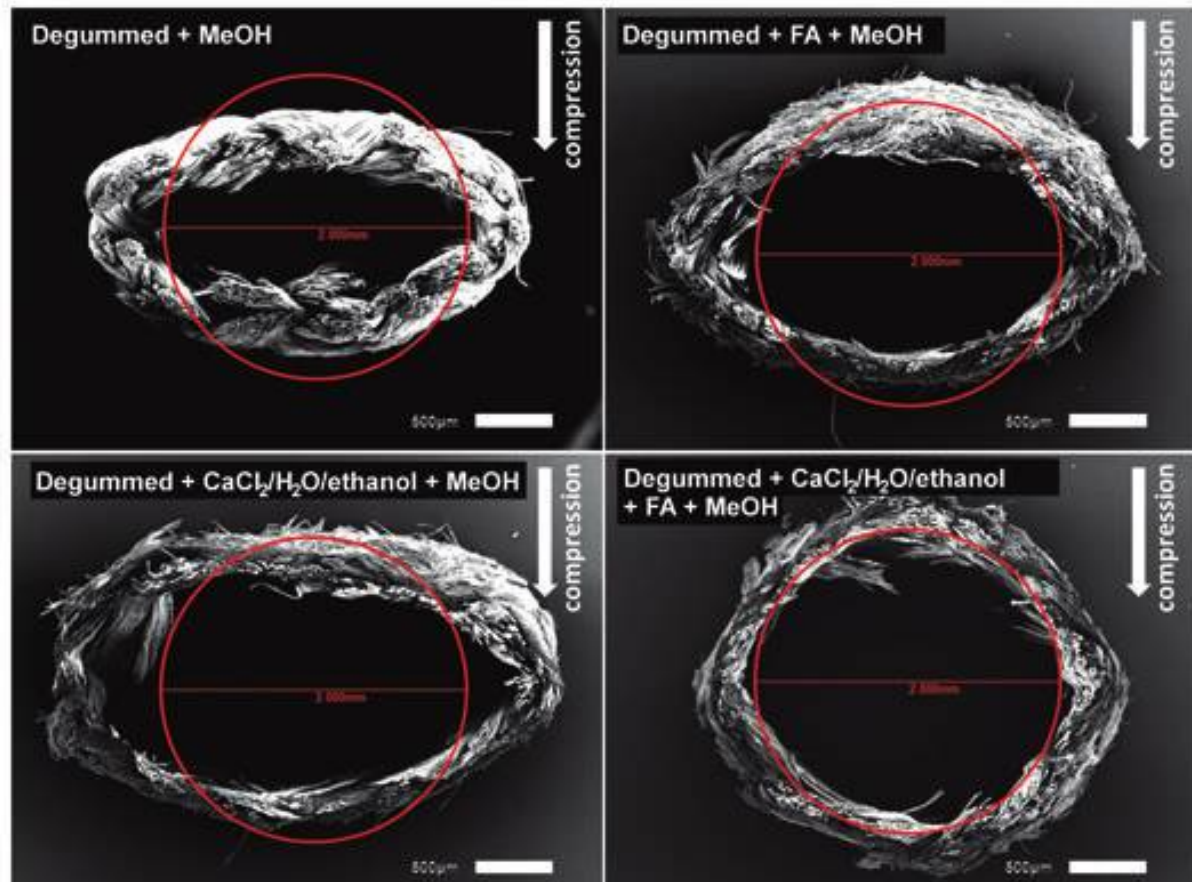
Figure 28: Compression test by using a custom-made test system to prove the improved elasticity of modified degummed tubu- lar structures shows that the CaCl$_2$/H$_2$O/ethanol-FA- MeOH modification is the most resistant to mechanical compression load. Red circles indicate the initial lumen (2 mm in diameter). Scale bars indicate 500 mm

Cell permeability

A cell migration assay was applied to test the impermeability of the SF-NGC wall to invading cells. The test was based on the chemotactic properties of PDGF-AA embedded in a fibrin clot (Figure 29 A). The efficacy of NIH/3T3 fibroblasts to penetrate and pass through the wall of the silk tube was tested. Degummed silk tube walls were suitable structures for the fibroblasts to migrate through their braided structure similar to positive controls, where the cells were able to pass through the mesh of a cell strainer (100 µm pore size) (Figure 29 B-C). In contrast SF-NGC with a completely closed outer surface did not support the penetration of fibroblast into the wall of the conduit (Figure 29 C).

88
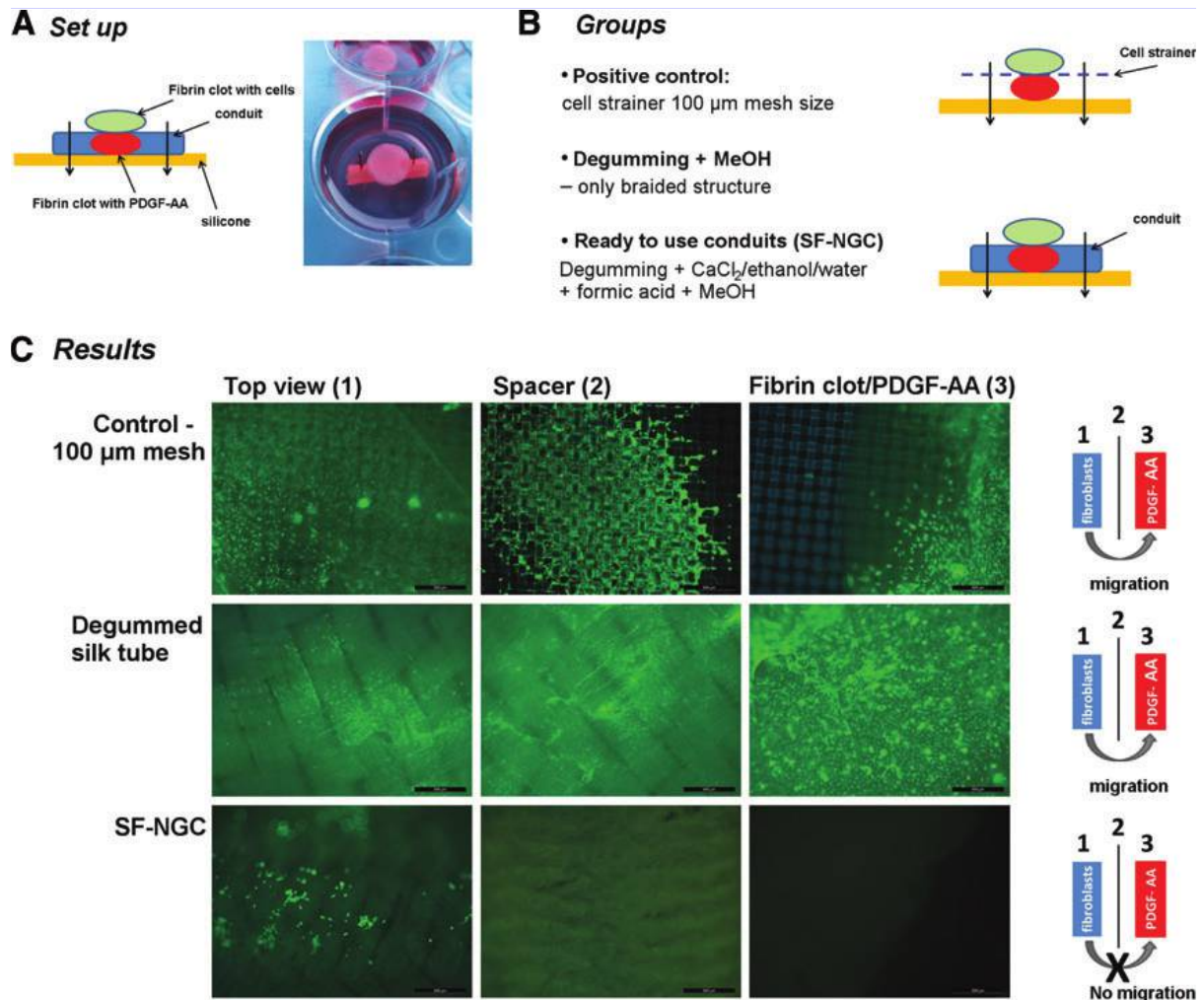
Figure 29: Results of the cell permeability assay using a fibrin clot containing NIH/3T3 fibroblasts and a second clot loaded with platelet-derived growth factor-AA (PDGF-AA) as a chemoattractant (A) in the various experimental groups (B). Fibroblasts passed through different spacers, including a cell strainer mesh of 100 mm pore size [(C), positive control, panel top row] and the unprocessed tubular silk structure [(C), panel middle row], but were not able to penetrate the applied SF- NGC [(C), panel bottom row]. Columns 1, 2, and 3 represent the view from the initial cell containing fibrin clot, the opposite side of the used spacer, and the initial fibrin clot containing PDGF-AA, respectively. All samples were stained for residual or invaded cells with Calcein AM staining. Scale bar is 500 mm.

Short term in vivo studies - general observations

The implanted SF-NGCs were explored and thoroughly checked under the operating microscope one and three weeks after surgery. Figure 30 A shows the proximal and distal nerve stumps coaptated to the SF-NGC by two epineurial sutures at the time of surgery. One week after implantation, visual inspection revealed that the SF-NGC did not exhibit substantial degradation (Figure 30 B). Furthermore, no signs of inflammatory reaction or neuroma formation at the coaptation sites could be detected. The entire outer surface of the implanted graft was covered by a thin layer of connective tissue. Interestingly, the proximal as well as the distal end of the implanted SF-NGC shows a partial integration of the nervous

tissue with the SF-NGC (Figure 30 B). Moreover, the thin layer of connective tissue on the surface of the SF-NGC contained small blood vessels (Figure 30 C-D). At 3 weeks after implantation the lumen of the SF-NGC was completely filled with regenerated tissue (Figure 30 E). Careful dissection of the SF-NGC (Figure 30 F) revealed a complete reconnection of the proximal and distal nerve stumps.
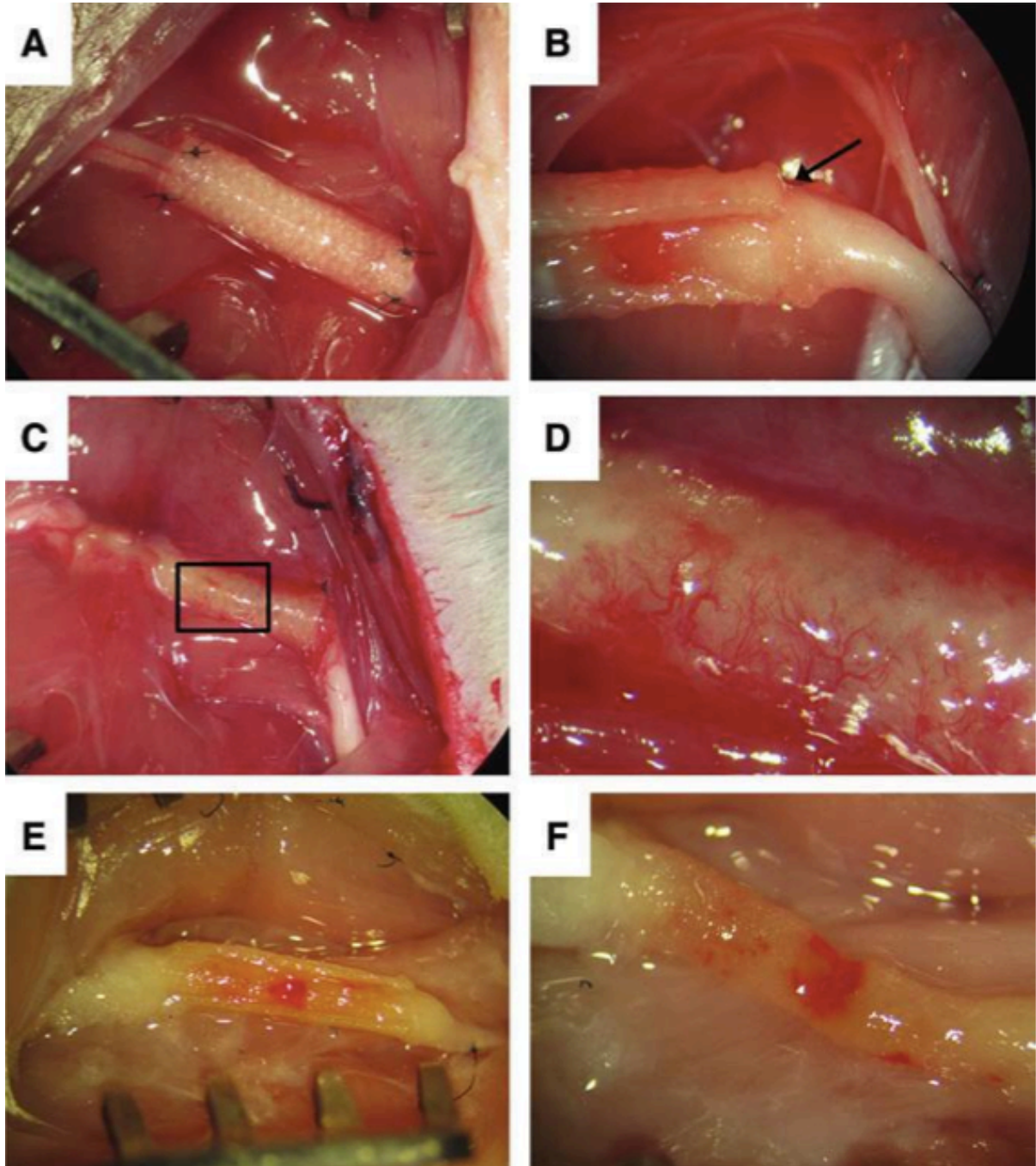
Figure 30: Integration of the silk-fibroin conduit in the defect site. (A) Photograph of an SF-NGC immediately after implantation between the sciatic nerve stumps. (B) Proximal side of the SF-NGC 1 week after implantation. Arrow indicates a thin layer of newly formed connective tissue capping the end of the SF-NGC. (C) Area of peripheral nerve surgery (1 week survival), showing small blood vessels in the thin layer of connective tissue around the conduit. (D) Enlarged photograph of the framed area in (C). Note the fine network of blood vessels.

(E) At 3 weeks after implantation, the lumen of the SF-NGC was completely filled with newly formed tissue. (F) Dissection of the SF-NGC in (E) revealed a reconnection of the distal and proximal nerve stumps.

Axonal regeneration

Our results showed that an 8 mm gap in the rat sciatic nerve could be bridged by implanting an SF-NGC in the gap. To compare the axon growth promoting capacity of the three conduits used in the study we looked at the axon outgrowth from the proximal nerve stump into the conduits ten days after grafting by using neurofilament staining. Autologous nerve grafts were already populated with regenerated axons along their whole length at this time-point and the axons approached the distal coaptation site (Figure 31 A). In contrast, the silk tubes were able to promote only limited outgrowth of the axons at this stage. The regenerating axons have grown to a distance of approximately 2 mm in both conduits (1.7 and 1.8 mm in empty tubes and 2 and 2.1 mm in collagen-filled tubes, n=2 in each group) without considerable difference between them (Figure 31 B, C). The autologous nerve grafts 10 days after postoperatively are well vascularized (Figure 31 A). A similar range of vascularization of the silk tubes could be observed on day 10 after surgery. No considerable number of macrophages were seen in the implanted silk tubes (Figure 31 B,C).
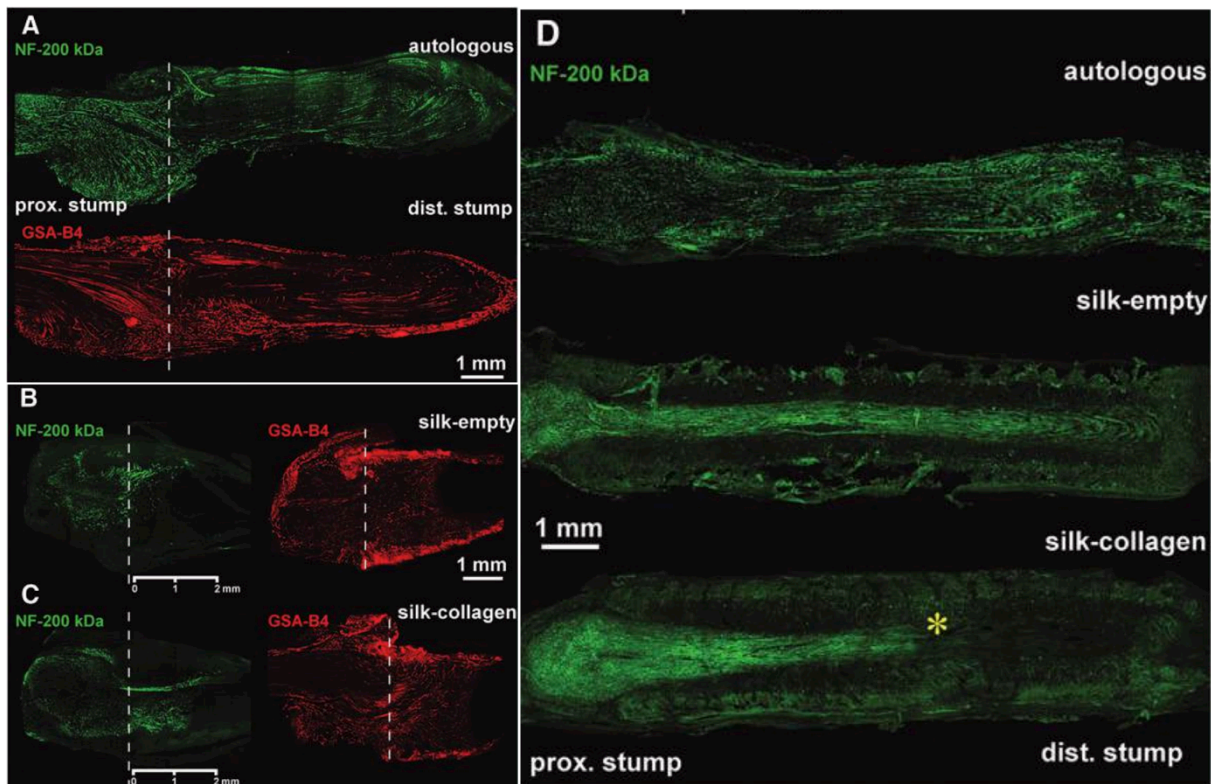
Figure 31: Axonal regeneration and vascular ingrowth in the various experimental groups. (A) Regenerating axons (green) reach the distal coaptation site (indicating by broken lines) in the autologous nerve grafts 10 days postoperatively and the nerves are also well vascularized, as shown with the GSA-B4 lectin histochemistry (red). Note the lack of macrophages in these grafts. (B, C) The regenerating axons extend ca 2 mm into the silk tubes

with a similar range of vascularization on day 10 after surgery. No considerable number of macrophages was seen in the implanted silk tubes. Broken lines indicate the proximal coaptation zone. (D) Representative examples of axon growth through various con- duits 12 weeks after surgery. Note the robust regeneration via the autologous nerve graft, although numerous axons are able to also regenerate through the silk tube-based conduits. Axons were stained via neurofilament 200 kDa immunostaining, which failed to label the regenerating axons in the distal one- third of the empty silk tube (asterisk).

Three months after transplantation the course of regenerated axons throughout the lumen of the implanted SF-NGCs and autologous nerve grafts was clearly visible (Figure 31D-F). Although the axon bundle was present in the empty silk tubes the immune-histochemical analysis did not reveal a significant staining pattern for neurofilament 200 kD in the distal portion of the tubes. On the other hand, myelinated axon counts showed significantly less myelinated axons in the empty SF-NGC as well as the collagen-filled SF-NGC compared to the autologous nerve graft empty SF-NGC: 1274 ± 146, collagen-filled SF-NGC: 1678 ± 303, autologous nerve graft: 6252 ± 474; Figure 32). Accordingly, filling the silk tubes with collagen did not influence the short and long term regeneration of axons.
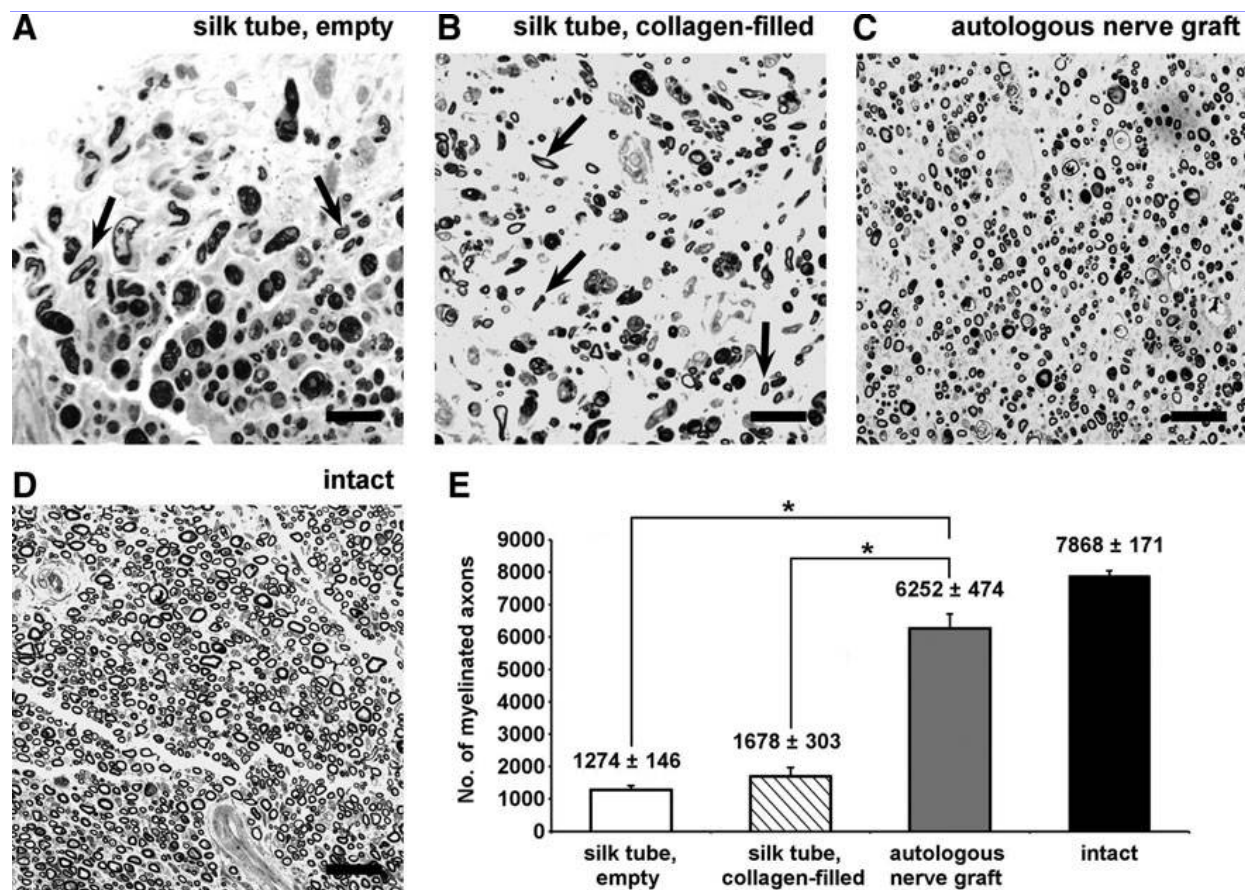
Figure 32: Numbers of myelinated axons in the various experimental groups 12 weeks after implantation. Arrows point to well-myelinated axons in the distal stumps (A–D). The scale bar is 20 mm. Note the significant differences between the myelinated axon numbers found in autologous nerve graft and the silk tube-based conduits (E). All data are means of six animals – SD. *Indicates significant difference of $p < 0.005$.

Functional recovery – Catwalk analysis

Twelve weeks after surgery the functional recovery parameters (Figure 33A-D) including mean stance time, mean print area, mean duty cycle and the mean maximally exerted intensity of the right hind limb were evaluated. In three out of four parameters (excluding limb print area) there was a significant difference between the extent of recovery of the autologous nerve grafts compared to the empty silk tube, whereas in the case of duty cycle the animals receiving an autologous nerve graft performed significantly better in comparison to both silk tube groups. A minor, statistically not significant difference was found between the two silk tube groups in case of all parameters (Figure 33A-D). It should be noted that animals treated with autologous nerve grafts displayed functional parameters approaching but never closely reaching the pre-training values.
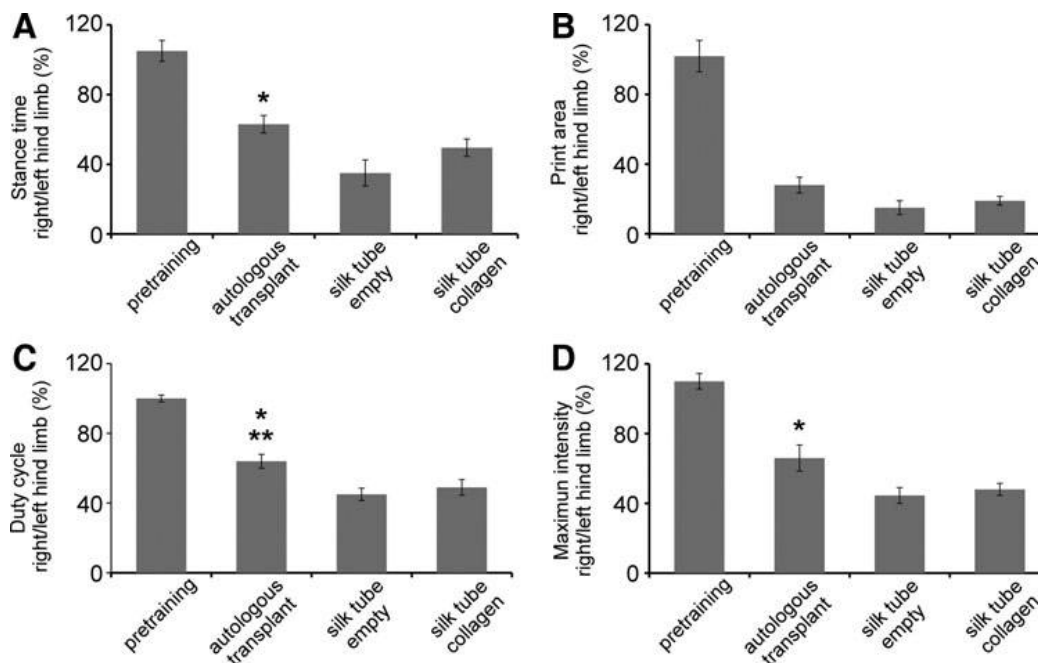
Figure 33: Quantitative CatWalk gait analysis of locomotor functional recovery 12 weeks after implantation, including stance duration time (A), print area (B), duty cycle (C) and intensity exerted at maximum floor contact area (D) of the operated right hind limb relative to the unoperated left hind limb. Pretraining data show intact values recorded 1 week before surgery. All data are means of six animals +/- SD. *Indicates significant difference (p < 0.005) between the autologous grafting and the empty silk tube groups, whereas ** indicates significant difference between the autologous grafting (auto- logous transplant) and both silk tube groups either empty (silk tube empty) or filled with collagen (silk tube collagen).

Electrophysiology

The results of the electrophysiological analysis strongly correlate with the functional data described above. Electrophysiological recordings were carried out twelve weeks after transplantation. Compound nerve action potential (CNAP) and nerve conduction velocity (NCV) values were significantly improved in the autologous nerve grafting group (CNAP:

22,8 ±7,5; NCV: 49,2 ±14,2) compared to both silk tube groups (empty SF-NGC, CNAP: 6,5 ±3,1; NCV: 23,9 ±6,6. Collagen-filled SF-NGC, CNAP: 9,7 ±4,4; NCV 25,9 ±7,3; Figure 34). No difference could be detected between the groups receiving the various silk tubes, although the animals with empty silk tubes displayed slightly impaired electrophysiological data.
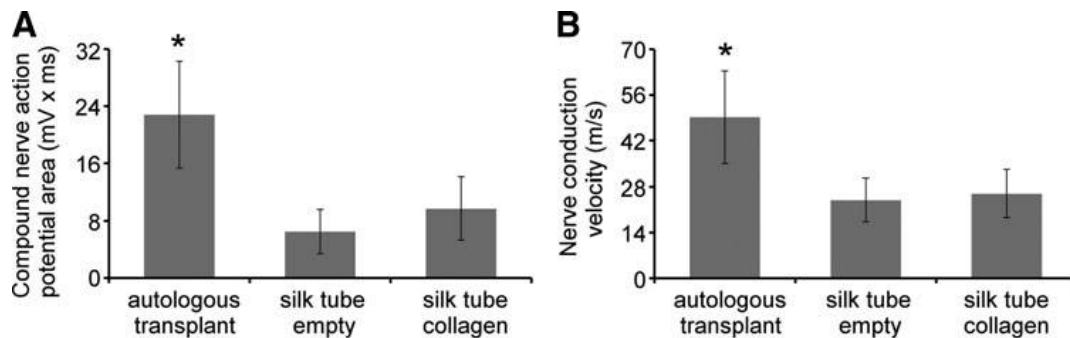
Figure 34: Electrophysiological analysis of the effect of axonal regeneration through the various conduits. The compound nerve action potential area (A) and nerve conduction velocity values (B) were significantly improved in cases of autologous nerve grafts (autologous transplant) compared with silk conduits. All data are means of six animals–SD. *Indicates a significant difference of $p < 0.005$ between the autologous grafting and both silk tube groups either empty (silk tube empty) or filled with collagen (silk tube collagen).

DISCUSSION

In this study we have investigated the mechanical properties and biocompatibility of a novel nerve guidance conduit manufactured from a braided tubular structure of silk fibroin fibres. Moreover, the ability of this novel conduit to bridge a peripheral nerve gap and support the regeneration of injured rat sciatic nerve axons has been tested.

The nature of the chemical treatment to transform a braided structure into a mechanically resistant, flexible tube, non-permeable for externally invading cells made it necessary to investigate cytotoxicity and cellular viability prior to *in vivo* implantation. The mixture of $CaCl_2/H_2O$/ethanol dissolves native silk fibres (186,187), while methanol induces the formation of β-sheets, leading to a crystalline-like structure of the silk fibroin (188,189). Formic acid functions as a solving and crystallizing agent. Um *et al.* (190,191) reported that formic acid induces an ordered structure and molecular arrangement. As the end result, this combination treatment resulted in a homogenous crystalline-like outer layer of the nerve conduit wall. In addition, by controlling the incubation times we were able to design the structure and thickness of the outer crystalline layer. All together the treatment steps resulted in the generation of a mechanically stable tubular conduit.

Apart from the favourable mechanical properties the question remained whether this construct maintained its biocompatibility, was able to prevent invasion of connective tissue cells from

the environment and provided a supportive luminal surface for proliferating Schwann cells. According to our findings these conduits fulfilled all these requirements.

Our short term *in vivo* studies have provided evidence that the implanted silk tube conduits were able to integrate into the host environment without generating significant inflammatory reactions and on the other hand could successfully bridge an eight millimeter long nerve defect. These features may enable this type of silk tube conduit to act as a strong candidate for nerve repair. From a practical point of view, the best available nerve conduit is an autologous nerve graft, frequently regarded as the gold standard for experimental and clinical use of nerve grafting. There is, however, an urging need for nerve conduits in the clinical use when autologous nerve grafts are not available. These conduits should preferably fulfill a number of requirements: they should be biocompatible, long enough to bridge large defects, able to support Schwann cell proliferation followed by rapid axonal regeneration and accept external vascular ingrowth, while they resist to invasion of external cell populations especially that of fibroblast.

It is evident that a chemically inert silk tube bears several of the above mentioned features still is unlikely to guide significant number of degenerating axons over long distances. The longest distances that can still be bridged by artificial or natural conduits are frequently called "critical gap", and they are thought to range between 2 and 6 cm in humans (38-40). Gaps longer than 6 cm can only be reconnected by using autologous nerve grafts or nerve allografts (40,41). The intriguing question is raised how nerve conduits should be altered in order to make them suitable for grafting in long nerve defects. The silk tube conduit presented in this study is likely to undergo a number of further modifications to suit these requirements. It could be argued that by making the silk tubes permeable for growing vessels and modifying their luminal environment in order to foster axonal regeneration the silk tube conduits would be transformed into structures with features closely resembling peripheral nerve grafts. Such conduits should carry features normally present in an intact or freshly degenerated peripheral nerve e.g. the presence of axonal growth promoting cells (like Schwann cells or Schwann cell -like cells) (43-45) and the extracellular matrix compounds produced by these cells. Recently advances in experimental bridging of larger nerve defects have been made including the strategies outlined above. We suggest that the next generation of biologically inert silk tube conduits could possibly include treatment with the peripheral nerve specific extracellular matrix molecules fibronectin and laminin along with sequential transplantation of Schwann cells or Schwann cell-like cells into the conduit.

These novel methodological approaches may open new horizons in the field of peripheral nerve regeneration and repair and may contribute to better treatment opportunities of large human nerve defects.

CONCLUSION

In this study we describe the production of a novel nerve guidance conduit based on raw silk textile tubular structures. The chemical treatment of the raw silk tube resulted in a biocompatible and mechanically stable conduit, which was able to bridge relatively short gaps in the rat sciatic nerve. It can be concluded that these silk tube conduits are subject to further studies and modifications in order to produce cellularised bioartificial conduits that would support long distance nerve regeneration.

SUPPLEMENT

Custom-made compression test system

Side view
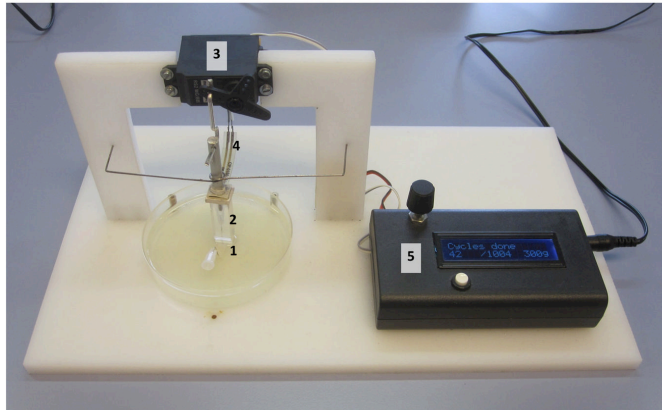
Front view

1. silk tube scaffold mounted on silicone mat
2. piston
3. servo motor
4. force sensitive resistor
5. controller board / microcontroller
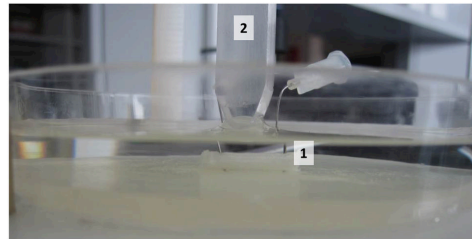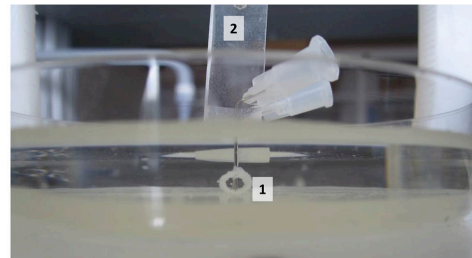
Supplementary Figure 1: Custom-made compression testing machine. The test sample (1) is mounted on a silicone mat that fits in a petri dish via pins. A piston (2) is moved downwards via a servo motor (3) at a speed of approximately 5 mm/s in a linear manner until it touches the probe. The piston continually stresses the probe until a predefined force threshold is reached. A force sensitive resistor (4), which is integrated into the piston, works as a sensor and is part of a voltage divider. The resistance and thus the applied force is constantly sampled at 50 Hz sampling frequency using the built-in 10 bit ADC of the microcontroller (5). Once the threshold is reached, the piston is returned to the top position, where it remains for a time set by the user.

Covalent Binding of Placental Derived Proteins Improves Adhesion of Schwann Cells to Fibroin

Christina Schuh[1,2], Johannes Hackethal[1,2], Xavier Monforte[2,3],
Heinz Redl[1,2], Andreas Teuschl[2,3]

[1]Ludwig Boltzmann Institute for Experimental and Clinical Traumatology, AUVA Research Center, Donaueschingenstraße 13, A-1200 Vienna, Austria
[2]Austrian Cluster for Tissue Regeneration, Austria
[3]University of Applied Sciences Technikum Wien – Department of Biochemical Engineering, Vienna, Austria

ABSTRACT

Schwann cells play a key role in peripheral nerve regeneration. Failure in sufficient formation of Büngner bands due to impaired Schwann cell proliferation has significant effects on the functional outcome after regeneration. Therefore the growth substrate for Schwann cells should be considered with highest priority. Due to its excellent biocompatibility silk fibroin has attracted considerable interest as a biomaterial for use as a conduit in peripheral nerve regeneration. In this study we established a protocol to covalently bind collagen and laminin to silk fibroin utilizing carbodiimide chemistry, evaluating adhesion, viability and proliferation of Schwann cells. A cell adhesion assays revealed that laminin and collagen significantly improved Schwann cell adhesion to silk fibroin and that laminin accelerated adhesion. Furthermore Schwann cell proliferation and viability assessed with BrdU and MTT assay were increased in the laminin coated groups. The results suggest beneficial effects of laminin on both, cell adhesion as well as proliferative behaviour of Schwann cells.

Key words: silk fibroin; Schwann cells; cell adhesion; laminin;

INTRODUCTION

Peripheral nerve lesions occur with a prevalence of approximately 5% in trauma associated injuries. Even though autologous nerve grafts are the clinical gold standard, the functional regeneration often is not satisfactory and autografts show several severe disadvantages such as limited availability and potential donor site morbidity (9,102,132,192). Alternatives are sought to facilitate nerve regeneration, such as artificial nerve guidance tubes, luminal fillers containing neurotrophic substances and/or Schwann cells. Some of these approaches are currently used in clinical nerve repair, though there is an ongoing debate as concerns their appropriate use, effectiveness and side-effects (103,104). One of the major reasons for the unsatisfactory outcome after repair of long distance gaps is the limited proliferative capacity of Schwann cells (105) and their selective adhesion to surfaces (193). Schwann cells play a key role in peripheral nerve regeneration: they participate in the removal of myelin and axonal remnants, start proliferating and align to build the so called bands of Büngner (106). After the axon has elongated along these bands of Büngner, the Schwann cells start to remyelinate the newly formed axon to complete the regenerative process. Failure in sufficient formation of Büngner bands due to impaired Schwann cell proliferation has significant effects on the functional outcome after regeneration (43). Therefore the growth substrate for Schwann cells should be considered with highest priority.

Silk fibroin has attracted considerable interest as a biomaterial for use as a conduit in peripheral nerve regeneration due to its excellent biocompatibility (194–197). In previous studies our group demonstrated that carbodiimide chemistry could be utilized to covalently bind the plant lectin wheat germ agglutinin to silk fibroin- improving adhesion time of anterior cruciate ligament fibroblasts and adipose derived stem cells significantly compared to the native silk fibroin. Laminin and collagen interact with integrins on the surface of Schwann cells, supporting adhesion and proliferation of Schwann cells (198).

We hypothesize that covalent binding of laminin and collagen I/III to silk fibroin improves cell adhesion and might have beneficial effects on Schwann cells cultured on silk fibroin. Aim of this study was to investigate the influence of covalently bound laminin and collagen I/III on the adhesion, viability and proliferation of Schwann cells.

MATERIAL AND METHODS

Schwann cell isolation and culture

All animals were euthanized according to established protocols, which were approved by the City Government of Vienna, Austria in accordance with the Austrian Law and Guide for the Care and Use of Laboratory Animals as defined by the National Institute of Health. Animals and treatment/control groups were randomly chosen and analysed without pre- or post selection of the respective nerves or cultures.

Sciatic nerves of adult male Sprague Dawley rats were dissected and kept in phosphate buffered saline (PBS; PAA, Austria) pre-chilled on ice until further use, but not longer than one hour. Schwann cells were isolated from the treated and non-treated sciatic nerve tissues according to a method adapted from Kaekhaw *et al.* (108) Briefly, the epineurium was removed and nerves were strained and minced. Nerve fragments were incubated with 0.05% collagenase for 1 hour at 37°C subsequently filtered through a 40 μm cell strainer and centrifuged at 400 x g for 6 minutes. After washing the cell pellet in Dulbecco's Modified Eagle Medium (DMEM; PAA, Austria) containing 10% fetal calf serum (FCS; PAA, Austria), the pellet was resuspended in DMEM-D-valine (PAA, Austria), supplemented with 10% FCS, 2 mM L-Glutamine (PAA, Austria), 1% antibiotics (PAA, Austria), N_2 supplement (Invitrogen, Germany), 10 μg/mL bovine pituitary extract (Sigma-Aldrich), 5 μM forskolin (Sigma-Aldrich). Cell suspension was seeded on 6-well plates (PAA, Austria) coated with poly-L-lysin (Sigma-Aldrich) and laminin (Sigma-Aldrich). Purity of Schwann cell cultures was assessed with flow cytometry and common Schwann cell markers S100, P75 and P0.

Preparation of silk films

Silk films were prepared as described by Teuschl *et al.* (199). Briefly, sericin was removed from white raw *Bombyx mori* silkworm fibres (20/22den, 250T/m, Testex AG, Switzerland) by boiling in 0.2 M boric acid in a 0.05 M sodium borate buffer at pH 9.0, followed by rinsing in ddH$_2$O. Subsequently fibres were dissolved in calcium chloride, ethanol and ddH$_2$O (1:2:8) for 6h. The solution was then filtered (0.22 μm, Rotilab, Germany), dialyzed against ddH$_2$O using, a Slide-a-Lyzer dialysis cassette (Pierce) with a molecular weight cut off of 3.500 Da and lyophilized. Silk films were prepared after reconstitution with hexafluoro-2-propanol (25 mg/ml) in 96 well plates (50 μl) or 24 well plates (150 μl) respectively, air-dried and stored at 4°C.

Coating of silk films with laminin and collagen

Placental collagen and laminin were resuspended in HEPES pH 7.4 to a concentration of 1mg/ml and a blend of collagen/laminin to a concentration of 1 mg/ml each over night on a roller mixer. Plates/fibres were immersed in 100% methanol for an hour and allowed to air-dry. After hydration over night in 20 mM HEPES/NaOH (pH 7.0) buffer, the carboxy groups were activated by adding 0.5 mg/mL 1-ethyl-3-(dimethylaminopropyl) carbodiimide hydrochloride (EDC) and 0.7 mg/mL *N*-hydroxysuccinimide (NHS) solution in 20 mM HEPES/NaOH (pH 7.0) (2 hours) and subsequently rinsed in 20 mM HEPES pH 7.0. Coating with laminin, collagen and laminin/collagen was perfomed at 4°C over night and films were subsequently rinsed. For all assays uncoated wells (ctrl), poly-L-lysin/laminin coated wells and fibroin coated wells acted as control groups.

Cell adhesion assay

To evaluate alterations in Schwann cell adhesion to the silk films after coating with placental proteins, an attachment assay was performed. Schwann cells were detached from cell culture plastic with Accutase to preserve cell viability and ensure most efficient re-attachment. Accutase activity was stopped with cell culture medium and cells were counted using a cell counter (BioRad T20). $5x10^4$ cells (60 µl) were pipetted onto the silk films as well as control wells of a 96 well plate (triplicates per Schwann cell culture; 1 triplicate of 1 donor equals n=1), and tube containing cell suspension was inverted after every triplicate. The plates were incubated for 30 min under standard cell culture conditions (37°C, 5% CO_2 and 95% humidity). Subsequently supernatant containing non-adhered cells was collected and residual cells were added after washing step with PBS (60 µl). Cells were counted using a cell counter.

Cell viability

Cell viability of Schwann cells on the coated silk fibres was determined using MTT assay. Schwann cells, seeded at a density of $4x10^4$ cells/cm^2 (triplicates / Schwann cell culture; 1 triplicate of 1 donor equals n=1), incubated with culture medium containing 650 µg/ml MTT [3-(4,5- dimethylthiazol-2-yl)-2,5-diphenyltetrazolium] bromide (Sigma Aldrich) for 1 hour at standard cell culture conditions (37°C and 5%) (30 hours after seeding). Medium was discarded and MTT formazan precipitate was dissolved in 100 µl DMSO (Sigma Aldrich) by

shaking in dark for 20 minutes. Light absorbance at 540 nm was measured immediately and optical density (OD) values were corrected for an unspecific background on an automatic microplate reader (Tecan Sunrise; Tecan).

Proliferation

Proliferation of Schwann cells on the coated silk fibres was evaluated using a 5- bromo-2-deoxyuridine uptake assay (BrdU; Cell Proliferation ELISA assay Kit; Roche Diagnostics, Switzerland), according to manufacturer's instructions. Briefly, coated and control 96 well plates were seeded with Schwann cells at a density of 4×10^4 cells/cm^2 (triplicates / Schwann cell culture; 1 triplicate of 1 donor equals n=1). Cells were left to adhere for 24 hours and 72 hours. Subsequently medium was changed to Schwann cell medium containing 100 µM BrdU and cells were incubated for 24 hours at standard cell culture conditions (37°C and 5% CO_2). The culture plates were fixated with FixDenat® solution and incubated with anti-BrdU POD antibody solution for 60 minutes at room temperature. After washing the plate with PBS twice, substrate solution (tetramethyl benzidine) was added for 20 minutes. The reaction was stopped with 1 M H_2SO_4 and absorption was measured at 450 nm with 690 nm as reference wavelength on an automatic microplate reader (Tecan Sunrise; Tecan, Switzerland). Results were normalized on cell count after 30 hour attachment period.

Visualization of cells on silk fibres

Schwann cells were seeded on functionalized fibroin matts (woven) and fibroin fibres at an initial seeding density of 4×10^4 cells/cm^2. 48 hours after cell seeding, cell adherence on the fibres was visualized using a live/dead staining (Calcein AM/Propidium iodide; Thermo Fisher) according to manufacturer's instructions. Briefly, cell-fibre constructs were incubated with Calcein AM (3 µM in DMSO) and propidium iodide (2.5 µM in water) in cell culture medium for 30 minutes. Subsequently cell-fibre constructs were washed twice with PBS and kept in PBS until evaluation with fluorescence microscopy.

Statistical analysis

Statistical difference was analysed using one-way ANOVA (analysis of variance) followed by Tukey range test for significant differences between the means. Significance was considered for $P < 0.05$. For statistical calculations GraphPad Prism 5 for Mac OS X, Version 5.0b (GraphPad Software, Inc., La Jolla, CA, USA) was used. All data in this study are shown as mean ± standard deviation (SD).

RESULTS

Improved immediate Schwann cell adhesion to modified silk films

Prior to assays Schwann cell purity and proliferative status were assessed using flow cytometry and common Schwann cell specific markers. As seen in Figure 35A, Schwann cells expressed the Schwann cell marker S100b and the proliferation-associated marker P75, while myelin marker P0 is only mildly expressed. Figure 35B depicts Schwann cells expressing typical bipolar, spindle shaped Schwann cell morphology.
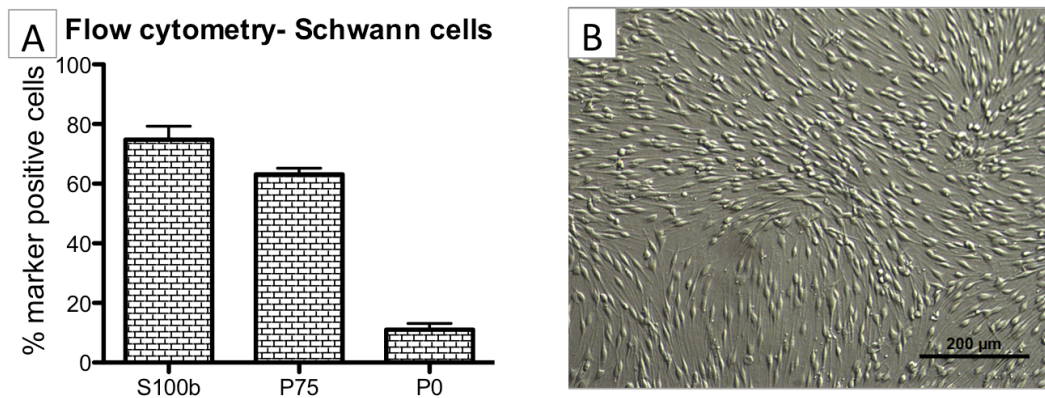
Figure 35: A) Flow cytometric analysis of Schwann cells using Schwann cell specific markers S100b, P75 and P0; B) light microscopy image depicting typical Schwann cell morphology;

Schwann cell adhesion was evaluated in a cell attachment assay. 20 minutes, 2 hours and 24 hours after cells were pipetted onto the films, residual non-adhered cells were counted and viability assessed with trypan blue exclusion. Uncoated control (ctrl) and the standard coating for Schwann cells (Lysin/Laminin) acted as negative and positive control respectively. Cell viability of the non-adhered Schwann cells decreased significantly over time (Figure 36A). While after 20 minutes around 95% of the non-adhered cells were negative for trypan blue, the amount of viable cells decreased to 35% after 24 hours (Figure 36 B). Figure 36B depicts that in all three time points significantly more cells adhered to the standard coating than to the untreated control, allowing a comparison of the treatment groups. Schwann cells adhered faster and overall better to fibroin, independent of coating, than to uncoated control. However, a significant improvement of attachment could be observed in the fibroin group coated with laminin, also compared to the standard coating group.
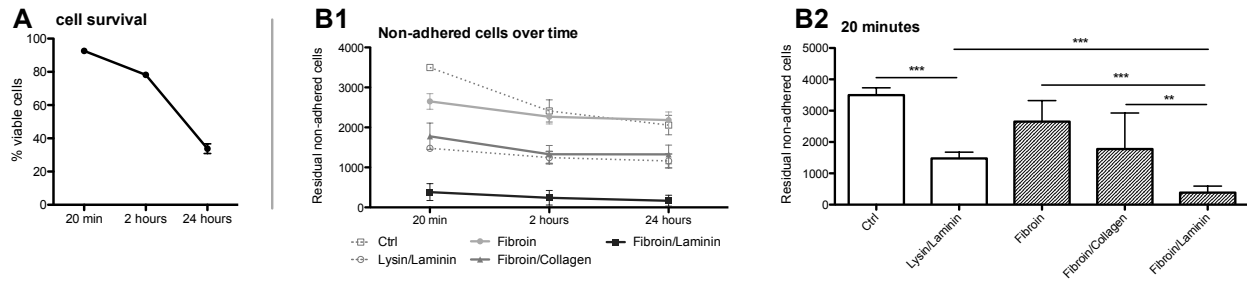
Figure 36: Schwann cell adhesion to silk fibroin films; (A) percentage of viable cells assessed with trypan-blue exclusion after 20 min, 2 hours and 24 hours; B) cell count of residual cells after 20 min (B2), 2 hours and 24 hours after seeding on uncoated control (ctrl-dotted light grey), standard Schwann cell coating (Lysin/Laminin-dotted dark grey) or fibroin films coated with Collagen or Laminin; statistical significance was tested with 1-way ANOVA and Tukey range test; data is presented as Mean ± SD; *P<0.05, **P<0.01, ***P<0.0001; 1 triplicate of 1 donor equals n=1; n=12;

Schwann cells proliferate on modified silk films

Proliferation behaviour on fibroin films was assessed with a BrdU incorporation assay. Cells were seeded on the films and left to adhere for 24 and 72 hours. Uncoated control (ctrl) and the standard coating for Schwann cells (Lysin/Laminin) acted as negative and positive control respectively. Schwann cells proliferated on both time points significantly more on lysin/laminin films than on the uncoated control (Figure 37). Proliferation on fibroin films was improved compared to the uncoated control, but lower than in the lysin/laminin group. Modification of the fibroin film with collagen negatively affected proliferation, while modification with laminin led to a significant improvement, comparable to the positive control lysine/laminin. (Figure 37). Between the early time point and later time point proliferation increased in all groups between 25-30%.
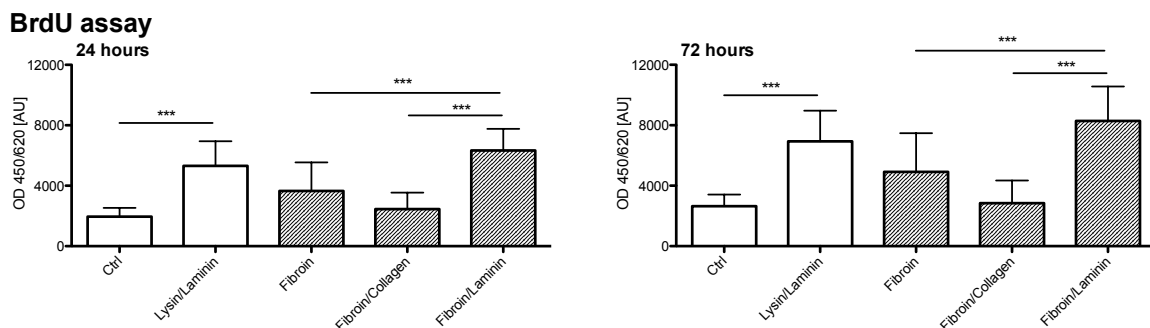
Figure 37: Improved Schwann cell proliferation on silk fibroin films modified with laminin; BrdU assay of Schwann cells seeded on uncoated tissue culture plastic (ctrl), standard Schwann cell coating (Lysin/Laminin) and fibroin films coated with Collagen or Laminin; OD values were normalized on BrdU start point cell counts per group; statistical significance was tested with 1- way ANOVA and Tukey range test; data is presented as Mean ± SD; *P<0.05, **P<0.01, ***P<0.0001; 1 triplicate of 1 donor equals n=1; n=12;

Schwann cell viability on modified fibroin films

Influence on viability of Schwann cells was evaluated with an MTT assay. Cells were seeded on the films and left to adhere for 24 and 72 hours. Uncoated control (ctrl) and the standard coating for Schwann cells (Lysin/Laminin) acted as negative and positive control respectively. As seen in Figure 38, no significant differences in cell viability could be observed after 24 hours, with a slight tendency towards a decreased viability in the uncoated control group (ctrl) and the fibroin/collagen group. However, after 72 hours Schwann cell viability was significantly higher in the lysine/laminin and fibroin/laminin group. OD values normalized on start point cell count revealed an increase between the early time point (24 hours) and the later time point (72 hours) of approximately 60% in the lysin/laminin and fibroin/laminin group, while in the other groups OD values increased only 25-30% (Figure 38).
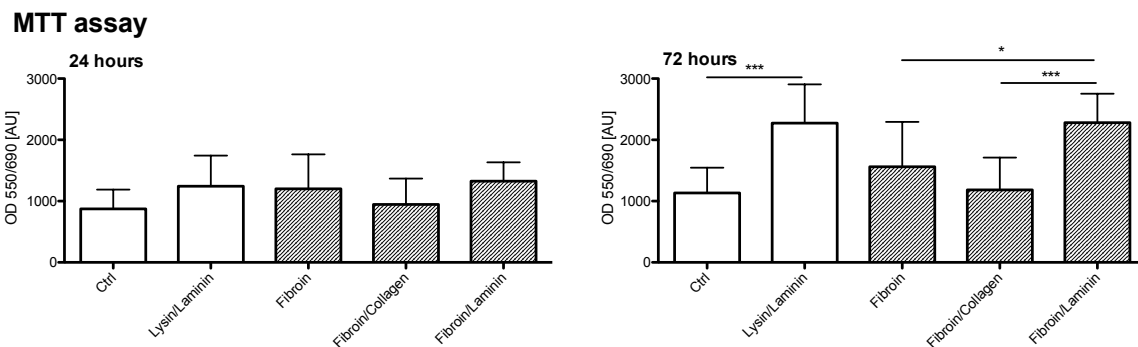

Figure 38: Increased Schwann cell viability on fibroin films modified with laminin; MTT assay of Schwann cells seeded on uncoated tissue culture plastic (ctrl), standard Schwann cell coating (Lysin/Laminin) and fibroin films coated with Collagen or Laminin; OD values were normalized on BrdU start point cell counts per group; statistical significance was tested with 1- way ANOVA and Tukey range test; data is presented as Mean ± SD; *$P<0.05$, **$P<0.01$, ***$P<0.0001$; 1 triplicate of 1 donor equals n=1; n=12;

Improved adhesion to laminin-modified silk fibre matts and silk fibres

To investigate efficacy of the coating on single fibres and matts in terms of Schwann cell attachment, cells were visualized using a live/dead stain. Cells were seeded on the matts and fibres and left to adhere for 48 hours. After staining procedure, silk matts and fibres were positioned with the surface containing the cells facing the light beam of the microscope. Calcein AM/PI staining shows a high number of viable cells adhered to the laminin-coated fibroin matts and fibres, while only a few cells could be detected on the uncoated and collagen-coated fibres and matts. (Figure 39)
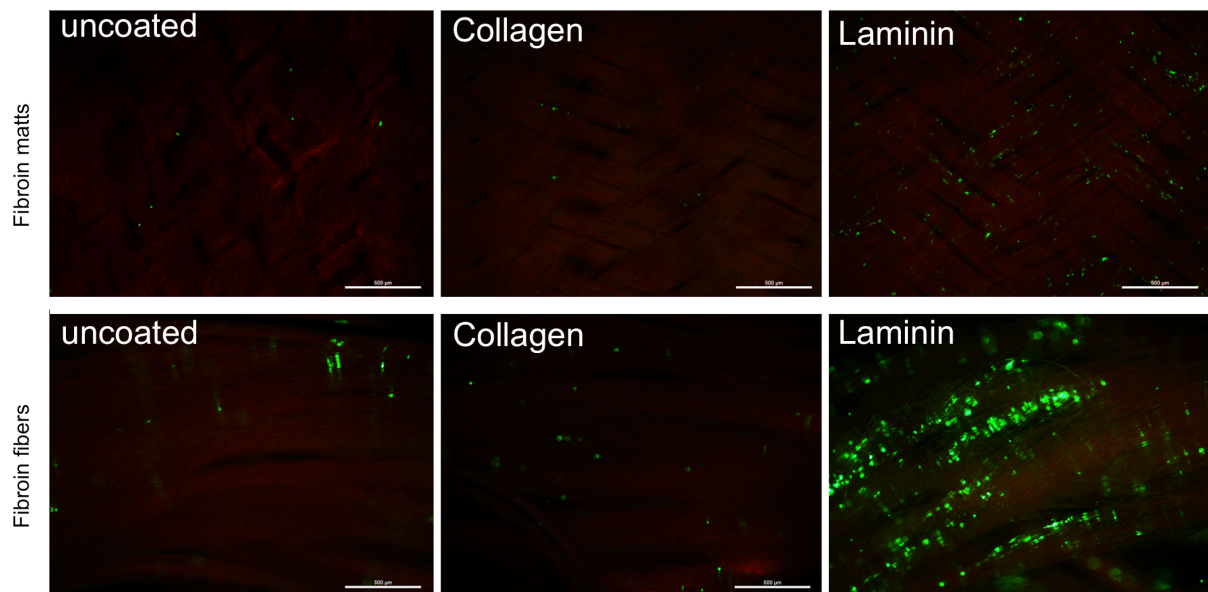
Figure 39: Representative fluorescence micrographs of Schwann cells visualized using a Calcein AM/propidium iodide staining; viable cells appear green; upper panel: Schwann cells seeded on woven silk fibroin matts coated with collagen or laminin; lower panel: Schwann cells seeded on silk fibroin fibres coated with collagen or laminin;

DISCUSSION

In this study we hypothesized that covalent binding of laminin and collagen I/III to silk fibroin could accelerate cell adhesion and as a result have beneficial effects on Schwann cell viability and proliferation cultured on silk fibroin.

A well-known method was used to isolate Schwann cells by first dissociating the nerve and then cultivating the cells in a selective medium introduced by Kaekhaw *et al.* 2012 (108). Purity of the Schwann cells used was proven with S100b, P75 and P0 antibody staining, evaluated with flow cytometry. Furthermore cells showed the typical Schwann cell bipolar, spindle-like morphology.

Vleggert *et al.* (200) showed that Schwann cells can adhere to a number of materials, contradicting the common opinion that attachment is limited to an exclusive materials coated with ECM molecules and therefore an important consideration for Schwann cultures (200,201). In our study we demonstrated that - seeded in a low concentration - Schwann cells adhered to a certain degree to all substrates, even to the negative control (uncoated tissue culture plastic), but there were significant differences between the substrates providing ECM molecules and the uncoated controls at all three time points evaluated. Covalent binding of laminin to fibroin significantly improved cell adhesion, also compared to the standard coating used for Schwann cells (lysine/laminin). Moreover it accelerated attachment: more than 90%

of the seeded cells adhered within the first 20 minutes. As seen in Figure 36, time is a crucial factor. Percentage of viable cells within the non-adhered cells decreased significantly after 2 hours and 24 hours. This effect might not only result in high variations of cell numbers, but also in a selection of sub-populations within the Schwann cells. A faster and more efficient cell seeding results in a lower initial cell number needed and a reduction of donor material necessary.

It is known that laminin and collagen interact with integrins on the surface of Schwann cells, supporting adhesion and proliferation (198). We observed a positive effect of both, laminin and collagen, on Schwann cell adhesion compared to the control groups. However, only the laminin-coated groups showed an increase in proliferation, while proliferation on the collagen-coated fibroin films was comparable to the negative control and even lower than fibroin alone. Simultaneously, cell metabolism assessed by MTT assay revealed no differences between the groups after 24 hours, but a significant increase in laminin coated groups after 72 hours. This increase in metabolic activity may be reflected in the increased proliferation. It has been shown that a number of neural cells respond with an increased viability and a later onset of apoptosis to adhesion on laminin (14,202,203). The increase in viability is in accordance with our findings, in further studies long term effects (eg on adhesion and apoptosis) have to be evaluated.

Concluding, collagen and laminin covalently bound to silk fibroin increased cell adhesion, while only laminin also improved proliferation and cell viability.

SUMMARY

Regeneration of peripheral nerves is more than other tissues a complex interplay of cells, growth factors and extracellular matrix. The unique trait of Schwann cells having a regenerative phenotype and in this state being extremely reactive to outer stimuli is challenge and possibility at the same time.

When Schwann cells were treated with extracorporeal shockwaves, we observed a higher proliferative activity without phenotype commitment, increased purity of the culture as well as reduced expression of senescence associated markers even after long cultivation periods. Our *in vitro* study reflects a well-known *in vivo* problem, but also presents a possible solution: limited proliferative capacity of Schwann cells can be improved with extracorporeal shockwave treatment. Treated Schwann cells are thought to be building a growth substrate faster and for a longer period of time. The resulting *in vivo* effect could be twofold: not only results extracorporeal shockwave treatment in an acceleration of regeneration by activating autologous Schwann cells, but also allows reimplantation of a high number of autologous Schwann cells – or highly committed Schwann cell-like cells- expanded *ex vivo,* in a decidedly regenerative state.

Nerve conduit luminal fillers have been topic of discussion for many years. Ideas of an ideal luminal filler include gels, single fibres, to composite gel/fibre fillers or multiple channels containing different growth factors and/or cells. We developed a gel/fibre composite material including fibrin in both components, which is known for its Schwann cell phenotype modifying characteristics: as long as fibrin is present Schwann cells cannot switch to their myelinating phenotype, and continue proliferating. We could show that mesenchymal stem cells differentiated into activated, proliferating SCLs react to minimal changes in stimulus, switching to a pro-myelinating phenotype. Aligned electrospun fibrin-PGLA fibres promoted the formation of Büngner-like structures in Schwann cell-like cells.

In an attempt to develop a novel nerve conduit a braided silk fibroin tube was modified with a ternary solvent to improve its stability and topographic characteristics. Migration assays revealed that the modified tube is permeable for nutrients, but not for potentially ingrowing fibroblasts. *In vitro* cell viability tests confirmed cytocompatibility for Schwann cells. Short term *in vivo* studies in the rat proved that the silk fibroin did not trigger host inflammatory responses, while long term *in vivo* studies showed promising histologic and functional outcome.

Furthermore a protocol has been established to covalently bind laminin to silk fibroin utilizing carbodiimide chemistry, resulting in improved adhesion, viability and proliferation of Schwann cells.

Summarizing, promising results have been found improving several aspects of nerve regeneration. Extracorporeal Shockwave Treatment appears to have a beneficial influence on a variety of cells, including mesenchymal stem cells and Schwann cells. Electrospun fibrin supports formation of Büngner like structures of Schwann cells and Schwann cell-like cells, qualifying it as luminal filler for mechanically stable silk fibroin tubes.

REFERENCES

1. Belkas JS, Shoichet MS, Midha R. Peripheral nerve regeneration through guidance tubes. Neurol Res. 2004;26:151–60.

2. Haftek J. Autogenous cable nerve grafting instead of end to end anastomosis in secondary nerve suture. Acta Neurochir (Wien). 1976;34(1-4):217–21.

3. Siemionow M, Brzezicki G. Chapter 8 Current Techniques and Concepts in Peripheral Nerve Repair. International Review of Neurobiology. 2009. p. 141–72.

4. Mumenthaler Marco, Stöhr Manfred, Müller-Vahl Hermann. Läsionen peripherer Nerven und radikuläre Syndrome. Thieme; 2007.

5. Sunderland S. Nerves and Nerve Injuries. Journal of neurology, neurosurgery, and psychiatry. 1969. p. 165.

6. Carp S. Peripheral Nerve Injury An Anatomical and Physiological Approach for Physical Therapy Intervention. FA Davis; 2015.

7. Oldfors A, Ullman M. Motor nerve conduction velocity and nerve fibre diameter in experimental protein deprivation. Studies on rat peripheral nerve during development. Acta Neuropathol. 1980;51(3):215–21.

8. Avellino AM, Hart D, Dailey AT, MacKinnon M, Ellegala D, Kliot M. Differential macrophage responses in the peripheral and central nervous system during wallerian degeneration of axons. Exp Neurol. 1995;136(2):183–98.

9. Millesi H. Bridging defects: autologous nerve grafts. Acta Neurochir Suppl. 2007;100:37–8.

10. Daly W, Yao L, Zeugolis D, Windebank A, Pandit A. A biomaterials approach to peripheral nerve regeneration: bridging the peripheral nerve gap and enhancing functional recovery. Journal of The Royal Society Interface. 2012. p. 202–21.

11. Yannas I V. Tissue and organ regeneration in adults. Springer; 2001.

12. de Luca AC, Terenghi G, Downes S. Chemical surface modification of poly-ε-caprolactone improves Schwann cell proliferation for peripheral nerve repair. J Tissue Eng Regen Med. 2014;8(2):153–63.

13. Schaakxs D, Kalbermatten DF, Pralong E, Raffoul W, Wiberg M, Kingham PJ. Poly-3-hydroxybutyrate strips seeded with regenerative cells are effective promoters of peripheral nerve repair. J Tissue Eng Regen Med. 2014;n/a – n/a.

14. di Summa PG, Kalbermatten DF, Raffoul W, Terenghi G, Kingham PJ. Extracellular Matrix Molecules Enhance the Neurotrophic Effect of Schwann Cell-Like Differentiated Adipose-Derived Stem Cells and Increase Cell Survival Under Stress Conditions. Tissue Eng Part A. 2013 Feb 24;19(3-4):368–79.

15. Harley BA, Yannas I V. Induced peripheral nerve regeneration using scaffolds. Minerva Biotecnol. 2006;18(2):97–120.

16. Jin J, Limburg S, Joshi SK, Landman R, Park M, Zhang Q, et al. Peripheral nerve repair in rats using composite hydrogel-filled aligned nanofiber conduits with incorporated nerve growth

factor. Tissue Eng Part A. 2013;19:2138–46.

17. Daud MFB, Pawar KC, Claeyssens F, Ryan AJ, Haycock JW. An aligned 3D neuronal-glial co-culture model for peripheral nerve studies. Biomaterials. 2012;33(25):5901–13.

18. Daly WT, Yao L, Abu-rub MT, O'Connell C, Zeugolis DI, Windebank AJ, et al. The effect of intraluminal contact mediated guidance signals on axonal mismatch during peripheral nerve repair. Biomaterials. 2012;33(28):6660–71.

19. Hausner T, Schmidhammer R, Zandieh S, Hopf R, Schultz A, Gogolewski S, et al. Nerve regeneration using tubular scaffolds from biodegradable polyurethane. Acta Neurochir Suppl. 2007;100:69–72.

20. Wang G, Hu X, Lin W, Dong C, Wu H. Electrospun PLGA-silk fibroin-collagen nanofibrous scaffolds for nerve tissue engineering. Vitr Cell Dev Biol - Anim. 2011;47(3):234–40.

21. Han H, Ao Q, Chen G, Wang S, Zuo H. A novel basic fibroblast growth factor delivery system fabricated with heparin-incorporated fibrin-fibronectin matrices for repairing rat sciatic nerve disruptions. Biotechnol Lett. 2010;32(4):585–91.

22. Wood MD, MacEwan MR, French AR, Moore AM, Hunter D a., Mackinnon SE, et al. Fibrin matrices with affinity-based delivery systems and neurotrophic factors promote functional nerve regeneration. Biotechnol Bioeng. 2010;106(6):970–9.

23. Hobson MI, Green CJ, Terenghi G. VEGF enhances intraneural angiogenesis and improves nerve regeneration after axotomy. J Anat. 2000;197 Pt 4:591–605.

24. di Summa PGG, Kingham PJJ, Raffoul W, Wiberg M, Terenghi G, Kalbermatten DFF. Adipose-derived stem cells enhance peripheral nerve regeneration. J Plast Reconstr Aesthetic Surg [Internet]. 2010;63(9):1544–52.

25. Rodríguez FJ, Verdú E, Ceballos D, Navarro X. Nerve guides seeded with autologous schwann cells improve nerve regeneration. Exp Neurol. 2000;161:571–84.

26. Jessen KR, Mirsky R. The origin and development of glial cells in peripheral nerves. Nat Rev Neurosci. 2005;6(9):671–82.

27. Brady S, Siegel G, Albers RW, Price D. Basic neurochemistry: molecular, cellular and medical aspects. Academic Press; 2005.

28. Sherman DL, Brophy PJ. Mechanisms of axon ensheathment and myelin growth. Nat Rev Neurosci. 2005;6(9):683–90.

29. Jessen KR, Mirsky R. Schwann cells and their precursors emerge as major regulators of nerve development. Trends Neurosci. 1999;22(9):402–10.

30. Arthur-Farraj PJ, Latouche M, Wilton DK, Quintes S, Chabrol E, Banerjee A, et al. c-Jun Reprograms Schwann Cells of Injured Nerves to Generate a Repair Cell Essential for Regeneration. Neuron. 2012;75(4):633–47.

31. Funakoshi H, Frisén J, Barbany G, Timmusk T, Zachrisson O, Verge VMK, et al. Differential expression of mRNAs for neurotrophins and their receptors after axotomy of the sciatic nerve. J Cell Biol. 1993;123(2):455–65.

32. Höke a, Cheng C, Zochodne DW. Expression of glial cell line-derived neurotrophic factor family of growth factors in peripheral nerve injury in rats. Neuroreport. 2000;11(8):1651–4.

33.   Mudó G, Persson H, Timmusk T, Funakoshi H, Bindoni M, Belluardo N. Increased expression of trkB and trkC messenger RNAs in the rat forebrain after focal mechanical injury. Neuroscience. 1993;57(4):901–12.

34.   Thornton MR, Shawcross SG, Mantovani C, Kingham PJ, Birchall M a, Terenghi G. Neurotrophins 3 and 4 differentially regulate NCAM, L1 and N-cadherin expression during peripheral nerve regeneration. Biotechnol Appl Biochem. 2008;49(Pt 2):165–74.

35.   Provenzano MJ, Minner SA, Zander K, Clark JJ, Kane CJ, Green SH, et al. p75(NTR) expression and nuclear localization of p75(NTR) intracellular domain in spiral ganglion Schwann cells following deafness correlate with cell proliferation. Mol Cell Neurosci. 2011;47(4):306–15.

36.   Cosgaya JM, Chan JR, Shooter EM. The neurotrophin receptor p75NTR as a positive modulator of myelination. Science. 2002;298(5596):1245–8.

37.   Hausner T, Pajer K, Halat G, Hopf R, Schmidhammer R, Redl H, et al. Improved rate of peripheral nerve regeneration induced by extracorporeal shock wave treatment in the rat. Exp Neurol. Austrian Cluster for Tissue Regeneration and Ludwig Boltzmann Institute for Experimental and Clinical Traumatology at the Research Centre for Traumatology of the Austrian Workers' Compensation Board (AUVA), Donaueschingenstr. 13, A-1200 Vienna, Austria. t; 2012;236(2):363–70.

38.   Weihs A, Fuchs C, Teuschl A, Hartinger J, Slezak P, Mittermayr R, et al. Shock wave treatment enhances cell proliferation and improves wound healing by ATP release-coupled extracellular signal-regulated kinase (ERK) activation. J Biol Chem. 2014;Sep 26(289(39)):27090–104.

39.   Williams LR, Longo FM, Powell HC, Lundborg G, Varon S. Spatial-temporal progress of peripheral nerve regeneration within a silicone chamber: parameters for a bioassay. J Comp Neurol. 1983;218(4):460–70.

40.   Yang Y, Chen X, Ding F, Zhang P, Liu J, Gu X. Biocompatibility evaluation of silk fibroin with peripheral nerve tissues and cells in vitro. Biomaterials. 2006/12/26 ed. 2007;28(9):1643–52.

41.   Madduri S, Papaloizos M, Gander B. Trophically and topographically functionalized silk fibroin nerve conduits for guided peripheral nerve regeneration. Biomaterials. 2009/12/17 ed. 2010;31(8):2323–34.

42.   Tohyama K, Ide C. The localization of laminin and fibronectin on the Schwann cell basal lamina. Arch Histol Jpn Nippon soshikigaku kiroku. 1984;47(5):519–32.

43.   Wang GY, Hirai K, Shimada H. The role of laminin, a component of Schwann cell basal lamina, in rat sciatic nerve regeneration within antiserum-treated nerve grafts. Brain Res. 1992;570(1-2):116–25.

44.   Chiono V, Tonda-Turo C, Ciardelli G. Chapter 9 Artificial Scaffolds for Peripheral Nerve Reconstruction. International Review of Neurobiology. 2009. p. 173–98.

45.   Chernousov MA, Yu W-M, Chen Z-L, Carey DJ, Strickland S. Regulation of Schwann cell function by the extracellular matrix. Glia. 2008;56(14):1498–507.

46.   Javazon EH, Beggs KJ, Flake AW. Mesenchymal stem cells: paradoxes of passaging. Exp Hematol; 2004;32(5):414–25.

47.   Bianco P, Riminucci M, Gronthos S, Robey PG. Bone marrow stromal stem cells: nature, biology, and potential applications. Stem Cells. 2001;19(3):180–92.

48.   Lee OK, Kuo TK, Chen W-M, Lee K-D, Hsieh S-L, Chen T-H. Isolation of multipotent mesenchymal stem cells from umbilical cord blood. Blood. 2004;103(5):1669–75.

49.   Kern S, Eichler H, Stoeve J, Klüter H, Bieback K. Comparative analysis of mesenchymal stem cells from bone marrow, umbilical cord blood, or adipose tissue. Stem Cells. 2006;24(5):1294–301.

50.   Fan H, Liu H, Toh SL, Goh JCH. Enhanced differentiation of mesenchymal stem cells co-cultured with ligament fibroblasts on gelatin/silk fibroin hybrid scaffold. Biomaterials. 2008;29(8):1017–27.

51.   Väänänen HK. Mesenchymal stem cells. Ann Med. 2005;37(7):469–79.

52.   Dominici M, Le Blanc K, Mueller I, Slaper-Cortenbach I, Marini F, Krause D, et al. Minimal criteria for defining multipotent mesenchymal stromal cells. The International Society for Cellular Therapy position statement. Cytotherapy. 2006;8(4):315–7.

53.   Strem BM, Hicok KC, Zhu M, Wulur I, Alfonso Z, Schreiber RE, et al. Multipotential differentiation of adipose tissue-derived stem cells. Keio J Med. 2005;54(3):132–41.

54.   Dezawa M, Takahashi I, Esaki M, Takano M, Sawada H. Sciatic nerve regeneration in rats induced by transplantation of in vitro differentiated bone-marrow stromal cells. Eur J Neurosci. 2001;14(11):1771–6.

55.   Jiang L, Zhu J-K, Liu X-L, Xiang P, Hu J, Yu W-H. Differentiation of rat adipose tissue-derived stem cells into Schwann-like cells in vitro. Neuroreport. 2008;19(10):1015–9.

56.   Barry FP, Murphy JM. Mesenchymal stem cells: clinical applications and biological characterization. Int J Biochem Cell Biol. 2004;36(4):568–84.

57.   Chamberlain G, Fox J, Ashton B, Middleton J. Concise review: mesenchymal stem cells: their phenotype, differentiation capacity, immunological features, and potential for homing. Stem Cells. 2007;25(11):2739–49.

58.   Kronsteiner B, Wolbank S, Peterbauer A, Hackl C, Redl H, van Griensven M, et al. Human mesenchymal stem cells from adipose tissue and amnion influence T-cells depending on stimulation method and presence of other immune cells. Stem Cells Dev. 2011;20(12):2115–26.

59.   Nasef A, Mathieu N, Chapel A, Frick J, Francois S, Mazurier C, et al. Immunosuppressive effects of mesenchymal stem cells: Involvement of HLA-G. Transplantation. 2007;84:231–7.

60.   Siddappa R, Licht R, van Blitterswijk C, de Boer J. Donor variation and loss of multipotency during in vitro expansion of human mesenchymal stem cells for bone tissue engineering. J Orthop Res. 2007;25(8):1029–41.

61.   Kretlow JD, Jin Y-Q, Liu W, Zhang WJ, Hong T-H, Zhou G, et al. Donor age and cell passage affects differentiation potential of murine bone marrow-derived stem cells. BMC Cell Biol. 2008;9:60.

62.   Bonab MM, Alimoghaddam K, Talebian F, Ghaffari SH, Ghavamzadeh A, Nikbin B. Aging of mesenchymal stem cell in vitro. 2006;7:14.

63.   Ross SE, Hemati N, Longo KA, Bennett CN, Lucas PC, Erickson RL, et al. Inhibition of adipogenesis by Wnt signaling. Sci (New York, NY). 2000;289(5481):950–3.

64. Bourin P, Bunnell BA, Casteilla L, Dominici M, Katz AJ, March KL, et al. Stromal cells from the adipose tissue-derived stromal vascular fraction and culture expanded adipose tissue-derived stromal/stem cells: a joint statement of the International Federation for Adipose Therapeutics and Science (IFATS) and the International So. Cytotherapy.; 2013;15(6):641–8.

65. Maioli M, Rinaldi S, Santaniello S, Castagna A, Pigliaru G, Delitala A, et al. Radio and Electric Asymmetric Conveyed Fields and Human Adipose-derived Stem cells Obtained with a non-enzymatic Method and Device: a Novel Approach to Multipotency. Cell Transplant. 2013;

66. Kang KS, Hong JM, Kang JA, Rhie J-W, Cho D-W. Osteogenic differentiation of human adipose-derived stem cells can be accelerated by controlling the frequency of continuous ultrasound. J Ultrasound Med; 2013;32(8):1461–70.

67. Raabe O, Shell K, Goessl A, Crispens C, Delhasse Y, Eva A, et al. Effect of extracorporeal shock wave on proliferation and differentiation of equine adipose tissue-derived mesenchymal stem cells in vitro. Am J Stem Cells. 2013;2(1):62–73.

68. Kaude J V, Williams CM, Millner MR, Scott KN, Finlayson B. Renal morphology and function immediately after extracorporeal shock-wave lithotripsy. AJR Am J Roentgenol. 1985;145(2):305–13.

69. Schaden W, Fischer A, Sailler A. Extracorporeal shock wave therapy of nonunion or delayed osseous union. Clin Orthop Relat Res. 2001;(387):90–4.

70. Furia JP, Juliano PJ, Wade AM, Schaden W, Mittermayr R. Shock wave therapy compared with intramedullary screw fixation for nonunion of proximal fifth metatarsal metaphyseal-diaphyseal fractures. J bone Jt Surg Am Vol. 2010;92(4):846–54.

71. Elster EA, Stojadinovic A, Forsberg J, Shawen S, Andersen RC, Schaden W. Extracorporeal shock wave therapy for nonunion of the tibia. J Orthop Trauma. 2010;24(3):133–41.

72. Mittermayr R, Hartinger J, Antonic V, Meinl A, Pfeifer S, Stojadinovic A, et al. Extracorporeal shock wave therapy (ESWT) minimizes ischemic tissue necrosis irrespective of application time and promotes tissue revascularization by stimulating angiogenesis. Ann Surg. 2011;253(5):1024–32.

73. Schaden W, Thiele R, Kölpl C, Pusch M, Nissan A, Attinger CE, et al. Shock wave therapy for acute and chronic soft tissue wounds: a feasibility study. J Surg Res. 2007;143(1):1–12.

74. Saggini R, Figus A, Troccola A, Cocco V, Saggini A, Scuderi N. Extracorporeal shock wave therapy for management of chronic ulcers in the lower extremities. Ultrasound Med Biol. 2008;34(8):1261–71.

75. Haupt G. Use of extracorporeal shock waves in the treatment of pseudarthrosis, tendinopathy and other orthopedic diseases. J Urol. Department of Urology, Ruhr-University Bochum, Germany.; 1997;158(1):4–11.

76. Davis TA, Stojadinovic A, Anam K, Amare M, Naik S, Peoples GE, et al. Extracorporeal shock wave therapy suppresses the early proinflammatory immune response to a severe cutaneous burn injury. Int Wound J. 2009;6(1):11–21.

77. Rompe JD, Hope C, Küllmer K, Heine J, Bürger R. Analgesic effect of extracorporeal shock-wave therapy on chronic tennis elbow. J bone Jt Surg Br Vol. 1996;78(2):233–7.

78. Ogden JA, Tóth-Kischkat A, Schultheiss R. Principles of shock wave therapy. Clin Orthop Relat Res. 2001;(387):8–17.

79.   Chen YJ, Wurtz T, Wang CJ, Kuo YR, Yang KD, Huang HC, et al. Recruitment of mesenchymal stem cells and expression of TGF-β1 and VEGF in the early stage of shock wave-promoted bone regeneration of segmental defect in rats. J Orthop Res. 2004;22:526–34.

80.   Wolbank S, Peterbauer A, Fahrner M, Hennerbichler S, van Griensven M, Stadler G, et al. Dose-dependent immunomodulatory effect of human stem cells from amniotic membrane: a comparison with human mesenchymal stem cells from adipose tissue. Tissue Eng. 2007;13(6):1173–83.

81.   Holfeld J, Tepeköylü C, Kozaryn R, Urbschat A, Zacharowski K, Grimm M, et al. Shockwave Therapy Differentially Stimulates Endothelial Cells: Implications on the Control of Inflammation via Toll-Like Receptor 3. Inflammation. 2014;37:65–70.

82.   Moviglia GA, Blasetti N, Zarate JO, Pelayes DE. In vitro differentiation of adult adipose mesenchymal stem cells into retinal progenitor cells. Ophthalmic Res. 2012;48 Suppl 1:1–5.

83.   Song K, Wang Z, Li W, Zhang C, Lim M, Liu T. In vitro culture, determination, and directed differentiation of adult adipose-derived stem cells towards cardiomyocyte-like cells induced by angiotensin II. Appl Biochem Biotechnol. 2013;170(2):459–70.

84.   Sen A, Lea-Currie YR, Sujkowska D, Franklin DM, Wilkison WO, Halvorsen YD, et al. Adipogenic potential of human adipose derived stromal cells from multiple donors is heterogeneous. J Cell Biochem. 2001;81(2):312–9.

85.   Zhu M, Kohan E, Bradley J, Hedrick M, Benhaim P, Zuk P. The effect of age on osteogenic, adipogenic and proliferative potential of female adipose-derived stem cells. J Tissue Eng Regen Med. 2009;3(4):290–301.

86.   Tsutsumi S, Shimazu A, Miyazaki K, Pan H, Koike C, Yoshida E, et al. Retention of multilineage differentiation potential of mesenchymal cells during proliferation in response to FGF. Biochem Biophys Res Commun. 2001;288(2):413–9.

87.   Lai W-T, Krishnappa V, Phinney DG. Fibroblast growth factor 2 (Fgf2) inhibits differentiation of mesenchymal stem cells by inducing Twist2 and Spry4, blocking extracellular regulated kinase activation, and altering Fgf receptor expression levels. Stem Cells. 2011;29(7):1102–11.

88.   Shahdadfar A, Frønsdal K, Haug T, Reinholt FP, Brinchmann JE. In vitro expansion of human mesenchymal stem cells: choice of serum is a determinant of cell proliferation, differentiation, gene expression, and transcriptome stability. Stem Cells. 2005;23(9):1357–66.

89.   Stolzing A, Coleman N, Scutt A. Glucose-induced replicative senescence in mesenchymal stem cells. Rejuvenation Res. 2006;9(1):31–5.

90.   Schätti O, Grad S, Goldhahn J, Salzmann G, Li Z, Alini M, et al. A combination of shear and dynamic compression leads to mechanically induced chondrogenesis of human mesenchymal stem cells. Eur Cell Mater. 2011;22:214–25.

91.   Zorick TS, Lemke G. Schwann cell differentiation. Curr Opin Cell Biol. 1996;8(6):870–6.

92.   Cosgaya JM, Chan JR, Shooter EM. The neurotrophin receptor p75NTR as a positive modulator of myelination. Sci (New York, NY). 2002;298(5596):1245–8.

93.   Boland GM, Perkins G, Hall DJ, Tuan RS. Wnt 3a promotes proliferation and suppresses osteogenic differentiation of adult human mesenchymal stem cells. J Cell Biochem. 2004;93(6):1210–30.

94.   Fierro F, Illmer T, Jing D, Schleyer E, Ehninger G, Boxberger S, et al. Inhibition of platelet-

derived growth factor receptorbeta by imatinib mesylate suppresses proliferation and alters differentiation of human mesenchymal stem cells in vitro. Cell Prolif. 2007;40(3):355–66.

95.   Stenderup K, Justesen J, Eriksen EF, Rattan SI, Kassem M. Number and proliferative capacity of osteogenic stem cells are maintained during aging and in patients with osteoporosis. J Bone Miner Res. 2001;16(6):1120–9.

96.   Chen C-S. Phorbol ester induces elevated oxidative activity and alkalization in a subset of lysosomes. BMC Cell Biol. 2002;3:21.

97.   Bergman RJ, Gazit D, Kahn AJ, Gruber H, McDougall S, Hahn TJ. Age-related changes in osteogenic stem cells in mice. J Bone Miner Res. 1996;11(5):568–77.

98.   McIntosh K, Zvonic S, Garrett S, Mitchell JB, Floyd ZE, Hammill L, et al. The immunogenicity of human adipose-derived cells: temporal changes in vitro. Stem Cells. 2006;24(5):1246–53.

99.   Frairia R, Berta L. Biological effects of extracorporeal shock waves on fibroblasts. A review. Muscles Ligaments Tendons J. 2011;1:138–47.

100.   Huang C, Holfeld J, Schaden W, Orgill D, Ogawa R. Mechanotherapy: Revisiting physical therapy and recruiting mechanobiology for a new era in medicine. Trends in Molecular Medicine. 2013. p. 555–64.

101.   Lauer U, Bürgelt E, Squire Z, Messmer K, Hofschneider PH, Gregor M, et al. Shock wave permeabilization as a new gene transfer method. Gene Ther. 1997;4:710–5.

102.   Mukhatyar V, Karumbaiah L, Yeh J, Bellamkonda R. Tissue Engineering Strategies Designed to Realize the Endogenous Regenerative Potential of Peripheral Nerves. Adv Mater. 2009;21(46):4670–9.

103.   Arino H, Brandt J, Dahlin LB. Implantation of Schwann cells in rat tendon autografts as a model for peripheral nerve repair: long term effects on functional recovery. Scand J Plast Reconstr Surg Hand Surg. 2008;42(6):281–5.

104.   Johnson EO, Soucacos PN. Nerve repair: Experimental and clinical evaluation of biodegradable artificial nerve guides. Injury. 2008;39(3 SUPPL.):29–33.

105.   Saheb-Al-Zamani M, Yan Y, Farber SJ, Hunter DA, Newton P, Wood MD, et al. Limited regeneration in long acellular nerve allografts is associated with increased Schwann cell senescence. Exp Neurol. 2013;247:165–77.

106.   Chen Z-L, Yu W-M, Strickland S. Peripheral regeneration. Annu Rev Neurosci. 2007;30:209–33.

107.   Schuh CMAP, Heher P, Weihs AM, Banerjee A, Fuchs C, Gabriel C, et al. In vitro extracorporeal shock wave treatment enhances stemness and preserves multipotency of rat and human adipose-derived stem cells. Cytotherapy. 2014;16(12):1666–78.

108.   Kaewkhaw R, Scutt AM, Haycock JW. Integrated culture and purification of rat Schwann cells from freshly isolated adult tissue. Nature Protocols. 2012. p. 1996–2004.

109.   Frostick SP, Yin Q, Kemp GJ. Schwann cells, neurotrophic factors, and peripheral nerve regeneration. Microsurgery. 1998;18(7):397–405.

110.   Toy D, Namgung U. Role of glial cells in axonal regeneration. Exp Neurobiol. 2013;22(2):68–76.

111. Bhatheja K, Field J. Schwann cells: Origins and role in axonal maintenance and regeneration. International Journal of Biochemistry and Cell Biology. 2006. p. 1995–9.

112. Casella GTB, Bunge RP, Wood PM. Improved method for harvesting human Schwann cells from mature peripheral nerve and expansion in vitro. Glia. 1996;17(4):327–38.

113. Thi AD, Evrard C, Rouget P. Proliferation and differentiation properties of permanent Schwann cell lines immortalized with a temperature-sensitive oncogene. J Exp Biol. 1998;201(Pt 6):851–60.

114. Lehmann HC, Chen W, Mi R, Wang S, Liu Y, Rao M, et al. Human Schwann Cells Retain Essential Phenotype Characteristics After Immortalization. Stem Cells and Development. 2012. p. 423–31.

115. Lemke G, Chao M. Axons regulate Schwann cell expression of the major myelin and NGF receptor genes. Development. 1988;102(3):499–504.

116. Lemke G. Molecular biology of the major myelin genes. Trends Neurosci. 1986;9:266–70.

117. Triolo D, Dina G, Lorenzetti I, Malaguti M, Morana P, Del Carro U, et al. Loss of glial fibrillary acidic protein (GFAP) impairs Schwann cell proliferation and delays nerve regeneration after damage. J Cell Sci. 2006;119(Pt 19):3981–93.

118. Parkinson DB, Bhaskaran A, Arthur-Farraj P, Noon LA, Woodhoo A, Lloyd AC, et al. c-Jun is a negative regulator of myelination. J Cell Biol. 2008;181(4):625–37.

119. Schwiebert EM, Zsembery A. Extracellular ATP as a signaling molecule for epithelial cells. Biochim Biophys Acta. 2003;1615(1-2):7–32.

120. Abbracchio MP, Burnstock G, Boeynaems J-M, Barnard EA, Boyer JL, Kennedy C, et al. International Union of Pharmacology LVIII: update on the P2Y G protein-coupled nucleotide receptors: from molecular mechanisms and pathophysiology to therapy. Pharmacol Rev. 2006;58(3):281–341.

121. Lazarowski ER. Vesicular and conductive mechanisms of nucleotide release. Purinergic Signalling. 2012. p. 359–73.

122. Junger WG. Immune cell regulation by autocrine purinergic signalling. Nat Rev Immunol. 2011;11(3):201–12.

123. Liu GJ, Bennett MR. ATP secretion from nerve trunks and Schwann cells mediated by glutamate. Neuroreport. 2003;14(16):2079–83.

124. Samara C, Poirot O, Domènech-Estévez E, Chrast R. Neuronal activity in the hub of extrasynaptic Schwann cell-axon interactions. Front Cell Neurosci. 2013;7:228.

125. Jeftinija SD, Jeftinija K V. ATP stimulates release of excitatory amino acids from cultured Schwann cells. Neuroscience. 1997;82(3):927–34.

126. Stevens B, Fields RD. Response of Schwann cells to action potentials in development. Science. 2000;287(5461):2267–71.

127. Fields RD, Burnstock G. Purinergic signalling in neuron-glia interactions. Nat Rev Neurosci. 2006;7(6):423–36.

128. Steven B, Ishibashi T, Chen J-F, Fields RD. Adenosine: an activity-dependent axonal signal regulating MAP kinase and proliferation in developing Schwann cells. Neuron Glia Biology.

2004.

129. Saitoh F, Araki T. Proteasomal degradation of glutamine synthetase regulates schwann cell differentiation. J Neurosci. 2010;30(4):1204–12.

130. Boison D, Singer P, Shen H-Y, Feldon J, Yee BK. Adenosine hypothesis of schizophrenia--opportunities for pharmacotherapy. Neuropharmacology. Elsevier Ltd; 2012;62(3):1527–43.

131. Li Q, Ping P, Jiang H, Liu K. Nerve conduit filled with GDNF gene-modified Schwann cells enhances regeneration of the peripheral nerve. Microsurgery. 2006;26:116–21.

132. Rutkowski GE, Miller CA, Jeftinija S, Mallapragada SK. Synergistic effects of micropatterned biodegradable conduits and Schwann cells on sciatic nerve regeneration. J Neural Eng. 2004;1:151–7.

133. Ahmed Z, Brown RA. Adhesion, alignment, and migration of cultured Schwann cells on ultrathin fibronectin fibres. Cell Motil Cytoskeleton. 1999;42:331–43.

134. Hoffman-Kim D, Mitchel JA, Bellamkonda R V. Topography, cell response, and nerve regeneration. Annu Rev Biomed Eng. 2010;12:203–31.

135. Huang ZM, Zhang YZ, Kotaki M, Ramakrishna S. A review on polymer nanofibers by electrospinning and their applications in nanocomposites. Compos Sci Technol. 2003;63:2223–53.

136. Pham QP, Sharma U, Mikos AG. Electrospinning of polymeric nanofibers for tissue engineering applications: a review. Tissue Eng. 2006;12:1197–211.

137. Katti DS, Robinson KW, Ko FK, Laurencin CT. Bioresorbable nanofiber-based systems for wound healing and drug delivery: optimization of fabrication parameters. J Biomed Mater Res B Appl Biomater. 2004;70:286–96.

138. Casper CL, Stephens JS, Tassi NG, Chase DB, Rabolt JF. Controlling surface morphology of electrospun polystyrene fibers: Effect of humidity and molecular weight in the electrospinning process. Macromolecules. 2004;37(2):573–8.

139. Wong C, Inman E, Spaethe R, Helgerson S. New Technologies and Diagnostic Tools Fibrin-based biomaterials to deliver human growth factors. Thromb Haemost. 2003;89:573–82.

140. Weinand C, Gupta R, Weinberg E, Madisch I, Jupiter JB, Vacanti JP. Human shaped thumb bone tissue engineered by hydrogel-beta-tricalciumphosphate/poly-epsilon-caprolactone scaffolds and magnetically sorted stem cells. Ann Plast Surg. 2007;59:46–52; discussion 52.

141. Peled E, Boss J, Bejar J, Zinman C, Seliktar D. A novel poly(ethylene glycol)-fibrinogen hydrogel for tibial segmental defect repair in a rat model. J Biomed Mater Res A. 2007;80:874–84.

142. Kaipel M, Schützenberger S, Schultz A, Ferguson J, Slezak P, Morton T, et al. BMP-2 but not VEGF or PDGF in fibrin matrix supports bone healing in a delayed-union rat model. J Orthop Res. 2012;30:1563–9.

143. Falanga V, Iwamoto S, Chartier M, Yufit T, Butmarc J, Kouttab N, et al. Autologous bone marrow-derived cultured mesenchymal stem cells delivered in a fibrin spray accelerate healing in murine and human cutaneous wounds. Tissue engineering. 2007.

144. Mittermayr R, Branski L, Moritz M, Jeschke MG, Herndon DN, Traber D, et al. Fibrin biomatrix-conjugated platelet-derived growth factor AB accelerates wound healing in severe

thermal injury. J Tissue Eng Regen Med. 2013;

145.   Hildner F, Concaro S, Peterbauer A, Wolbank S, Danzer M, Lindahl A, et al. Human adipose-derived stem cells contribute to chondrogenesis in coculture with human articular chondrocytes. Tissue Eng Part A. 2009;15:3961–9.

146.   Hong HJ, Chang JW, Park J-K, Choi JW, Kim YS, Shin YS, et al. Tracheal reconstruction using chondrocytes seeded on a poly-(L-lactic-co-glycolic acid)-fibrin/Hyaluronan. J Biomed Mater Res A. 2014;

147.   Syroid DE, Maycox PJ, Soilu-Hänninen M, Petratos S, Bucci T, Burrola P, et al. Induction of postnatal schwann cell death by the low-affinity neurotrophin receptor in vitro and after axotomy. J Neurosci. 2000;20(15):5741–7.

148.   Arras MML, Grasl C, Bergmeister H, Schima H. Electrospinning of aligned fibers with adjustable orientation using auxiliary electrodes. Science and Technology of Advanced Materials. 2012. p. 035008.

149.   Huang Y-C, Dennis RG, Larkin L, Baar K. Rapid formation of functional muscle in vitro using fibrin gels. J Appl Physiol. 2005;98:706–13.

150.   Son YJ, Thompson WJ. Schwann cell processes guide regeneration of peripheral axons. Neuron. 1995;14:125–32.

151.   Meyer zu Hörste G, Hu W, Hartung H-P, Lehmann HC, Kieseier BC. The immunocompetence of Schwann cells. Muscle Nerve. 2008;37:3–13.

152.   Shen YJ, DeBellard ME, Salzer JL, Roder J, Filbin MT. Myelin-associated glycoprotein in myelin and expressed by Schwann cells inhibits axonal regeneration and branching. Mol Cell Neurosci. 1998;12(1-2):79–91.

153.   Haastert K, Mauritz C, Chaturvedi S, Grothe C. Human and rat adult Schwann cell cultures: fast and efficient enrichment and highly effective non-viral transfection protocol. Nat Protoc. 2007;2:99–104.

154.   Tanaka K, Webster HD. Myelinated fiber regeneration after crush injury is retarded in sciatic nerves of aging mice. J Comp Neurol. 1991;308:180–7.

155.   Song XY, Zhou FHH, Zhong JH, Wu LLY, Zhou XF. Knockout of p75NTR impairs re-myelination of injured sciatic nerve in mice. J Neurochem. 2006;96:833–42.

156.   Bellamkonda R V. Peripheral nerve regeneration: An opinion on channels, scaffolds and anisotropy. Biomaterials. 2006;27:3515–8.

157.   Nezarati R. Effects of Humidity and Solution Viscosity on Electrospun Fiber Morphology. Tissue Eng Part C. 2013;19(10):1–10.

158.   Loesberg WA, te Riet J, van Delft FCMJM, Schön P, Figdor CG, Speller S, et al. The threshold at which substrate nanogroove dimensions may influence fibroblast alignment and adhesion. Biomaterials. 2007;28:3944–51.

159.   Yim EKF, Reano RM, Pang SW, Yee AF, Chen CS, Leong KW. Nanopattern-induced changes in morphology and motility of smooth muscle cells. Biomaterials. 2005;26:5405–13.

160.   Lietz M, Dreesmann L, Hoss M, Oberhoffner S, Schlosshauer B. Neuro tissue engineering of glial nerve guides and the impact of different cell types. Biomaterials. 2006;27:1425–36.

161. Millesi H, Meissl G, Berger A. The interfascicular nerve-grafting of the median and ulnar nerves. J Bone Jt Surg Am. 1972/06/01 ed. 1972;54(4):727–50.

162. Battiston B, Geuna S, Ferrero M, Tos P. Nerve repair by means of tubulization: literature review and personal clinical experience comparing biological and synthetic conduits for sensory nerve repair. Microsurgery. 2005/06/04 ed. 2005;25(4):258–67.

163. Chalfoun CT, Wirth G a, Evans GRD. Tissue engineered nerve constructs: where do we stand? J Cell Mol Med. 2006;10(2):309–17.

164. Chiu DT, Janecka I, Krizek TJ, Wolff M, Lovelace RE. Autogenous vein graft as a conduit for nerve regeneration. Surgery. 1982 Feb;91(2):226–33.

165. Walton RL, Brown RE, Matory WE, Borah GL, Dolph JL. Autogenous vein graft repair of digital nerve defects in the finger: a retrospective clinical study. Plast Reconstr Surg. 1989 Dec;84(6):944–9; discussion 950–2.

166. Itoh S, Shinomiya K, Samejima H, Ohta T, Ishizuki M, Ichinose S. Experimental study on nerve regeneration through the basement membrane tubes of the nerve, muscle, and artery. Microsurgery. 1996 Jan;17(10):525–34.

167. Geuna S, Nicolino S, Raimondo S, Gambarotta G, Battiston B, Tos P, et al. Nerve regeneration along bioengineered scaffolds. Microsurgery. 2007/06/29 ed. 2007;27(5):429–38.

168. Ichihara S, Inada Y, Nakamura T. Artificial nerve tubes and their application for repair of peripheral nerve injury: an update of current concepts. Injury. 2008/09/23 ed. 2008 Oct;39 Suppl 4:29–39.

169. Nectow AR, Marra KG, Kaplan DL. Biomaterials for the development of peripheral nerve guidance conduits. Tissue Eng Part B Rev. 2012 Feb;18(1):40–50.

170. Kameswaran N, Cullen DK, Pfister BJ, Ranalli NJ, Huang JH, Zager EL, et al. A novel neuroprosthetic interface with the peripheral nervous system using artificially engineered axonal tracts. Neurol Res. 2008/12/17 ed. 2008;30(10):1063–7.

171. Kingham PJ, Terenghi G. Bioengineered nerve regeneration and muscle reinnervation. J Anat. 2006/09/29 ed. 2006;209(4):511–26.

172. Soffer L, Wang X, Zhang X, Kluge J, Dorfmann L, Kaplan DL, et al. Silk-based electrospun tubular scaffolds for tissue-engineered vascular grafts. J Biomater Sci Polym Ed. 2008 Jan;19(5):653–64.

173. Zhang X, Baughman CB, Kaplan DL. In vitro evaluation of electrospun silk fibroin scaffolds for vascular cell growth. Biomaterials. 2008 May;29(14):2217–27.

174. Marelli B, Alessandrino A, Farè S, Freddi G, Mantovani D, Tanzi MC. Compliant electrospun silk fibroin tubes for small vessel bypass grafting. Acta Biomater. Acta Materialia Inc.; 2010 Oct;6(10):4019–26.

175. Park SY, Ki CS, Park YH, Lee KG, Kang SW, Kweon HY, et al. Functional recovery guided by an electrospun silk fibroin conduit after sciatic nerve injury in rats. J Tissue Eng Regen Med. 2012 Oct;

176. Lovett M, Cannizzaro C, Daheron L, Messmer B, Vunjak-Novakovic G, Kaplan DL. Silk fibroin microtubes for blood vessel engineering. Biomaterials. 2007/08/31 ed. 2007 Dec;28(35):5271–9.

177. Ghaznavi AM, Kokai LE, Lovett ML, Kaplan DL, Marra KG. Silk fibroin conduits: a cellular and functional assessment of peripheral nerve repair. Ann Plast Surg. 2011/01/26 ed. 2011 Mar;66(3):273–9.

178. Lovett ML, Cannizzaro CM, Vunjak-Novakovic G, Kaplan DL. Gel spinning of silk tubes for tissue engineering. Biomaterials. Elsevier Ltd; 2008 Dec;29(35):4650–7.

179. Lovett M, Eng G, Kluge JA, Cannizzaro C, Vunjak-Novakovic G, Kaplan DL. Tubular silk scaffolds for small diameter vascular grafts. Organogenesis. 2011/01/12 ed. 2010;6(4):217–24.

180. Yang Y, Ding F, Wu J, Hu W, Liu W, Liu J, et al. Development and evaluation of silk fibroin-based nerve grafts used for peripheral nerve regeneration. Biomaterials. 2007/09/22 ed. 2007;28(36):5526–35.

181. Teuschl AH, van Griensven M, Redl H. Sericin Removal from Raw Bombyx mori Silk Scaffolds of High Hierarchical Order. Tissue Eng Part C Methods. 2014;20:431–9.

182. Ai H, Lvov YM, Mills DK, Jennings M, Alexander JS, Jones S a. Coating and selective deposition of nanofilm on silicone rubber for cell adhesion and growth. Cell Biochem Biophys. 2003 Jan;38(2):103–14.

183. Rüdeberg C. A rapid method for staining thin sections of vestopal W-embedded tissue for light microscopy. Experientia. 1967 Sep;23(9):792.

184. Deumens R, Bozkurt A, Meek MF, Marcus M a E, Joosten E a J, Weis J, et al. Repairing injured peripheral nerves: Bridging the gap. Prog Neurobiol. Elsevier Ltd; 2010 Nov;92(3):245–76.

185. Bozkurt a, Deumens R, Scheffel J, O'Dey DM, Weis J, Joosten E a, et al. CatWalk gait analysis in assessment of functional recovery after sciatic nerve injury. J Neurosci Methods. 2008 Aug;173(1):91–8.

186. Bessa PC, Balmayor ER, Azevedo HS, Nürnberger S, Casal M, van Griensven M, et al. Silk fibroin microparticles as carriers for delivery of human recombinant BMPs. Physical characterization and drug release. J Tissue Eng Regen Med. 2010 Jul;4(5):349–55.

187. Bessa PC, Balmayor ER, Hartinger J, Zanoni G, Dopler D, Meinl A, et al. Silk fibroin microparticles as carriers for delivery of human recombinant bone morphogenetic protein-2: in vitro and in vivo bioactivity. Tissue Eng Part C Methods. 2010 Oct;16(5):937–45.

188. Vepari C, Kaplan DL. Silk as a Biomaterial. Prog Polym Sci. 2007 Jan;32(8-9):991–1007.

189. Rockwood DN, Preda RC, Yücel T, Wang X, Lovett ML, Kaplan DL. Materials fabrication from Bombyx mori silk fibroin. Nat Protoc. 2011 Sep;6(10):1612–31.

190. Um IC, Kweon HY, Park YH, Hudson S. Structural characteristics and properties of the regenerated silk fibroin prepared from formic acid. Int J Biol Macromol. 2001 Aug;29(2):91–7.

191. Um IC, Kweon HY, Lee KG, Park YH. The role of formic acid in solution stability and crystallization of silk protein polymer. Int J Biol Macromol. 2003/11/11 ed. 2003 Dec;33(4-5):203–13.

192. Höke A, Redett R, Hameed H, Jari R, Zhou C, Li ZB, et al. Schwann cells express motor and sensory phenotypes that regulate axon regeneration. J Neurosci. 2006;26(38):9646–55.

193. Armstrong SJ, Wiberg M, Terenghi G, Kingham PJ. ECM molecules mediate both Schwann cell proliferation and activation to enhance neurite outgrowth. Tissue Eng. 2007;13:2863–70.

194. Teuschl AH, Schuh CMAP, Halbweis R, Pajer K, Márton G, Hopf R, et al. A new preparation method for anisotropic silk fibroin nerve guidance conduits and its evaluation in vitro and in a rat sciatic nerve defect model. Tissue Eng Part C Methods. 2015 Mar 28;

195. Yang Y, Chen X, Ding F, Zhang P, Liu J, Gu X. Biocompatibility evaluation of silk fibroin with peripheral nerve tissues and cells in vitro. Biomaterials. 2007;28(9):1643–52.

196. Madduri S, Papaloïzos M, Gander B. Trophically and topographically functionalized silk fibroin nerve conduits for guided peripheral nerve regeneration. Biomaterials. 2010;31(8):2323–34.

197. Kundu B, Rajkhowa R, Kundu SC, Wang X. Silk fibroin biomaterials for tissue regenerations. Adv Drug Deliv Rev. 2013;65(4):457–70.

198. Chernousov M a, Carey DJ. Schwann cell extracellular matrix molecules and their receptors. Histol Histopathol. 2000;15(2):593–601.

199. Teuschl AH, Neutsch L, Monforte X, Rünzler D, Van Griensven M, Gabor F, et al. Enhanced cell adhesion on silk fibroin via lectin surface modification. Acta Biomater. 2014;10(6):2506–17.

200. Vleggeert-Lankamp CLA-M, Pêgo AP, Lakke EAJF, Deenen M, Marani E, Thomeer RTWM. Adhesion and proliferation of human Schwann cells on adhesive coatings. Biomaterials. 2004 Jun;25(14):2741–51.

201. Pêgo AP, Vleggeert-Lankamp CL a M, Deenen M, Lakke E a JF, Grijpma DW, Poot A a, et al. Adhesion and growth of human Schwann cells on trimethylene carbonate (co)polymers. J Biomed Mater Res A. 2003;67(3):876–85.

202. Ciara C. Tate, Deborah A. Shear, Matthew C. Tate, David R. Archer DS, LaPlaca and MC. Laminin and fibronectin scaffolds enhance neural stem cell transplantation into the injured brain. J Tissue Eng Regen Med. 2010;4(7):524–31.

203. Santiago LY, Nowak RW, Rubin JP, Marra KG. Peptide-surface modification of poly(caprolactone) with laminin-derived sequences for adipose-derived stem cell applications. Biomaterials. 2006;27(15):2962–9.

ABBREVIATIONS

ANOVA   Analysis of Variance

APS   Ammonium persulfate

ASC   Adipose derived stem cells

ATP   Adenosine triphosphate

BDNF   Brain derived neurotrophic factor

bidest   Bidestillatus/ double distilled

BrdU assay   5-bromo-2-deoxyuridine uptake assay

BSA   Bovine serum albumin

CNAP   Compound nerve action potential

CNS   Central nervous system

CTRL   Control

DEPC   Diethyl pyrocarbonate

DMEM   Dulbecco's Modified Eagle Medium

DMSO   Dimethyl sulfoxide

DNA   Deoxyribonucleic acid

dNTPs   Deoxyribonucleotides

EDTA   Ethylenediaminetetraacetic acid

ESWT   Extracorporeal Shockwave Treatment

FA   Formic acid

FACS   Fluorescence activated cell sorting

FGF   fibroblast growth factor

FGF   Peripheral nervous system

GDNF   Glial derived neurotrophic factor

HFP   Hexafluoroisopropanol

Hz   Hertz

kV   kilo Volt

LDH   Lactate Dehydrogenase

m/s   Meters per second

MAG   Myelin associated glycoprotein

$MgCl_2$ Magnesium chloride

mL	Milliliter
MPa	Mega Pascal
MSC	Mesenchymal stem cell
MTT	[3-(4,5- dimethylthiazol-2-yl)-2,5-diphenyltetrazolium] bromide
NGF	Nerve growth factor
NGFR	Nerve growth factor receptor
OD	Optical Density
P0	Protein 0
P1	Cell Passage 1
P75	Neurotrophin receptor P75
PBS	Phosphate buffered saline
PCR	Polymerase chain reaction
PDGF	Platelet derived growth factor
PGLA	Poly(Lactic-co-Glycolic Acid)
PI	Propidium iodide
PNS	Peripheral nervous system
RNA	Ribonucleic acid
SCLs	Schwann cell like cells
SD	Standard Deviation
SDS-PAGE	Sodium dodecyl sulfate polyacrylamide gelelectrophoresis
SF-NGC	Silk fibroin based nerve guidance conduits
TE	Tissue Engineering
v/v	Volume per volume
VEGF	Vascular endothelial growth factor
w/v	Weight per volume

CURRICULUM VITAE

Name:	Christina Maria Anna Pia Schuh
Date/Place of birth:	29.5.1985, Vienna, Austria
Nationality:	Austria

Experience

01/2014 - present

Group manager
Department for nerve regeneration at the Ludwig Boltzmann Institute for experimental and clinical traumatology

03/2013 - present

PhD studies
Ludwig Boltzmann Institute for experimental and clinical traumatology

03/2012 - 02/2013

Lab manager
University of Applied Sciences Technikum Wien, Vienna, Austria

03/2009 - 02/2013

Research associate, FHplus project NewTissue
University of Applied Sciences Technikum Wien, Vienna, Austria

07/2008 - 03/2009

Research associate
University of Applied Sciences Technikum Wien, Vienna, Austria

other
09/2012 - present

Teacher for cell culture technique
TGM- die Schule der Technik

Education

10/2012 - present

PhD studies (Medical University/University of Technology Vienna)
Supervisor: Prof. Heinz Redl
Topic: Novel approaches in peripheral nerve regeneration

09/2010 - 06/2012

Master Study Program „Biomedical Engineering Sciences" University of Applied Sciences Technikum Wien, Vienna, Austria
(graduated with highest distinctions)

09/2007 – 06/2010

Bachelor Study Program „Biomedical Engineering"
University of Applied Sciences Technikum Wien, Vienna, Austria
(graduated with highest distinctions)

Further education	
2015	**TERMIS Winterschool „Vitro/Vivo Preclinical Models and Imaging in Musculoskeletal Tissue Regeneration"**
2013	**TERMIS Winterschool „Vitro/Vivo Preclinical Models and Imaging in Musculoskeletal Tissue Regeneration"**
2011	**ESAO Summerschool „Biomaterials"**
	ESAO Winterschool „Biomaterials"
2009	**TERMIS Winterschool „Preclinical Models and Imaging in Musculoskeletal TE"**

Publications

Activated Schwann cell like Cells on Aligned Fibrin/PGLA Structures: a novel construct for application in peripheral nerve regeneration
Schuh C.M.A.P, Morton T.J., Banerjee A., Grasl C., Schima H., Schmidhammer R., Redl H., Rünzler D.
Cells Tissues Organs; accepted 22.6.2015;

A new preparation method for anisotropic silk fibroin nerve guidance conduits and its evaluation in vitro and in a rat sciatic nerve defect model
Teuschl A. H., Schuh C.M.A.P., Halbweis, R., Pajer, K., Márton, G., Hopf, R., Mosia S, Rünzler D, Redl H, Nógrádi A, Hausner, T.
Tissue Engineering Part C: Methods. Sept 2015;

In vitro extracorporeal shock wave treatment enhances stemness and preserves multipotency of rat and human adipose-derived stem cells
Schuh CM, Heher P, Weihs AM, Banerjee A, Fuchs C, Gabriel C, Wolbank S, Mittermayr R, Redl H, Rünzler D, Teuschl AH.
Cytotherapy. 2014 Aug 28. pii: S1465-3249(14)00700-2.
PMID: 25174738

In toto differentiation of human amniotic membrane towards the Schwann cell lineage.
Banerjee A, Nürnberger S, Hennerbichler S, Riedl S, **Schuh CM**, Hacobian A, Teuschl A, Eibl J, Redl H, Wolbank S.
Cell Tissue Bank. 2014 Jun;15(2):227-39
PMID: 24166477

Awards

TERMIS-AM Neural and Spine TWIG travel award:
Extracorporeal Shockwave Treatment accelerates peripheral nerve regeneration by altering Schwann cell phenotype- Poster presentation- *TERMIS- Tissue Engineering and Regenerative Medicine Society Annual Meeting* 2015

Best Poster Presentation: In vitro Extracorporeal Shockwave Treatment Enhances Stemness and Preserves Multipotency of Rat- and Human Adipose derived Stem Cells – Poster presentation – *TERMIS- Tissue Engineering and Regenerative Medicine Society Annual Meeting* 2013

Günther Schlag Award: "Extracorporeal Shockwave Treatment activates Schwann cells in vitro and in vivo" *LBG Meeting for Health Sciences, Vienna, Dec. 2014*

Conferences
2015

Silk fibroin for peripheral nerve regeneration: a novel preparation method improved mechanical characteristics and supports regeneration in rat sciatic nerves- Oral presentation *TERMIS Tissue Engineering and Regenerative Medicine Society World Congress*, Sept 2015

Extracorporeal Shockwave Treatment accelerates peripheral nerve regeneration by altering Schwann cell phenotype- Poster presentation; *TERMIS Tissue Engineering and Regenerative Medicine Society World Congress*, Sept 2015

-

Schwann cells and Schwann like cells for Peripheral Nerve Regeneration - Oral presentation TERMIS *Winterschool „Vitro/Vivo Preclinical Models and Imaging in Musculoskeletal Tissue Regeneration"* 2015

2014

In vitro Extracorporeal Shockwave Treatment in Adipose derived Stem Cells Leads to Enhanced Stemness and Preserves Multipotency- Oral presentation *ISMSTbasic biannual meeting* 2014

Schwann Cell like Cells for Peripheral Nerve Regeneration Approaches- Oral presentation *PACT- Platform for Advanced Cellular Therapy meeting* 2014

Extracorporeal Shockwave Treatment in vitro: Adipose derived Stem Cells show increased Stemness and Multipotency- Oral presentation TERMIS *Tissue Engineering and Regenerative Medicine Society Annual Meeting* 2014

Adipose derived Stem Cells Respond to in vitro Extracorporeal Shockwave Treatment With Increased Stemness and Multipotency – Oral presentation ECB *European Congress of Biotechnology* 2014

Extracorporeal Shockwave Treatment activates Schwann cells in vitro and in vivo- Oral presentation *LBG Health Meeting* 2014

2013	**In vitro Extracorporeal Shockwave Treatment has Beneficial Effects on Rat Schwann Cell Isolation and Culture –** Oral presentation *TERMIS- Tissue Engineering and Regenerative Medicine Society Annual Meeting* 2013
	In vitro Extracorporeal Shockwave Treatment Enhances Stemness and Preserves Multipotency of Rat- and Human Adipose derived Stem Cells – Poster presentation – *TERMIS- Tissue Engineering and Regenerative Medicine Society Annual Meeting* 2013
	Adipose derived Stem Cells: In vitro Treatment with Extracorporeal Shockwaves Enhances Stemness and Preserves Multipotency- Oral presentation *ISMST annual meeting* 2013
2012	**Schwann-like Cells- Neural Differentiation of rat Adipose Derived Stem Cells for improvement of Peripheral Nerve Regeneration-** Oral presentation *4th Vienna Symposium on Surgery of Peripheral Nerves* 2012
	Activated Schwann-like Cells Guided by Fibrin Structures Enhance Axonal Regeneration Poster presentation *TERMIS- Tissue Engineering and Regenerative Medicine Society Annual Meeting* 2012
2011	**Aligned Fibrin and Schwann-like Cells: a ready-to-use Neve Conduit-** Oral presentation *TERMIS- Tissue Engineering and Regenerative Medicine Society Annual Meeting* 2011
	Aligned Fibrin-PGLA Matrix as a Scaffold for Schwann-like Cells- Oral presentation *European Conference on Biomaterials* 2011
2010	**Electrospun Fibrin for peripheral Nerve Regeneration-** Poster presentation *European Conference on Biomaterials* 2010
	Aligned Electrospun Fibrin Nanofibres for Peripheral Nerve Regeneration- Poster presentation *BioNanoMed-International Congress on Nanotechnology in Medicine and Biology* 2010
Languages	**German**: fluent
	English: fluent
	Italian: fluent/profound knowledge
	Austrian Sign Language: profound knowledge
	Polish: knowledge

Vienna, February 2016